WELDABILITY STUDIES ON 12% AND 14% CHROMIUM STEELS

by

Christoffel Grobler

Submitted in fulfilment of the requirements for the degree of

PHILOSOPHIAE DOCTOR (Ph.D.)

in the Department of Materials Science and Metallurgical Engineering,
Faculty of Science, University of Pretoria, Pretoria

Supervisor : Professor Doctor G. T. van Rooyen

September 1987

TO MY WIFE LILI-MART

Where is the wise man? Where is the scholar? Where is the philosopher of this age? Has not God made foolish the wisdom of the world? For since in the wisdom of God the world through its wisdom did not know Him, God was pleased through the foolishness of what was preached to save those who believe.

1 Corinthians 1:20-21 (NIV)

ACKNOWLEDGEMENTS

The author wishes to express his appreciation to his supervisor, Prof. G. T. van Rooyen for his help and inspiration during the past three years of research for this project. Gratitude is expressed to the following persons for assistance with the experimental work and in preparing the final manuscript: Messrs. J. B. J. Barnard and P. L. Zietsman and Mmes. A. J. Steyn and E. L. Pretorius. A special word of thanks to Prof. J. G. Pretorius for his help with the language aspect of the text.

The writer also wishes to thank his wife in particular for her patience and encouragement during the course of this study.

This work was sponsored financially by Middelburg Steel and Alloys (Pty), Ltd.

Finally, to the living God who created everything through his Son, all praise and thanks.

SYNOPSIS

This thesis is a detailed study of some important aspects of the weldability of the well-known 12% chromium steel, known as 3CR12, and a 14% chromium steel, designated 3CR14.

3CR12 is a duplex ferrite-tempered-martensite steel which was developed as a corrosion resistant steel, from the ferritic stainless steel AISI 409, for application in mildly corrosive environments in the South African coal and gold mines. 3CR14 is a new higher chromium steel which is presently being developed for application in more aggressive corrosive environments than 3CR12. Although it is reported in the literature that the weldability of 3CR12 is superior to that of AISI 409, there is an increasing concern about the actual weldability of 3CR12 in comparison to the steels (mild and low alloy steels) it is replacing. This is particulary the case since 3CR12 is now also specified for, and used in, more and more structural applications.

The following aspects of the weldability of 3CR12 and 3CR14 were studied:

1. A study of the fusion line fracture behaviour of welds on 6 mm 3CR12 and 3CR14 plate in the presence of a triaxial stress field. A new bead-on-plate bend test was developed for measuring the fracture toughness of the narrow (0.25 mm - 0.35 mm) high-temperature (HT) weld heat-affected zone (HAZ) adjacent to the fusion line. The influence of factors like chemical composition, phase composition of the HT HAZ and loading rate on the HT HAZ fracture toughness, was studied.

2. A study was undertaken into the influence of weld metal and base metal mechanical properties on the fusion line fracture behaviour of highly restrained welds. A new fusion line notch fracture toughness test was developed to compare the suitability of different filler metals for welding 12 mm 3CR12 plate.

3. The mechanism of splitting in transverse Charpy specimens was studied and the relationship was established between splitting and the phenomenon of lamellar tearing which sometimes attends welding.

The experimental results are successfully explained in terms of two fracture mechanics theories.

The fracture toughness values measured in this thesis for the duplex ferrite-martensite HT HAZ of both 3CR12 and 3CR14 are much lower than the values reported in the literature. The HT HAZ ductile-brittle transition temperature of, e.g., 3CR12 is higher than 100°C, while values of below room temperature was reported in the literature. It is shown that the conventional Charpy V-notch test may not be used to measure reliably the toughness of the narrow HT HAZ. It is concluded that the weldability of 3CR12 is not really superior to that of AISI 409 and that the steel should not be used for structural applications in plate thicknesses above 3 mm if adequate joint toughness is required.

The HT HAZ fracture toughness of both 3CR12 and 3CR14 was found to be nearly independent of grain size and phase composition.

A type AISI 309L filler metal is recommended for welding 3CR12. The recently developed E3CR12 filler metal is not recommended due to its detrimental effect on the fusion line notch fracture toughness.

SAMEVATTING

Sekere belangrike sweisbaarheidsaspekte van die bekende 12% chroomstaal (3CR12) en 'n 14% chroomstaal (3CR14) is in detail bestudeer.

3CR12 is 'n sweisbare, dupleks ferriet-getemperde-martensietstaal wat ontwikkel is vanuit die ferritiese roesvrye staal AISI 409, vir aanwending in matige korrosiewe omgewings in Suid-Afrikaanse steenkool- en goudmyne. 3CR14 is 'n nuwe staal wat tans ontwikkel word vir toepassing in meer aggressiewe korrosiewe omgewings. Alhoewel daar in onlangse publikasies beweer word dat 3CR12 'n baie beter sweisbaarheid het as AISI 409, heers daar tans heelwat onsekerheid ten opsigte van die sweisbaarheid van 3CR12, aangesien die staal nou ook gespesifiseer word vir strukturele toepassings.

Die volgende aspekte van die sweisbaarheid van 3CR12 en 3CR14 is ondersoek:

1. Die smeltlynbreukgedrag van sweislasse in 6 mm 3CR12 en 3CR14 plaat in die teenwoordigheid van 'n triaksiale spanningsveld. 'n Nuwe toetsmetode is ontwikkel vir die meting van die breuktaaiheid van die nou (0.25 mm - 0.35 mm) hoë temperatuur (HT) sone in die sweis hitte-geaffekteerde-sone (HAS). Die invloed van faktore soos chemiese samestelling, fasesamestelling van die HT HAS en belastingstempo op die breuktaaiheid van die HT HAS is bestudeer.

2. Die invloed van die sweismetaal en basismetaal meganiese eienskappe op die breukgedrag van ingeklemde sweislasse. 'n Nuwe smeltlynbreuktaai-heidstoetstegniek is ontwikkel vir die toetsing van verskillende tipes sweiselektrodes vir die sweising van 12 mm 3CR12 plaat.

3. Die meganisme van delaminering in transversale Charpymonsters. Ondersoek is ingestel om te bepaal of hierdie verskynsel nie moontlik 'n aanduiding is van die vatbaarheid van 3CR12 vir lamellare skeuring gedurende en na sweising nie.

Die eksperimentele resultate word suksesvol verklaar aan die hand van twee breukmeganikateorieë.

Die breuktaaiheidswaardes wat in hierdie studie bepaal is vir die HT HAS

van 3CR12 sowel as 3CR14, is baie laer as die gepubliseerde waardes. Die HT HAS brosoorgangstemperatuur van 3CR12 is bv. hoër as 100°C terwyl waardes laer as 20°C gepubliseer is. Daar word aangetoon dat die taaiheid van die HT HAS nie akkuraat m.b.v. die konvensionele Charpytoets bepaal kan word nie. Die eksperimentele resultate dui daarop dat die sweisbaarheid van 3CR12 nie beter is as die van AISI 409 nie. Vir strukturele toepassings waar aanvaarbare sweislastaaiheid 'n vereiste is, word 3CR12 gevolglik nie aanbeveel vir plaatdiktes dikker as 3 mm nie.

Die breuktaaiheid van die HT HAS van beide 3CR12 en 3CR14 word nie noemenswaardig deur die korrelgroote en fasesamestelling van die sone beïnvloed nie.

'n Tipe AISI 309L sweiselektrode word aanbeveel vir die sweising van 3CR12 terwyl die nuwe E3CR12 sweiselektrode glad nie aanbeveel word nie as gevolg van die nadelige effek van die E3CR12 sweismetaal op die smeltlynbreuk-taaiheid.

TABLE OF CONTENTS

CHAPTER 1

AN INTRODUCTION TO THE WELDABILITY OF 3CR12

1. INTRODUCTION

The main purpose of this first chapter is to outline three important aspects of the weldability of a 12 percent chromium steel, designated 3CR12, on which little information is available yet. This thesis is a report on a detailed study of these aspects.

3CR12 is a low carbon (0.03%), titanium stabilised, 12 percent chromium, duplex ferritic-martensitic steel which was developed by Southern Cross Steel, the stainless steel producing division of Middelburg Steel and Alloys (Pty), Ltd. The steel was developed from the ferritic stainless steel AISI 409 by careful balancing of the ferrite (Cr, Si, Ti) and austenite (Ni, Mn, C, N) stabilising elements using Kaltenhauser's(1) relationship:

$$\text{Ferrite Factor (F.F.)} = Cr + 6Si + 8Ti - 2Mn - 4Ni - 40(C+N)$$

where F.F. = 11.5 for 3CR12.

The microstructure of the steel consists of slightly elongated to equiaxed ferrite and highly tempered martensite grains (grain size ASTM 7) with large blocky cubic titanium carbonitrides. This structure is obtained by tempering (750-770°C) of hot rolled plate of which the temperature during the final pass was within the dual-phase ferrite-austenite phase field. This results in a banded microstructure consisting of pancake shaped ferrite and martensite grains.

Two basic varieties of 3CR12, one containing 0.6 percent nickel (3CR12) and one containing 1.2 percent nickel (3CR12Ni), are being marketed by Southern Cross Steel. (See table 1.1 for chemical compositions.) The lower nickel variety is intended for general applications, while the higher nickel variety is produced for high strength applications.

3CR12 has been developed as a relatively inexpensive corrosion resisting steel and replacement for mild and structural steels for application in mildly corrosive environments where the corrosion resistance of these

Table 1.1: Chemical composition limits (wt-%) for AISI 409 and 3CR12.

Steel	C	S	P	Mn	Si	Cr	Ni	Ti	N
409 Limits	0.08 max	0.045 max	0.045 max	1.00 max	1.0 max	10.5-11.75	0.5 max	6 x C 0.75max	-
3CR12 Limits	0.03 max	0.030 max	0.030 max	1.50 max	1.0 max	11-12	1.5 max	4(C+N)min 0.6max	0.03 max
3CR12 Typical	0.025	0.012	0.020	1.2	0.5	11.2	0.6	0.3	0.015
3CR12Ni Typical	0.025	0.012	0.020	1.2	0.5	11.2	1.2	0.3	0.015

steels are inadequate. Sheet and plate are presently being marketed respectively within the thickness ranges 0.55 to 3.0 mm and 3.5 to 30 mm. The steel is presently finding application in the South African gold and coal mines for construction of transport wagons, coal bunkers, railway masts, storage tanks, containers, etc. It is also increasingly being used in structural applications for petro-chemical, metallurgical, pulp and paper, and sugar industries.

The mechanical properties, i.e. toughness, formability and weldability of 3CR12 are superior to that of AISI 409. This is due to the fine grained microstructure which contains large fractions of low carbon, highly tempered martensite. Typical mechanical properties of 3CR12 and 409 are(2):

		3CR12	AISI 409
Tensile strength, Rm (MPa)	:	530	450
0.2% Proof Stress, Rp (MPa)	:	380	250
Elongation, A (% in 50mm)	:	26	27
Brinell hardness (HB)	:	165	150

Typical Charpy V-notch values for 10 mm plate are(2):

		3CR12	AISI 409
Temperature (20°C)	:	85J	20J
Temperature (0°C)	:	65J	10J
D.B.T.T. (30J)	:	-20°C	40-100°C

2. WELDABILITY

The standard ferritic stainless steels exhibit a poor weldability due to undesirable heat-affected zone (HAZ) microstructural changes, i.e.

a. Excessive HAZ grain growth with a loss of both ductility and toughness.
b. Formation of chromium carbonitrides which lowers the corrosion resistance and toughness(3).
c. Loss in ductility and corrosion resistance due to the formation of small amounts martensite on the grain boundaries(4).

The poor weldabiltiy is the major constraining factor in using ferritic stainless steels in thicknesses exceeding 3 mm, which is generally the maximum recommended thickness, if adequate weldment toughness is to be maintained(5,6). The improvement of the weld HAZ toughness of 11.5 percent chromium ferritic stainless steels, e.g. AISI 409, is the critical factor in extending the applications of these steels to thicker plate material.

Since 3CR12 was developed from AISI 409, it is of some significance to consider attempts by Thomas and Apps(7) to improve the weldability of 6 mm AISI 409 plate by compositional variations within the AISI 409 specification. Table 1.2 shows the compositional range of their experimental steels together with the composition of one of the steels (steel A) which contained up to 20 percent martensite in the high temperature (HT) HAZ.

The weld HAZ toughness of TIG welds on 6 mm plate was determined with thermal simulated substandard (10 mm x 5 mm x 55 mm) Charpy V-notch specimens. Depending on the peak temperature during thermal simulation, steel A (table 1.2) contained up to 20 percent low carbon martensite in the HT HAZ. Ductile-brittle transition temperatures (30J) of 76°C and 86°C were

Table 1.2: Chemical compositional range (wt-%) of AISI 409 steels studied by Thomas and Apps(7).

-	C	N	Mn	Si	S	Cr	Ni	Ti	Aℓ
Range	0.020-0.027	0.012-0.015	0.72-0.98	0.39-0.51	0.015-0.023	11.42-11.57	0.32-0.60	0.17-0.30	0.09-0.028
Steel A	0.025	0.015	0.74	0.39	0.017	0.6	0.6	0.3	0.09

obtained respectively for specimens with 5-10% and 15-20% martensite in the HT HAZ. It should be remembered that higher transition temperatures will be obtained with standard size Charpy V-notch specimens. Thomas and Apps also found that the transition temperatures and therefore the weld HAZ toughness were not significantly influenced by subsequent low peak temperature thermal cycles which simulated the thermal effects of multipass welding. It was therefore concluded that, due to the very low weld HAZ toughness values of the experimental steels (high transition temperatures), compositional variations in the AISI 409 specification were unlikely to give any significant improvement in the weldability of these steels. Finally, it was suggested that attemps to improve the weldability of AISI 409 should concentrate on reducing both grain growth and martensite formation in the HAZ.

Although the HAZ toughness of the low carbon, titanium stabilised steel A in table 1.2 was not improved to any significant extent by up to 20 percent martensite, the superior weldability of 3CR12 (which was developed from AISI 409) is in fact partly attributed to the formation of about 40 percent of this low carbon lath martensite (2,4,8,9,10). The composition of 3CR12 falls within the AISI 409 limits (table 1.1), although certain elements such as Mn, Ni, and Ti may fall outside these limits. A comparison between the typical composition for 3CR12 in table 1.1 and the composition of steel A in table 1.2 reveals that 3CR12 exhibits a slightly higher manganese content which will result in the formation of a higher fraction martensite in the weld HAZ. Figure 1.1 shows such a weld HAZ of a bead-on-plate MIG welded weld on 6 mm tempered 3CR12 plate. The HT coarse

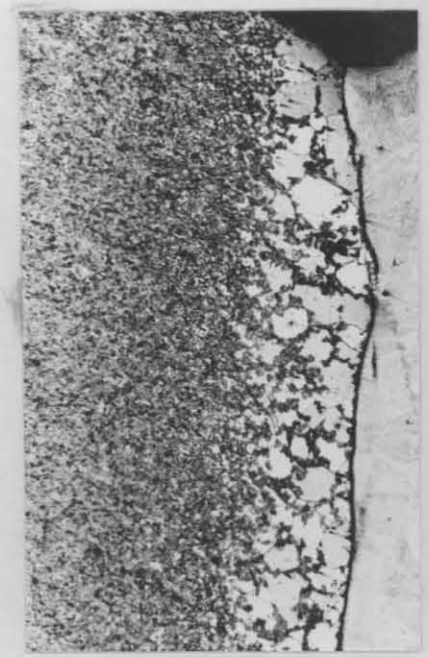

Figure 1.1: Weld HAZ of 3CR12 with 35 percent grain boundary martensite in the coarse grained, duplex ferrite-martensite high temperature HAZ adjacent to the fusion line (35X).

grained HAZ adjacent to the fusion line contains 35 percent grain boundary martensite with the balance ferrite. The HT HAZ of the high nickel 3CR12Ni contains up to 90 percent martensite, with even better toughness properties.

3CR12 has been developed to overcome the three major problems which limit the weld HAZ toughness and therefore the weldability of AISI 409:

a. The excessive grain growth which usually occurs in the HT HAZ is limited by the formation of about 40 percent grain boundary martensite(7,8,9).

b. The harmful effects of carbon and nitrogen on the toughness of ferritic stainless steels is limited by a low carbon and nitrogen content and titanium stabilization(8,11).

c. Ball and Hoffman(12) concluded that, since the hardness of the

martensite (HV 250) in the HT HAZ is equivalent to the hardness of martensite containing less than 0.05 percent carbon, the average toughness of the weld HAZ should not be less than the parent metal.

In summary, it appears therefore that the superior weld HAZ toughness of 3CR12, over AISI 409, results from the synergistic effect of the tough low carbon lath martensite and the restricted grain growth. The steel is claimed to be weldable in thicknesses up to 32 mm without any pre- or post weld heat treatments(8).

Hoffman(8) published a comprehensive summary of research, down to September 1984, done on the weldability of 3CR12. Satisfactory results were obtained with reference to the following factors determining the weldability: joint strength, ductility, toughness, fatigue strength, corrosion resistance, ease of welding and susceptability to hot cracking. Of particular interest is the half size Charpy V-notch ductile-brittle (10.2 Joule) transition temperature of less than room temperature which was obtained for the weld HAZ of 3CR12 and a ductile-brittle transition temperature of below 0°C which was obtained for the weld HAZ of 3CR12Ni. Melville et al.(2) reported average standard Charpy V-notch impact energy values of 49J and 35J, obtained at room temperature and 0°C, respectively.

Before discussing the excellent HAZ toughness values reported for 3CR12 in comparison to the poor HAZ toughness values obtained, respectively by Thomas and Apps(7) for AISI 409, and Gooch and Davey(13) for 3CR12, it is necessary to take a closer look at the weld HAZ microstructure of 3CR12 in figure 1.1. The HAZ may be divided into at least three zones; each with a different microstructure, phase composition and therefore mechanical properties. The microstructural changes which occurred in the three zones during welding may be described by means of the pseudo-binary phase diagram for 11.5% chromium steels in figure 1.2 and the microhardness transverse across the fusion line of the weld in figure 1.1 (fig. 1.3).

The three zones in the HAZ are:

1. A narrow coarse grained zone adjacent to the fusion line (figs. 1.1 and 1.3). The phase composition (δ -ferrite and granular blocky and

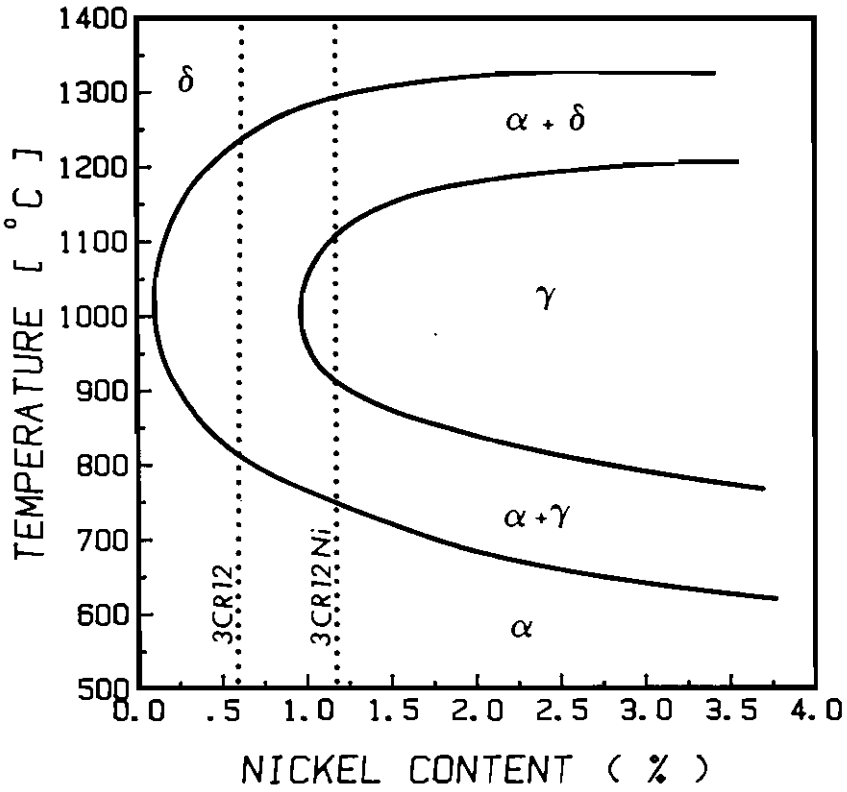

Figure 1.2: Pseudo-binary phase diagram for 11.5% chromium steels. (After Protopappas(14)). Typical compositions for 3CR12 and 3CR12Ni are also indicated.

angular Widmanstätten intergranular martensite(7)) of the zone is determined by the relative amount of ferrite and austenite stabilizing elements, while the width depends on the weld heat input. (For a very low heat input of 0.46 kJ/mm this zone has a typical thickness of 0.2 - 0.3 mm). During welding this zone was heated within the δ -ferrite phase field (above about 1250°C) in figure 1.2. Due to the very high peak temperatures in this zone, excessive δ-ferrite grain growth occurred, with subsequent transformation of some of the δ-ferrite to angular Widmanstätten austenite during subsequent cooling cycle. Grain refining actually occurred therefore during the δ-ferrite to austenite transformation. Any δ-ferrite that transforms to austenite will subsequently transform to martensite upon further cooling. The weighed average hardness of the ferrite and martensite in this zone is indicated in figure 1.3.

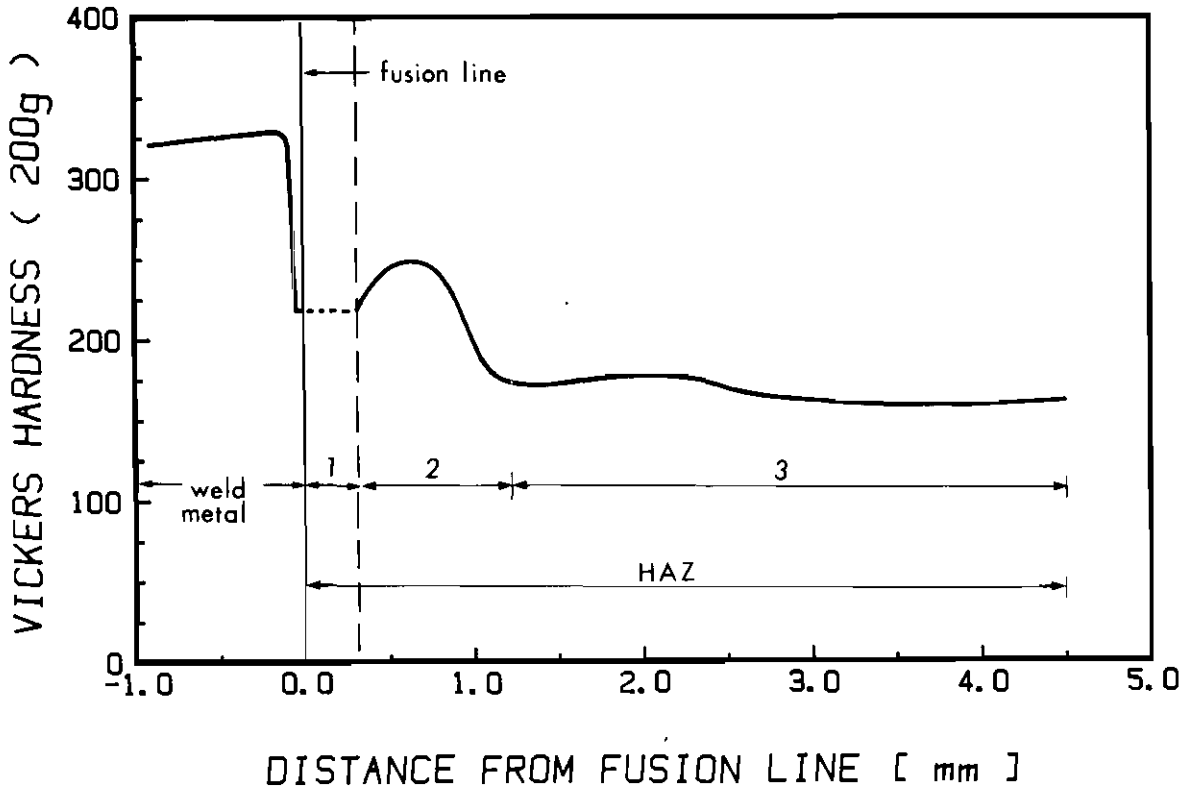

1: HT HAZ, 2: Fine grained HAZ, 3: Low temperature HAZ

Figure 1.3: Microhardness transverse across the fusion line of a bead-on-plate weld on 6.3 mm 3CR12 plate.

The only differences between this high temperature (HT) HAZ in 3CR12 and steel A in table 1.2 are the lower martensite content and coarser grain size of this zone in steel A.

2. A much wider duplex zone with fine grained ferrite and untempered inter- and intragranular martensite(7), right next to the coarse grained zone (figs. 1.1 and 1.3). This wider duplex zone originated when the material was heated to temperatures (900-1300°C) within the dual phase ferrite and austenite phase field in figure 1.2. The width of this zone depends on the weld heat input and the composition of the steel. The phase composition of this zone varies across the width of this zone. The maximum amount of martensite formed at the point in this zone at which the longest time was spent during welding, and at the temperature (1050°C in fig. 1.2) at which the maximum amount of austenite will form in 3CR12. The high

hardness of this zone in figure 1.3 results from the presence of the large amount of untempered martensite.

3. A third zone (low temperature HAZ) more distant from the fusion line that was heated to temperatures below the A_1 temperature (800°C in fig. 1.2) during welding. The hardness of the material in this zone is unchanged (fig. 1.2) since the plate was previously, subsequent to hot rolling, tempered at 750-770°C.

It is therefore clear that the weld HAZ of 3CR12 consists of at least three different zones with different microstructures and mechanical properties. For a proper comparison of the weld HAZ toughness of 3CR12 and AISI 409, it will therefore be necessary to compare the toughness of the various corresponding zones in the HAZ with each other. In the literature reference is made only to the weld HAZ toughness of 3CR12 and toughness values are only therefore being reported for the weld HAZ. In general it is actually not clear to which of the three zones in the weld HAZ these excellent toughness values apply.

The narrow high temperature (HT) zone in the HAZ adjacent to the fusion line, is considered to be the critical zone. The toughness of this zone is expected to be much lower than the toughness of the other two zones in the HAZ due to the relatively much larger grain size (fig. 1.1) and the possibility of high temperature embrittlement in this zone. The toughness of both the fine grained and low temperature zones in the HAZ of 3CR12 is expected to be superior to the toughness of the corresponding zones in AISI 409 as a result of the effective grain refining which occurred in the fine grained HAZ during welding and the superior original toughness of 3CR12 in the low temperature HAZ prior to welding. It is not clear whether the toughness of the HT HAZ of 3CR12 is superior to that of AISI 409. If the size of this zone is considered, it is doubtful whether the toughness of this zone, in actual welds, has ever been determined, since only the Charpy V-notch test has been used in the past. As far as the Charpy V-notch test is concerned it is questionable whether it is possible accurately to position the notch tip of the V-notch in this narrow HT HAZ, and guarantee that fracture will be limited exclusively to this zone.

The very low HT HAZ toughness which was obtained by Thomas and Apps for

steel A (table 1.2), with 20 percent martensite in the HT HAZ, seems to indicate that the toughness of this zone in 3CR12 is much lower than the reported values. This possibility is further strengthened by the Charpy V-notch weld HAZ toughness results which have been reported by Gooch and Davey(13) for 10 mm 3CR12 plate. Although Gooch and Davey have not been very successful in determining the toughness of the HT HAZ, their variable results, which are summarized in table 1.3, also seem to indicate that the actual toughness of the HT HAZ is much lower than that which is generally reported. The low toughness values in table 1.3 were obtained when

Table 1.3: Summary of weld HAZ Charpy values which was obtained by Gooch and Davey(13) for 10 mm 3CR12 plate.

Test Temperature (°C)	Absorbed energy (J)
-20	4 - 9
0	8 - 61
20	11 - 65
40	9 - 68

cleavage fracture occurred within three to four ferrite grain diameters of the fusion boundary. The high toughness values were obtained when ductile fracture occurred in the fine grained and low temperature HAZ.

It may therefore be concluded that there is an uncertainty as far as the actual toughness of the HT HAZ of welds on 3CR12 is concerned. If the actual toughness of this zone is much lower than the values reported by, e.g. Hoffman(8) and Melvill et al.(2), their values appear to apply to the fine grained zone in the HAZ, rather than the HT HAZ. The superior weldability of 3CR12 over the ferritic stainless steel AISI 409, from which it was developed, can therefore be seriously questioned.

3. WELDING CONSUMABLES FOR 3CR12

Although some ferritic filler metals are available for welding ferritic stainless steels, the resultant weld deposits are low in ductility. Austenitic steel fillers are therefore generally recommended for welding ferritic stainless steels(7). Hoffman investigated the influence of different MMA and MIG filler metals on the weldment properties of 3CR12 and recommended that any austenitic filler metal may be used for welding 3CR12. The use of AISI 308L, 309L and 309LMo is, however, preferred(8). Gooch and Davey also reported no significant differences in the weldment properties of welds on 3CR12, welded with AISI 308L, 309 and 310 electrodes(13). A high strength matching (composition) electrode, E3CR12, has also recently been developed by Pagani for welding 3CR12(15).

The evaluation of the mechanical properties of weldments, welded with the abovementioned filler metals, has been based on bend test and tensile test results only. These tests only evaluate the plane stress fracture behaviour of welds. With the toughness of the HT HAZ lower than the toughness of the rest of the HAZ, the suitability of a filler metal for welding 3CR12 should also be evaluated on the basis of its influence on the fusion line fracture behaviour of welds in the presence of a triaxial stress field. The HT HAZ is expected to have a significant effect on the fusion line fracture behaviour of welds on the presence of a triaxial stress field.

4. LAMELLAR TEARING

Mechanical tests on 3CR12 often reveal splitting or tearing in the rolling plane. Figure 1.4 shows such parallel splits on the fracture surface of a transverse 3CR12 Charpy specimen. These splits form in the rolling plane and is usually associated with a low through thickness fracture stress and the development of high through-thickness stresses during mechanical testing. Various mechanisms have already been suggested for the formation of these splits which are also common to hot rolled duplex steels.

Although Hoffman(8) do not consider these splits to be detrimental to the properties of 3CR12, the possibility of a correlation between splitting and the susceptability of 3CR12 to lamellar tearing during and after welding

in the rolling plane, has not yet been investigated. With 3CR12 being used in more and more higher strength structural applications, this aspect of the weldability of 3CR12 becomes even more important.

Figure 1.4: Parallel splits on the fracture surface of a transverse 3CR12 Charpy V-notch impact specimen. These splits developed in the rolling plane during impact testing.

5. EXPERIMENTAL

3CR12 is presently finding application as a replacement for mild steel, galvanized steel and coated structural steel. It finds use in more and more higher stress structural applications in the petro-chemical, metallurgical, pulp, paper and sugar industries due to its superior corrosion resistance and mechanical properties. There is therefore a growing concern about the actual weldability of 3CR12 over AISI 409 and the steels it is replacing due to the uncertainty concerning the true weld HAZ toughness and the higher constraint levels to which weldments are being subjected to.

A better understanding of the weld HAZ fracture behaviour, the effects of weld and base metal mechanical properties on the fusion line fracture toughness, and the susceptibility of welded 3CR12 to lamellar tearing, may greatly contribute towards confidence in the integrety of welded 3CR12 structures and the development of higher chromium duplex steels, e.g. 14 percent chromium steels (3CR14), with superior weldability.

The principal aims of this thesis may therefore, with reference to the various aspects of the weldability of 3CR12, be summarised as follows:

a. A study of the fusion line (HT HAZ) fracture behaviour of welds on 6 mm duplex 12 percent chromium (3CR12) and 14 percent chromium (3CR14) steel plate, in the presence of a triaxial stress field. A new test method was developed for measuring the fracture toughness of the HT HAZ of actual welds and to determine respectively the effects of factors such as chemical composition, phase composition, stabilising elements, loading rate, etc. on the fracture toughness of the HT HAZ (Chapters 3 and 4).

b. A study of both the effects of weld metal and base metal mechanical properties on the fusion line fracture behaviour of highly restrained welds. The suitability of different filler metals for welding of 10 mm 3CR12 plate is evaluated with another newly developed test method devised for measuring the fusion line fracture toughness of fillet welds (Chapter 5).

c. A study of the mechanism of splitting in the rolling plane of 10 mm 3CR12 plate and the correlation between splitting and the phenomenon of lamellar tearing which sometimes manifest during and after welding (Chapter 6).

The major results and conclusions on the different aspects of the weldability of 3CR12 and 3CR14 are discussed in Chapter 7.

CHAPTER 2

FRACTURE MECHANICS

1. INTRODUCTION

It has been pointed out in the previous chapter that the HAZ of a weld on 3CR12 consists of at least three different zones, each with a different microstructure and mechanical properties. The properties of the weld metal is determined by the type of filler metal and the dilution with the base metal. Hence, a weldment may therefore be treated as composite specimen which consists of at least five different materials with different properties. Any fracture mechanics analysis of the fracture behaviour of a weldment should therefore be based on the interaction between the different composite materials during loading and fracture. The fusion line or boundary fracture behaviour of welds on 3CR12 represents the most critical part of the fracture behaviour of welds since the fusion line is associated with the HT HAZ which has the lowest toughness.

2. NOTCH-TOUGHNESS TESTING

Masubuchi listed seventeen tests for evaluating the notch-toughness of welds(16). The Charpy V-notch and crack tip opening displacement methods (CTOD) are most commonly used for evualuating the HAZ notch-toughness of welds. Although these two methods are also the most probable methods for determining the notch-toughness of the narrow HT HAZ in 3CR12, they have certain practical limitations. Gooch and Davey have already demonstrated that the toughness of the HT HAZ of welds on 10 mm 3CR12 plate may not be successfully determined with the Charpy V-notch test(13). This is attributed to the following factors:

a. Even with a K-type weld preparation, Gooch and Davey did not succeed to produce a specimen with a planar HT HAZ which is also oriented normal to the plate surface.

b. With the size of the HT HAZ very similar to the notch tip radius of the Charpy V-notch, it is very difficult to position the notch tip in the HT HAZ.

In the case of 6 mm 3CR12 and 3CR14 plate, which is the thickness of the plate which was mainly used for this thesis, it is even more difficult to prepare Charpy and CTOD specimens from welded plate which will meet the abovementioned requirements. Another limitation of the Charpy and CTOD methods is the fact that the fusion line fracture initiation behaviour, which is an important aspect of the fracture behaviour of 3CR12 welds, may not be determined with an existing notch or fatigue crack in the HT HAZ.

A new notch-toughness test method was therefore developed (chapter 3) to study the fusion line fracture initiation and propagation behaviour of welds on 6 mm 3CR12 and 3CR14 plate. The notch-toughness of the HT HAZ is characterised by means of a fracture appearance transition temperature (FATT). The transition temperature approach has certain limitations as far as practical implementation of the FATT values are concerned. The FATT, for example, depends on the measurement criteria as well as the thickness of the test specimen. In this study it is used only on a qualitative basis to study the influences of factors like the chemical and phase composition of the HT HAZ, mechanical properties of the different weldment materials, and loading rate, etc., on the fusion line fracture behaviour of welds. The notch-toughness values which were obtained for the HT HAZ of 3CR12 are also compared with values which were determined for both the ferritic stainless steel AISI 409 and mild steel.

3. FRACTURE BEHAVIOUR OF WELDS

The resistance of a material to crack extension may be described by means of the stress and strain fields at the crack tip under load. When the material at the crack tip shows linear-elastic behaviour when subjected to a tensile load, the crack tip stress and strain field is described in terms of the stress intensity factor K_1 ($K_1 = Y\sigma\sqrt{a}$). The fracture behaviour of a material may then be predicted by means of linear-ealstic fracture mechanics (LEFM). LEFM is, however, only applicable when the crack tip plastic zone is small compared to the crack length and specimen thickness, and usually applies therefore to high strength steels with yield strengths in excess of 1240 MPa(16).

The fracture behaviour of a material, under conditions where crack extension is preceded by extensive plastic deformation, may be predicted

by means of elastic-plastic fracture mechanics (EPFM). The fracture toughness is then described in terms of the crack tip opening displacement (CTOD) parameter, which is actually a measure of the crack tip plastic zone size(17). The J-integral may also be used to characterise the fracture toughness of materials when crack extension is preceded by plastic deformation.

The abovementioned LEFM and EPFM parameters describe the critical crack tip conditions prior to the extension of an existing crack under load in a homogeneous material. Since these fracture toughness parameters were developed to describe the fracture behaviour of a homogeneous material, they may not be used to describe adequately the fracture initiation and propagation behaviour of a composite specimen, e.g. a weldment which consists of different zones with different properties. In the case of a notch on the fusion line of a weld on 3CR12, the stress field ahead of the notch tip during loading will extend into at least three different materials, i.e. the weld metal adjacent to the fusion line, the narrow HT HAZ and fine grained zone in the weld HAZ adjacent to the HT HAZ. It will be demonstrated in this thesis that the fusion line fracture initiation behaviour of defect-free welds and the fracture propagation behaviour of notched welds are critically dependent not only on the fracture toughness, but also on the mechanical properties of the different composite materials of the weldment.

The HAZ fracture behaviour of welds on 3CR12 and 3CR14 plate may therefore be adequately predicted only by means of a fracture theory which will describe the fracture behaviour in terms of the mechanical properties (yield strength, fracture strength, work hardening rate, etc.) of the different composite materials of the weldment. Cottrell and Petch(18) and Davidenkov and Ludwik(19) have respectively developed fracture theories to explain the grain size and temperature sensitive fracture mechanism transitions in steel. In Chapters 3, 4 and 5 it is demonstrated how these theories may also be used to describe the HAZ fracture behaviour of welds on 3CR12 and 3CR14.

3.1 Cottrell-Petch fracture theory

Cottrell and Petch used dislocation theory to develop relationships that could account for the effect temperature, grain size and various metallurgical factors have on the likehood for cleavage fracture for materials that undergo a temperature sensitive fracture mechanism transition. The following relationship was developed for the fracture stress

$$\sigma_f = \frac{4G\gamma_m}{k_y\sqrt{d}} \quad \ldots\ldots\ldots\ldots\ldots\ldots \quad 2.1$$

where
- σ_f = fracture stress
- G = shear modulus
- γ_m = plastic work around a crack as it moves through the crystal
- d = grain diameter
- k_y = dislocation locking term from the Hall-Petch relationship.

Both the fracture stress and yield strength increase with decreasing grain size. Petch demonstrated that the cleavage fracture stress is approximately doubled as the grain size is reduced from a very coarse grain size (250 μm) to a very fine grain size (25 μm)(20). The Hall-Petch relationship for the yield strength is given by

$$\sigma_{ys} = \sigma_i + \frac{k_y}{\sqrt{d}} \quad \ldots\ldots\ldots\ldots\ldots\ldots \quad 2.2$$

where
- σ_{ys} = yield strength
- σ_i = lattice resistance to dislocation movement resulting from various strenghtening mechanisms and intrinsic lattice friction (Peierls stress).
- k_y = dislocation locking term
- d = grain diameter

Low demonstrated that the fracture stress is more sensitive to grain size than the yield strength(21). The intersection of the fracture stress and yield stress curves represents a fracture mode transition in

material response. Since the fracture stress and yield stress are temperature sensitive properties, the critical grain size for fracture transition would be expected to vary with temperature. The transition temperature decrease strongly with decreasing grain size.

Tetelman and McEvily studied the significance of the terms in equation 2.1 in more detail and showed that with increasing temperature the fracture stress increases while the yield stress decreases(22). These effects are attributed to an increase in dislocation velocity and a reduction in the Peierls stress. In fact, anything that increases the number of mobile dislocations, their mobility and speed, and the time allowed for such movement, will increase γ_m and the fracture stress.

The temperature dependence of the fracture stress and yield strength is shown in figure 2.1. The intersection of the curves represents a transition in material response. At a temperature T_1 below the transition temperature T*, failure must await the onset of plastic flow at the yield strength. With the yield strength at T_1 higher than the fracture stress, an unstable cleavage fracture results in body centered cubic (BCC) materials. At a temperature T_2 above the transition temperature, yielding occurs first and is followed by eventual fracture after a certain amount of plastic flow. Fracture above the transition temperature is usually characterised by a ductile microvoid coalesence mechanism.

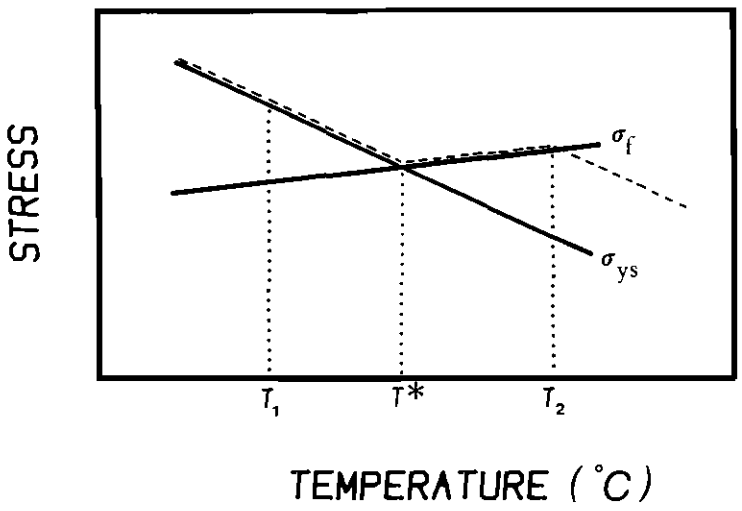

Figure 2.1: Temperature dependence of the fracture stress (σ_f) and yield strength (σ_{ys}).

3.2 Davidenkov-Ludwik fracture theory

Davidenkov developed a theory for fracture in 1936 which was actually initiated by Ludwik in 1923. They considered plastic flow and fracture to be independent phenomena with yielding obeying a critical shear stress criterion (Tresca), and fracture being dependent on the maximum principal stress. The fracture behaviour of a metal subjected to an uniaxial tensile stress is determined by the relative values of the fracture stress (σ_f) and flow stress (σ_{ys}) or yield curves in figure 2.3. The yield stress increases as the material is strain hardened, while the fracture stress is assumed to decrease (fig. 2.3a). Fracture will then occur at the intersection of the curves in figure 2.3a at a strain $\bar{\varepsilon}_1$.

The relative positions of the flow and fracture stress curves are changed with a change in stress state. The flow stress curve is lowered (according to the maximum shear stress criterion) with the application of a compressive stress R, perpendicular to the axis of a tensile specimen; while the fracture stress curve is unchanged (maximum principal stress criterion). The intersection of the curves now occur at a greater strain $\bar{\varepsilon}_2$ (fig. 2.3b), corresponding to increased ductility as found in practice with hydrostatic pressure or in a drawing die.

Conversly, a circumferential notch on a tensile test specimen produces tensile stresses perpendicular to the axis, due to the restraint on radial contraction of the material in the notch section by the unyielded material in the full section. The yield curve is therefore raised, giving reduced ductility as shown in figure 2.4

In 1936 Davidenko introduced the cleavage fracture curve (σ_{CL}) to represent fracture by cleavage (fig. 2.3c); the fracture stress curve (σ_f) now represents fibrous fracture or fracture by microvoid coalesence. The fracture mode transition from ductile to cleavage fracture with decreasing temperature is now explained, at least qualitatively, since the yield stress of materials which are susceptible to cleavage fracture increases sharply with reduced temperatures. The cleavage fracture curve may now, at lower temperatures, be intersected before the fibrous fracture curve (fig. 2.3c).

This latter situation reflects greater toughness with an increasing ratio of fracture stress to yield strength. This ratio will not increase indefinitely at higher temperatures. A maximum ratio may be correlated with the shelf energy of the Charpy impact energy curve. The shelf energy usually increases with improved steel cleanliness, thus the maximum ratio will also increase with improved steel cleanliness.

If the abovementioned considerations are taken into account a more realistic or correct fracture stress curve may be superimposed on figure 2.1 (dotted curve). Such a fracture stress curve was also obtained by Hahn et al.(19) for unnotched mild steel tensile specimens which were tested within the temperature range -250°C to 20°C (fig. 2.2).

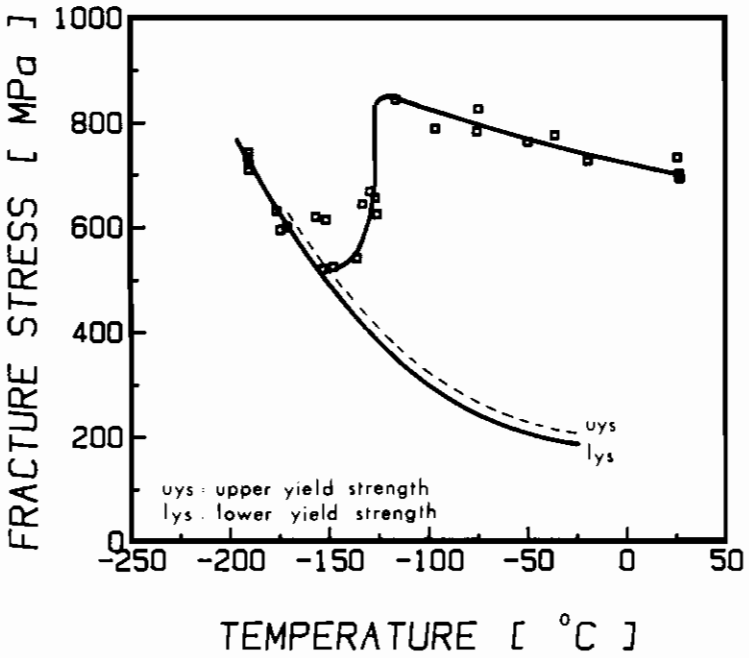

Figure 2.2: Unnotched tensile test data for 0.22 percent carbon steel versus test temperature (After Hahn et al.)

The fracture behaviour of a composite specimen, e.g. a weldment, may now be described by superimposing the fracture and yield stress curves of the different composite materials on the same figure.

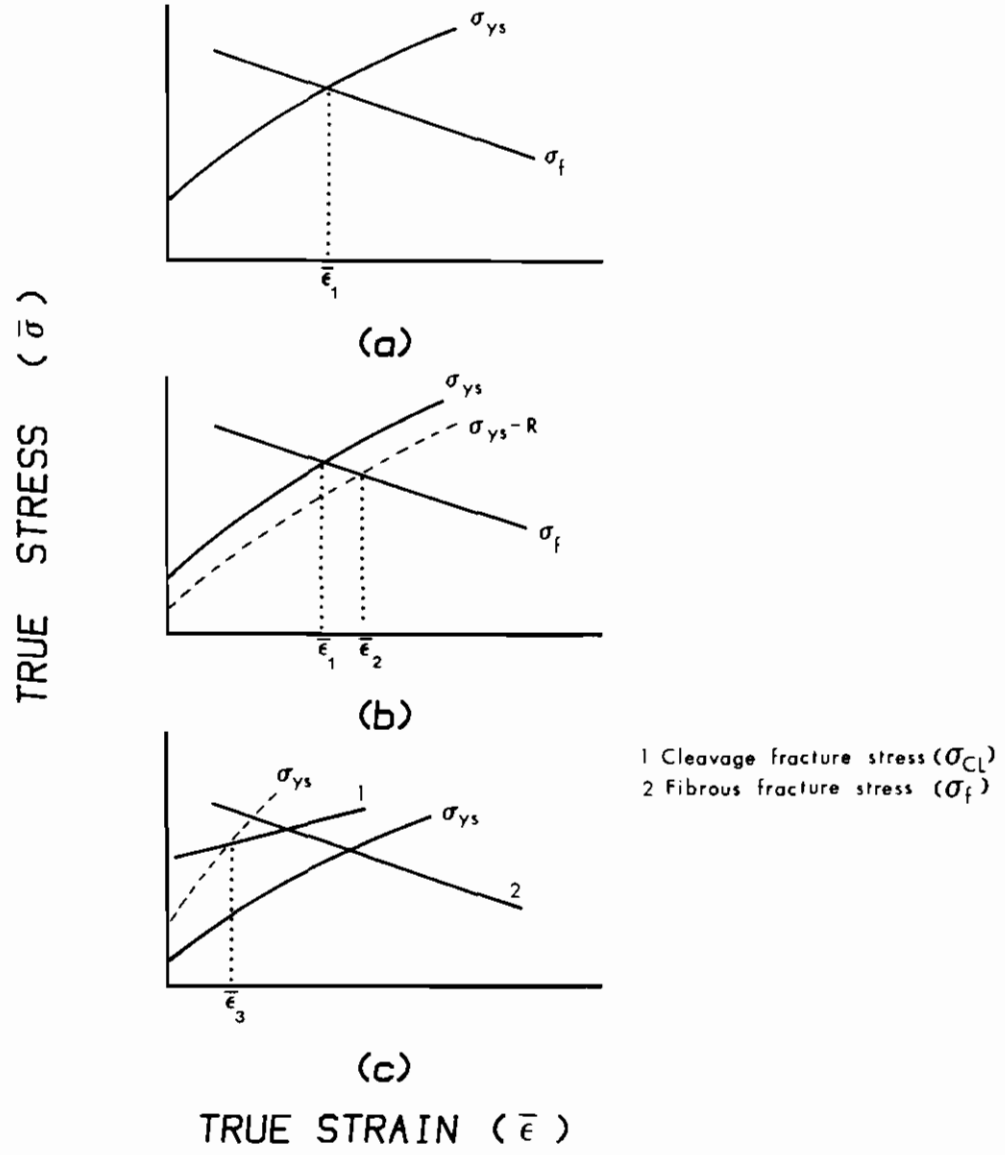

Figure 2.3: a. Fracture (σ_f) and flow stress (σ_{ys}) curves for simple tension.

b. With a superimposed compressive radial stress R, the yield curve is shifted to $\sigma_{ys}-R$ (dotted curve).

c. Davidenkov introduced cleavage and ductile fracture curves. The flow stress curve shifts to higher stresses with reducing temperature.

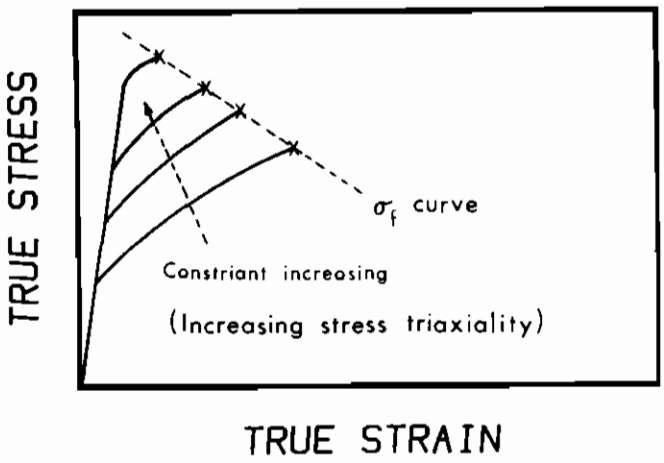

Figure 2.4: Elevation of flow stress (σ_{ys}) curves with increasing constraint or triaxial stress state.

There is a limit to the extent by which the yield stress or flow stress curve can be raised with increasing constraint. Orowan et al. demonstrated during 1945 to 1948 that the maximum principal stress can only reach three times the tensile yield stress. Thus only those materials for which the cleavage curve is not more than three times the flow stress curve (at test temperature), can be made to undergo cleavage fracture by increasing the degree of restraint. (The factors which determine the cleavage fracture stress have already been discussed.)

The fracture behaviour of a composite specimen may again be described in terms of the mechanical properties of the different composite materials by superimposing the fracture and flow stress curves of the different composite materials on the same figure.

CHAPTER 3

THE NOTCH-TOUGHNESS OF WELDED 14% CHROMIUM STEELS

SYNOPSIS

A new bead-on-plate bend test has been developed to measure the toughness of the narrow (0.25 - 0.35 mm), coarse grained, high temperature heat affected zone (HT HAZ), adjacent to the fusion line, in bead-on-plate welds on 6 mm hot rolled 14 percent chromium steel plate. The test is applied to study the influence of factors like stabilising elements (titanium vs. vanadium), phase composition of the HT HAZ, punch speed during bend testing and weld metal mechanical properties, on the fusion line notch fracture toughness of welds. The fracture toughness is characterised by a fracture appearance transition temperature (FATT).

The FATT temperature of the HT HAZ of steels with less than 60 percent ferrite in the HT HAZ increased at decreasing punch speeds below 133 mm/min. (during bend testing) and higher weld metal strength values. The HT HAZ FATT temperatures of two titanium stabilised steels with respectively 69 and 79 percent ferrite in the HT HAZ are respectively 67 and 74°C for slow bend testing. The HT HAZ FATT temperatures of both titanium and vanadium stabilised steels with less than 60 percent ferrite in the HT HAZ are higher than the reported values. This is due to the fact that the fusion line notch-toughness is enhanced by the ductile properties of the austenitic weld metal. The experimental results are explained in terms of Cottrell's and Davidenkov's fracture theories and the relative strain rate sensitivities of the yield and fracture strength of the austenitic weld metal and ferritic HT HAZ.

Large fractions, low carbon (< 0.028%), titanium stabilised martensite has not resulted in a significant improvement of the fracture toughness of the HT HAZ of welds on 6 mm hot rolled 14 percent chromium steel plate. It is suggested that the fracture toughness is determined by another important factor or phenomenon which has not yet been identified in this study so far.

THE NOTCH-TOUGHNESS OF WELDED 14% CHROMIUM STEELS

1. INTRODUCTION

3CR12 was developed as a replacement for mild and low alloy steels for application in mildly corrosive environments. In order to make provision for applications where more severe corrosive environments are encountered, attention was given to the development of a duplex ferrite-martensite stainless steel with a higher chromium and nickel content (3CR14), using the same principles employed in the development of 3CR12. Although a provisional patent has been lodged recently, the 14% chromium steels are currently not being produced commercially.

As far as the weldability of 3CR12 is concerned, the possibility of the fracture toughness of the narrow HT HAZ being much lower than anticipated, even at high low carbon martensite contents, has already been pointed out in chapter 1. A similar narrow coarse grained HT HAZ develops in welds of the 14% chromium steels. In fact the microstructure and phase composition of the weld HAZ (fig. 3.1) are very similar to that of 3CR12. The development of the microstructures of the different zones in the HAZ therefore may also be similary explained using the pseudo-binary phase diagram for 14% chromium steels(14). This particular study is therefore mainly concerned with the measurement of the fracture toughness of the HT HAZ, adjacent to the fusion line, of bead-on-plate welds on 6 mm plate. The contribution of this narrow HT zone to the notch-toughness of welds on 14% chromium steels has not been quantified as yet.

This HT HAZ appears to have no significant effect on the plane stress toughness of welds on 3CR12 and 14% chromium steels. Slow bend tests, with the weld root in tension and compression respectively, were performed in this study on welds made from tempered 6 mm plate and 180°C bends were successfully achieved. Satisfactory results were also obtained from crossweld tensile tests with fracture occurring in the low temperature HAZ. However, the HT HAZ may have a significant influence on the notch-toughness of welds in critical applications where plane strain conditions rather than plane stress conditions are approached. Brittle fracture may occur in this zone when subjected to a triaxial stress state due to the presence of fusion line defects or in weld configurations offering a high degree of

constraint.

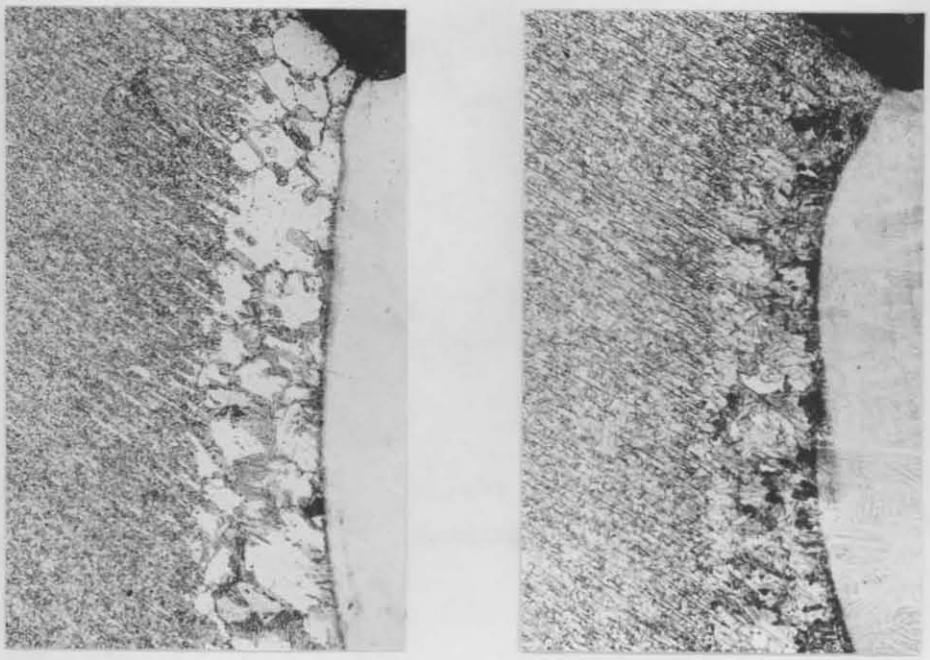

a. b.

Figure 3.1: Weld HAZ microstructure of bead-on-plate welds on hot rolled 6 mm 14% chromium steels.

a. 69% ferrite and 31% grain boundary martensite in the HT HAZ (80x).

b. 96% martensite in HT HAZ. Note the coarse microstructure of the HT HAZ relative to that of the rest of the HAZ even at such a high martensite content (80X).

The limitations of the Charpy impact and CTOD tests for measuring the fracture toughness of the narrow HT HAZ, in especially welded 6 mm plate, have already been dealt with in the first chapter. In theory the toughness of the HT HAZ can be studied by subjecting full Charpy specimens to the same thermal cycle. For this purpose the thermal cycle of this zone, during welding, can be determined experimentally and subsequently simulated in full or sub-size Charpy specimens, in order to produce a large specimen with a phase composition and structure similar to the coarse grained HAZ. This technique has certain important limitations. It is, for example,

difficult to obtain accurate measurements of the thermal cycle of the coarse grained HAZ, which is virtually heated to the solidus temperature. Furthermore, the maximum temperature as well as the subsequent fast cooling rate which are important variables, would be practically impossible to produce experimentally, if the phenomenon of high-temperature embrittlement of the ferrite phase, due to oversaturation with carbon and nitrogen, is considered(3). It is also doubtful whether it is possible to simulate the very fast cooling cycle even in a sub-size Charpy impact specimen and produce a specimen with a homogeneous microstructure and phase composition. Thomas and Apps found that it is generally impossible to match both grain size and hardness to actual weld HAZ structures(7). Even if it was possible to simulate the microstructure in a Charpy impact specimen, the measured toughness is still questionable due to the absence of the constraint associated with the adjacent weld and base metal. It will be shown in this study that the fracture behaviour of the narrow HT HAZ of actual welds is strongly dependent on the cumulative effect of the adjacent weld metal and fine grained HAZ which have totally different mechanical properties and fracture characteristics.

The fusion line fracture behaviour of welds on 14% chromium steel plate was investigated in the present study with particular reference to the following aspects:

a. The development of a new test method for measuring the fracture toughness of the HT HAZ of bead-on-plate welds on 6 mm plate.

b. The influence of factors like phase composition, weld metal mechanical properties and loading rate on the fracture response of the HT HAZ.

c. The relative effects of respectively titanium and vanadium on the fracture toughness of the HT HAZ. The possibility of substituting some of the titanium, which is commonly used as a stabilising element, with vanadium.

d. Interpretation of experimental results with flow stress-fracture stress theories.

2. EXPERIMENTAL PROCEDURE

2.1 Notch-toughness testing

During the past 30 years various tests have been developed to evaluate the brittle fracture characteristics of welds. Almost all of those tests involve the introduction of a notch and the determination of the ductile to brittle transition temperature. Although each test emphasizes a different feature of the brittle-fracture process, none was found suitable to evaluate the influence of this narrow coarse grained HAZ on the notch-toughness of welds on 6 mm 14% chromium steel plate. Among the various tests proposed, the Charpy test is the most widely used. (The limitations of this test for application to welds on 6 mm plate have already been dealt with in chapter 2).

After various attempts to develop a test method which will yield information on the effect of the HT HAZ on the fracture behaviour of actual welds, the test specimen shown in figure 3.2 was developed. It is a bead-on-plate welded specimen (6 mm x 10 mm x 58 mm) which was machined from 6 mm hot rolled plate on which a single bead was welded perpendicular to the rolling direction. The process variables were designed especially to obtain the excessive large welding bead together with the deep penetration with a fusion line which will ideally be oriented normal to the plate surface (fig. 3.3). Single beads were welded according to the following welding procedure:

Welding process	:	Gas metal-arc (MIG)
Welding wire	:	AISI 316L (1.6 mm dia.)
Shielding gas	:	84% Ar, 13% CO_2 , 3% O_2
Welding position	:	Flat
Current	:	360-380 amps.
Volts	:	20-22
Arc speed	:	93-95 cm/min.
Heat input	:	0.46-0.52 kJ/mm

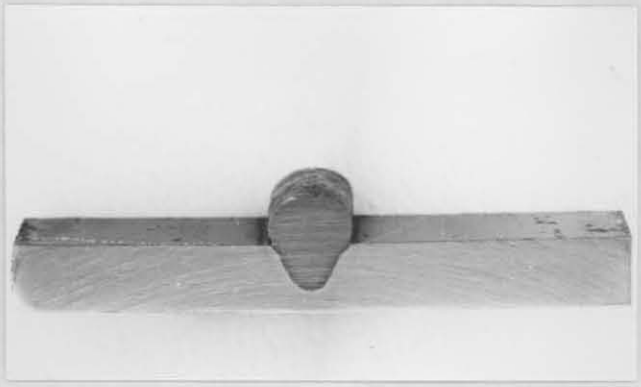

Figure 3.2: Bead-on-plate welded fusion line fracture toughness test specimen (6 mm x 10 mm x 55 mm).

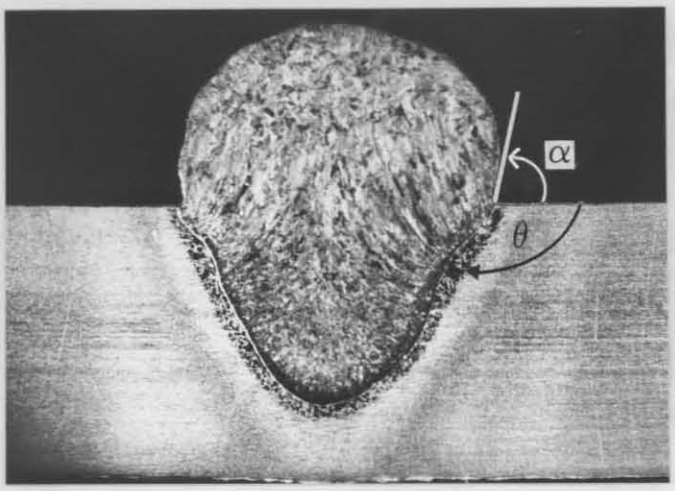

Figure 3.3: Weld bead details of bead-on-plate welded test specimen. Note the coarse grained HT HAZ adjacent to the fusion line.

Some of the details of the weld bead in figure 3.3 are as follows:

Penetration	:	60-65%
Dilution with base metal	:	40-45%
Fusion line orientation (θ)	:	119 - 125° (fig. 3.3)
Included angle (α) between weld bead and plate surface	:	58-62° (fig. 3.3)
Width of HT HAZ	:	0.2-0.3 mm

The welded bead-on-plate test specimens were tested by three-point face-bending at different temperatures to obtain a fusion line fracture appearance transition temperature (FATT). Bend testing was executed at a

punch speed of 133 mm/min., using an anvil with a radius equal to plate thickness. The weld bead which is subjected to tensile bending stresses is located with a transverse orientation in the centre of the bend test specimen.

The tip of the natural notch or stress concentration, which is created by the large welding bead, is located on the fusion line (fig. 3.4). The notch tip radius range from 0.15 mm to 0.25 mm. A triaxial stress field developes during bending at the notch tip due to the constraint produced by the large welding bead and the high strength of the hot rolled base metal. With the development of a triaxial stress field in both the weld metal and fine grained HAZ adjacent to the coarse grained HAZ at the notch tip, the cumulative effect of the fine grained HAZ, coarse grained HT HAZ, and the weld metal, on the fusion line notch fracture initiation and propagation behaviour may be studied.

Fracture of the 14% chromium steel specimens was found to occur only in the HT HAZ and/or weld metal adjacent to the fusion line. The FATT temperature was determined at 50% ductile (microvoid coalesence) fracture surface. The percentage of the fracture surface which failed in a ductile fashion was determined by area analysis of only that part of the fracture surface where the crack propagated in the HT HAZ and/or weld metal adjacent to the fusion line. Partially cracked as well as fractured specimens were also investigated by optical and scanning electron microscope (SEM) analysis in order to determine the crack path.

Figure 3.4: Notch tip on fusion line of bead-on-plate bend specimen. The tip radius ranged from 0.15 mm to 0.25 mm.

Although the test results of this new test method are dependent on such variables as the size of the HT HAZ (heat input), orientation of the fusion line relative to the plate surface, the base metal strength, loading rate and weld metal properties, an indication can be obtained of the performance of actual welds on 14% chromium steels during very severe loading conditions, where a high degree of constraint prevails. The effect of the fusion line orientation on the test results was kept constant by careful selection of only those specimens with fusion line orientations within the specified range.

2.2 Steel compositions and microstructures

Five titanium stabilised and six vanadium stabilised 14% chromium steels were designed in order to obtain different ferrite and martensite contents in the coarse grained HT HAZ. The steels were designed using Kaltenhauser's relation to obtain a large range of ferrite factors(1). (The ferrite factor is a measure of the relative amounts of ferrite and austenite stabilising alloying elements in stainless steel.) The chemical analysis (wt-%) of the experimental steels are shown in table 3.1. The steels were melted in a laboratory induction furnace in an inert gas atmosfere, cast into 5kg ingots and hot rolled into 6 mm thick plate.

Bead-on-plate welded bend test specimens were prepared from the hot rolled plate with a dual phase microstructure which consists of alternatively pancake shaped ferrite and martensite grains. During bending the HT HAZ is subjected to a larger constraint (higher triaxiality) by the relatively high strength hot rolled plate compared to a lower strength hot rolled-and-tempered plate. The microstructure of hot rolled-and-tempered plate consists of recrystallised ferrite and tempered martensite grains.

The ferrite contents of the HT HAZ of bead-on-plate welds on hot rolled 6 mm plate, of the experimental titanium and vanadium stabilised steels, ranged respectively from 4-79% and 17-55% ferrite. The phase composition of the HT HAZ was determined by area analysis on high contrast photographs prepared at a magnification of 150 times (table 3.1).

Table 3.1: Chemical analysis (wt-%) of experimental 14% chromium steels. The hardness (Vickers) of the hot rolled base metal is also indicated.

Steel	C	N	Mn	Cr	Ni	Si	Ti	V	F.F.*	Base metal hardness, HV
A	0.022	0.026	1.06	13.33	2.88	0.36	0.25	-	1.93	335
B	0.026	0.023	1.01	13,53	2.75	0.42	0.20	-	2.67	354
C	0.028	0.025	1.04	13.47	2.58	0.42	0.24	-	3.39	322
D	0.022	0.026	0.90	13.86	2.64	0.41	0.28	-	4.28	327
E	0.024	0.028	0.94	13.87	2.21	0.37	0.32	-	5.85	315
F	0.024	0.026	0.92	13.63	2.36	0.31	-	0.22	3.31	368
G	0.020	0.026	0.93	13.80	2.39	0.31	-	0.34	4.10	363
H	0.021	0.029	0.96	13.88	2.38	0.34	-	0.36	4.68	373
I	0.021	0.026	1.03	13.61	2.10	0.42	-	0.36	5.59	346
J	0.021	0.023	1.00	13.82	2.11	0.48	-	0.37	6.35	345
K	0.025	0.025	0.74	13.99	1.97	0.48	-	0.33	7.16	357

* Ferrite factor according to Kaltenhauser's (1) equation.

$$F.F. = -40\,(C+N) - 2Mn - 4Ni + Cr + 6Si + 8Ti + 2Al + 4Mo + 5V^{x}$$

x A factor of five was assumed for vanadium.

3. EXPERIMENTAL RESULTS AND DISCUSSION

3.1 Fracture behaviour of titanium stabilised steels with respectively 69 and 79% ferrite in the HT HAZ

The two welded titanium stabilised steels with respectively 69% and 79% ferrite in the HT HAZ fractured in a similar manner. Both cleavage and ductile fractures, which occurred respectively at temperatures below and above the FATT temperature, were confined to the HT HAZ. The other three titanium and all the vanadium stabilised steel specimens which contained less than 60% ferrite in the HT HAZ fractured in a different manner.

The fracture surfaces of specimens of steel D with 69% percent ferrite in the HT HAZ together with the FATT curve are shown in figure 3.5. The

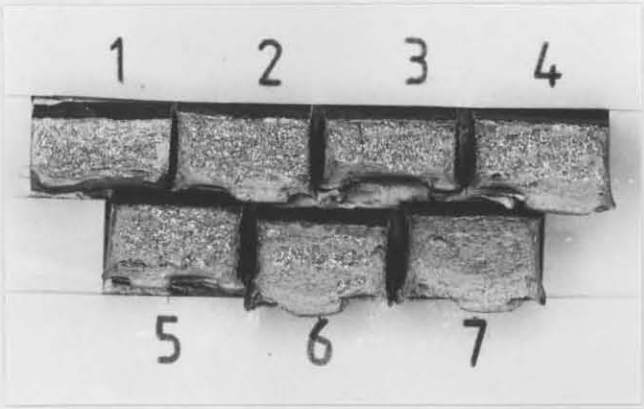

a.

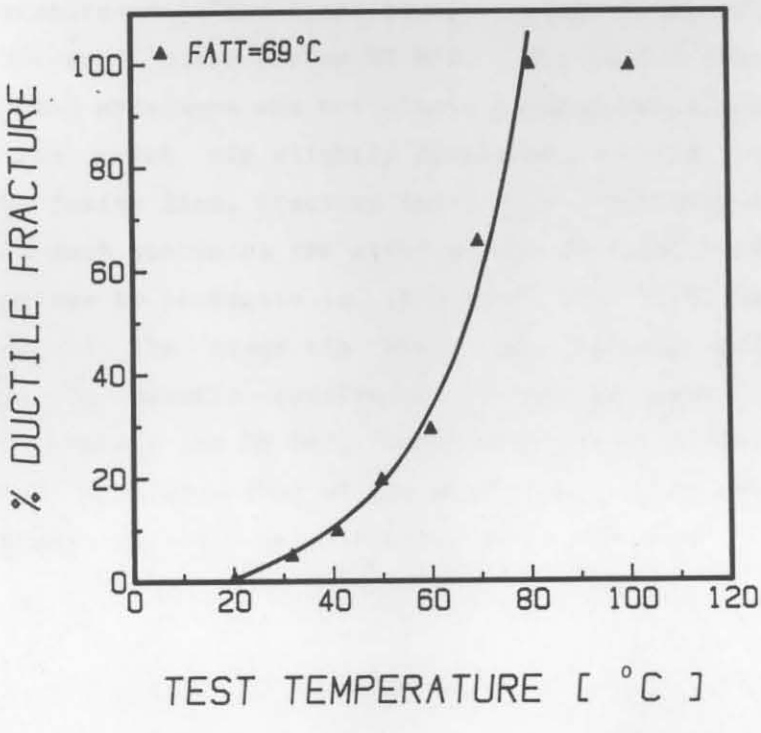

b.

Figure 3.5: a. Fracture surfaces of bead-on-plate bend specimens of steel D with 69% ferrite in the HT HAZ; tested at 1:20°C, 2:30°C, 3:40°C, 4:50°C, 6:70°C and 7:80°C.

b. Fracture appearance transition curve for the HT HAZ of steel D.

fracture path was established on partially cracked specimens. Figure 3.6 shows the crack path of specimens of steel E, with 79% ferrite in the HAZ,

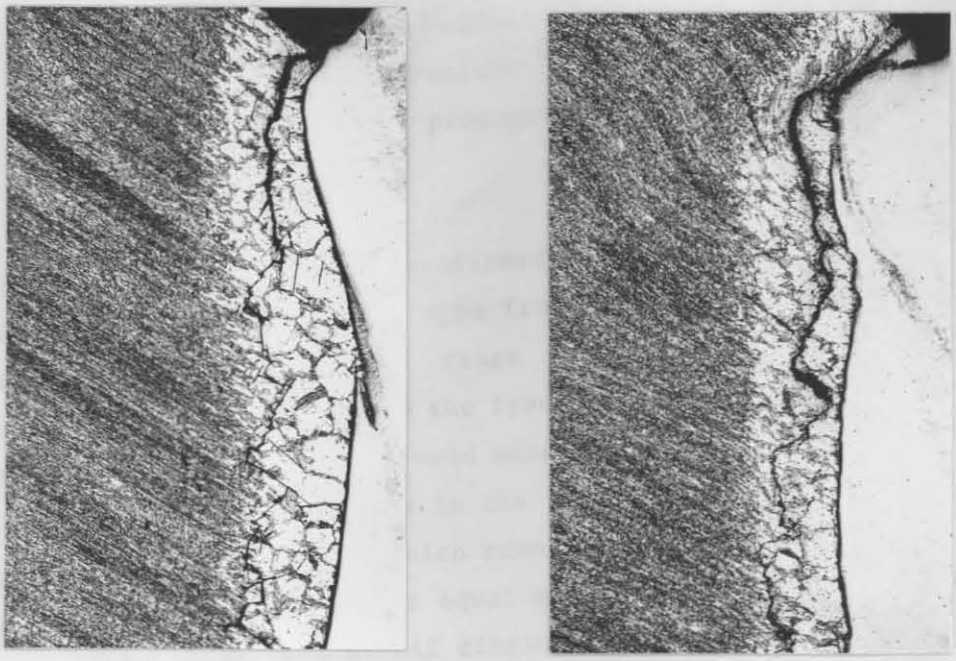

a. b.

Figure 3.6: Cleavage and ductile cracks in the HT HAZ of partially cracked bead-on-plate bend specimens of steel E, with 79% ferrite in the HT HAZ; tested respectively at 20°C (a) and 90°C (b). Magnification 35X. (The deformation which is evident in the specimen tested at 90°C occurred during reverse bending in order to close the ductile crack before polishing).

which were tested at temperatures below (20°C) and above (90°C) the FATT temperature of 74°C, respectively. Both fracture initiation and propagation occurred in the narrow HT HAZ. The fusion line notch tip of some of the bend specimens was not always located exactly on the fusion line. With the notch tip slightly displaced towards the weld metal adjacent to the fusion line, fracture initiation inevitably occurred in the weld metal. In such specimens the crack always deviated immediately to the HT HAZ to continue to propagate in this zone (fig. 3.7). Depending on the distance ahead of the crack tip where the maximum principal stress developes, due to plastic constraint, it can be argued that fracture initiation may occur in the HT HAZ, especially with the fracture stress of the HT HAZ much lower than that of the weld metal, with subsequent crack propagation through the weld metal towards the notch tip.

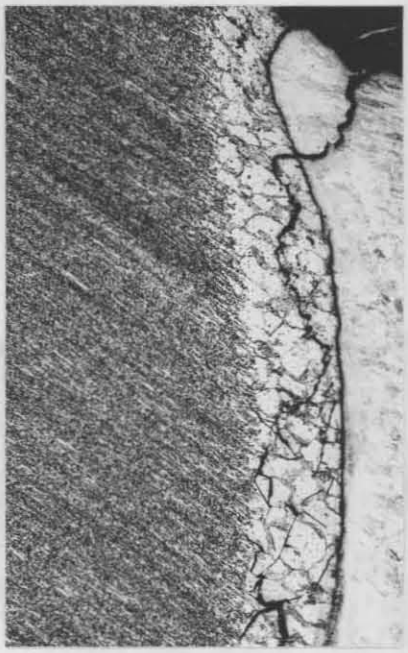

Figure 3.7: Partially cracked bead-on-plate bend specimen of steel D showing ductile fracture initiation in the weld metal and cleavage fracture propagation in the HT HAZ. Specimen tested at 90°C (35X).

The fracture path was also confirmed by SEM analysis of the fracture surfaces. Brittle cleavage type fractures occurred only in the HT HAZ within the test temperature range 0°C to 100°C. Certain distinct differences were observed in the fracture surface appearance of ductile fractures in respectively the weld metal, the coarse grained HT HAZ and the fine grained HAZ. The dimples in the fracture surface of respectively the weld metal and HT HAZ, which resulted from a micro-void coalesence mechanism, are nearly all of equal size, but the weld metal dimples are much smaller than the HT HAZ dimples (fig. 3.8). The ductile fracture surface which resulted from a ductile fracture in the fine grained, low temperature HAZ (the crack left the HT HAZ at the toe of the bead-on-plate weld), contains, however, a combination of relatively small and large dimples (fig. 3.9). It was therefore relatively easy to establish the fracture path by SEM analysis.

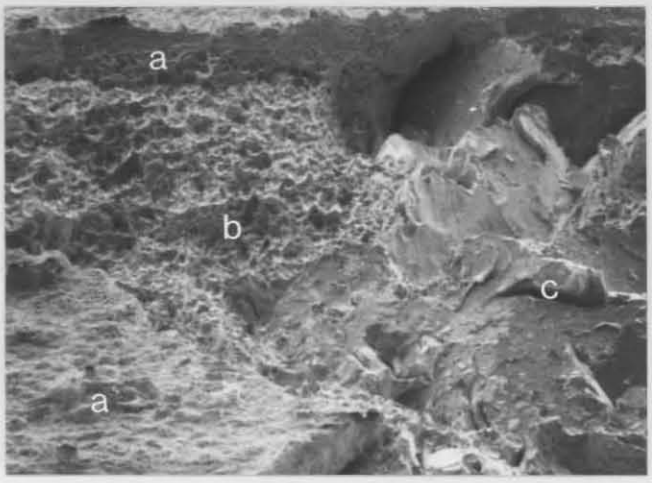

Figure 3.8: SEM fracture surface appearance of a bead-on-plate bent specimen; note ductile fracture in the weld metal (a) adjacent to the fusion line, ductile fracture in the HT HAZ (b) and cleavage fracture in the HT HAZ (c). The large cleavage facets resulted from the large grain size of the HT HAZ (100X).

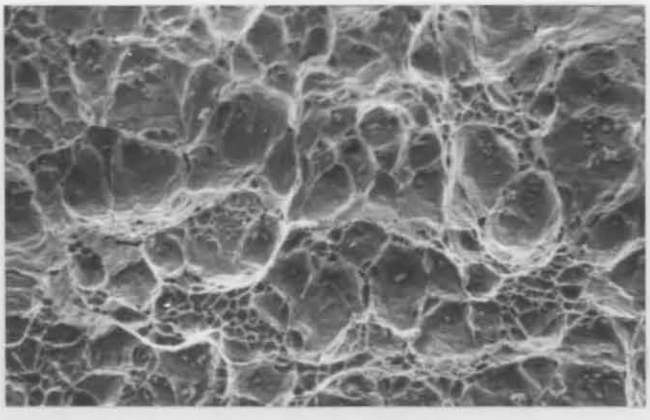

Figure 3.9: SEM fracture surface of a ductile fracture in the fine grained low temperature HAZ (825X).

3.2 Fracture behaviour of titanium and vanadium stabilised steels with less than 60% ferrite in the HT HAZ.

The three titanium and five vanadium stabilised steel bead-on-plate bend specimens with less than 60% ferrite in the HT HAZ fractured in a manner different from the titanium stabilised specimens with more than 60% ferrite in the HT HAZ. Brittle cleavage fracture at temperatures below the FATT and ductile fracture at temperatures above the FATT was confined respectively to the HT HAZ and weld metal adjacent to the fusion line (fig. 3.10). At the FATT temperature a ductile crack initiated in the weld metal and propagated for a certain distance in the weld metal, at a distance of 0.2 to 0.3 mm from the fusion line, before it deviated into the coarse grained HT HAZ to propagate further in a cleavage mode (fig. 3.11).

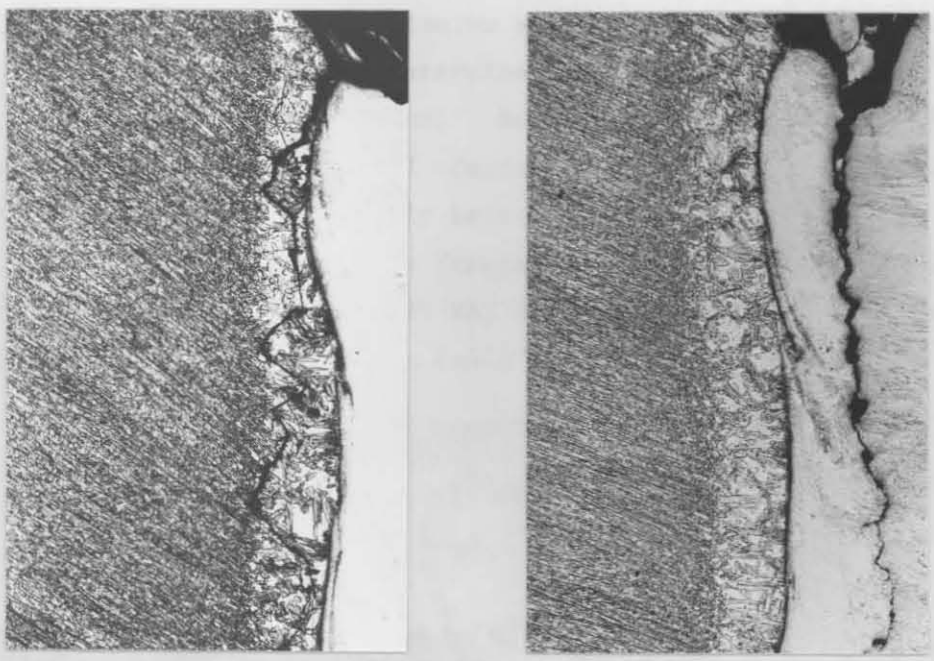

a. b.

Figure 3.10: Crack paths in partially fractured specimens of steel F with 17% ferrite in the HT HAZ (35X).
a. Brittle cleavage fracture in HT HAZ of a specimen tested at 5°C
b. Ductile fracture in weld metal of a specimen tested at 30°C

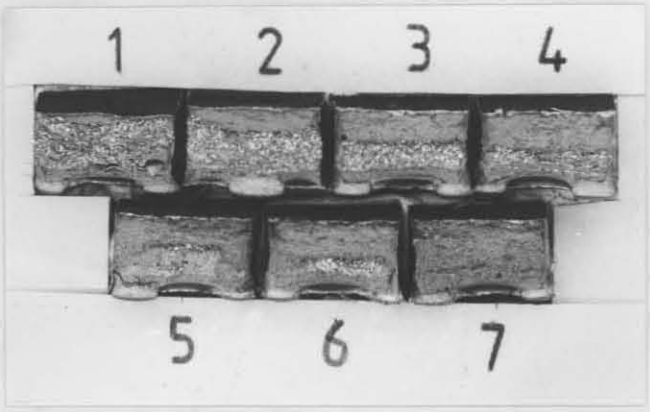

Figure 3.11: Fracture surfaces of bead-on-plate bend specimens of steel G with 24% ferrite in the HT HAZ, tested at: 1:10°C, 2:20°C, 3:32°C, 4:42°C, 5:52°C, 6:62°C and 7:72°C. The dull fracture surface resulted from ductile fracture in the weld metal while the bright fracture surface resulted from brittle cleavage fracture in the HT HAZ.

The phase composition and FATT values of the HT HAZ of the experimental steels in table 3.1 is summarized in table 3.2 and figure 3.12. A relationship was developed to calculate the amount of ferrite contained in the HT HAZ adjacent to the fusion line. The following equation was developed by multilinear regression analysis using the data in tables 3.1 and 3.2.

$$\%\ \text{ferrite in HT HAZ} = -798(\%C) + 4000(\%N) + 32(\%Mn) + 78(\%Cr) - 82(\%Ni) + 184(\%Si) - 180(\%Ti) - 320(\%V) - 777.$$

The FATT of the HT HAZ of the titanium stabilised steels with 69% and 79% ferrite in the HT HAZ, has been determined, since both brittle and cleavage fractures were limited to this zone. However, the FATT of the HT HAZ of the steels with less than 60% ferrite in this zone has not been determined, due to the completely brittle behaviour of this zone at the FATT temperature where 50% ductile fracture was confined exclusively to the weld metal. The FATT of the HT HAZ of these steels will therefore be higher than the values reported in table 3.2 and figure 3.12.

Table 3.2: Phase composition and FATT temperatures of the HT HAZ of bead-on-plate welds on 6 mm hot rolled plate of the steels in table 3.1.

Titanium stabilised 14% chromium steels

	Steel A	Steel B	Steel C	Steel D	Steel E
% Ferrite in HT HAZ	3.5	4	19	69	79
FATT (°C)	20	13	26	67*	74*

*Both ductile and brittle fractures occurred in the HT HAZ while ductile fracture occurred for all the other steels exclusively in the weld metal.

Vanadium stabilised 14% chromium steels

	Steel F	Steel G	Steel H	Steel I	Steel J	Steel K
% Ferrite in HT HAZ	17	24	32	44	48	55
FATT (°C)	13	39	37	40	56	60

Figure 3.12 shows a decrease in the FATT of the HT HAZ of both titanium and vanadium stabilised steels with a decrease in ferrite content. However, it is not possible at this stage to come to any conclusions as far as the relative effects of titanium and vanadium on the toughness of the HT HAZ are since the FATT of the HT HAZ of most of the steels have not yet been determined. The FATT values of the HT HAZ of the vanadium steels are expected to be higher than that of the titanium steels due to the lower stability of the vanadium carbonitrides and therefore higher total dissolved carbon and nitrogen contents.

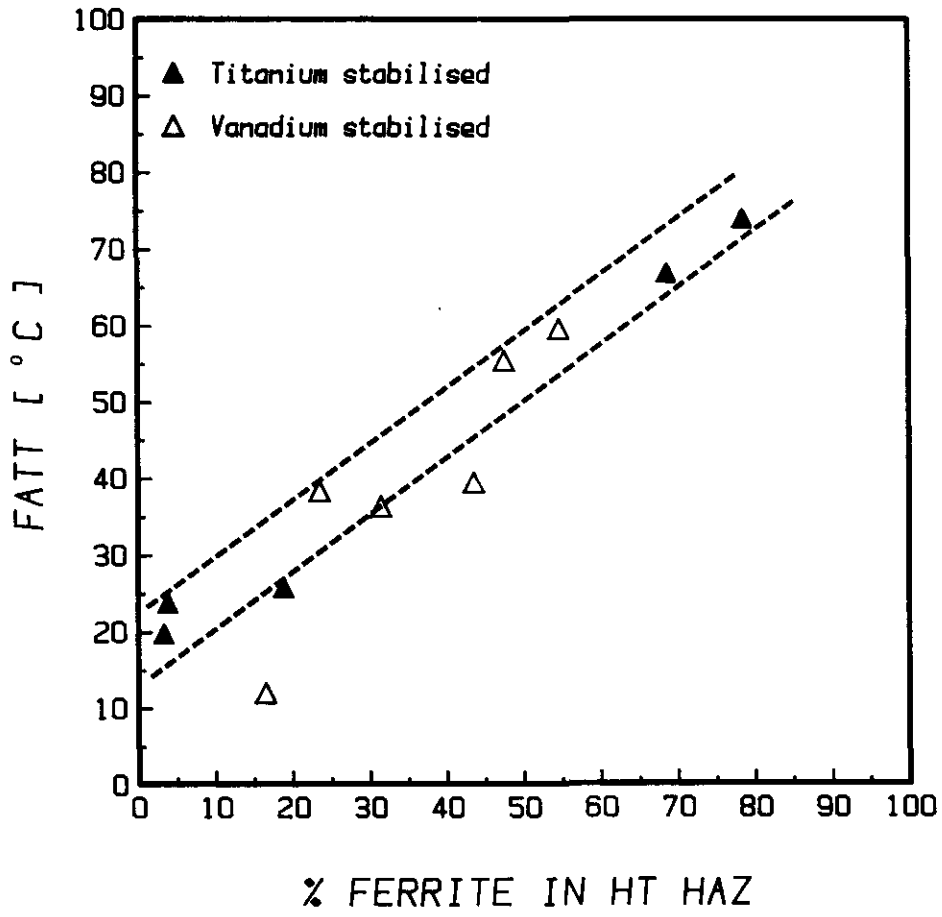

Figure 3.12: FATT temperature versus phase composition of the coarse grained HT HAZ of 14% chromium steels, stabilised respectively with titanium and vanadium.

3.3 The effect of loading rate and weld metal properties on the fusion line fracture behaviour of steels with less than 60% ferrite in the HT HAZ

The FATT temperatures of the HT HAZ of both the vanadium and titanium stabilised steels with less than 60% ferrite in the HT HAZ have not been determined yet since the fusion line fracture toughness, of welds on these steels, are artificially enhanced by the ductile property of the austenitic AISI 316L weld metal. The FATT temperature of the HT HAZ are therefore determined not only by the properties and size of this zone, but also by the mechanical properties and fracture toughness of the weld metal. Furthermore, since the yield strength of body-centered cubic metals (such as the HT HAZ) is far more sensitive to temperature and strain rate

changes, than it is in face-centered cubic metals (such as the austenitic weld metal), it was thought that the FATT temperature of the HT HAZ of steels with less than 60% ferrite in this zone might be sensitive to strain rate changes. This strain rate sensitivity in BCC metals may be related to the temperature-sensitive Peierls-Nabarro stress contribution to the yield strength, which is much larger in BCC metals than in FCC metals.

3.3.1 Loading rate or punch speed

The FATT temperatures in table 3.2 and figure 3.12 were determined at a loading rate or punch speed during bend testing of 133 mm/min. The FATT temperature of the HT HAZ of steel J with 48% ferrite in this zone increased from 56°C to 76°C with a decrease in punch speed from 133 mm/min. to 4 mm/min. (fig. 3.13). The FATT temperature of a homogeneous material is generally not sensitive to loading rate variations within this range. Even at this new FATT temperature of 76°C, the 50% ductile fracture surface resulted from ductile fracture in the weld metal with a completely cleavage fracture in the HT HAZ. The FATT of the HT HAZ is therefore even higher than 76°C.

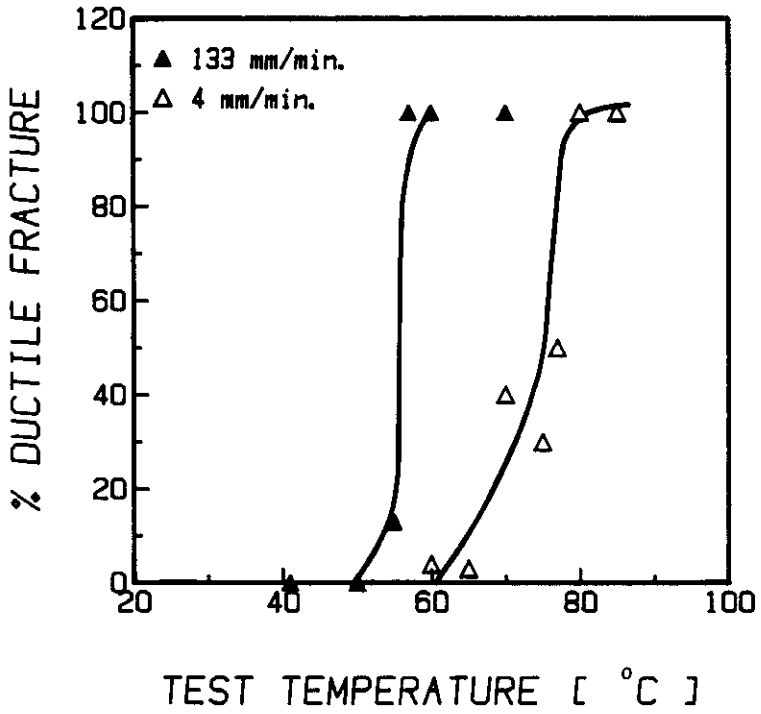

Figure 3.13: Fracture appearance transition curves for steel J with 48% ferrite in the HT HAZ determined at two punch speeds of respectively 133 mm/min. and 4 mm/min..

The FATT temperature of the titanium stabilised steel with 79% ferrite in the HT HAZ, determined at a punch speed of 133 mm/min., is 74°C (table 3.2). With the FATT of the HT HAZ of the vanadium stabilised steel with only 48% ferrite in this zone much higher than 76°C, it is clear that the FATT of this zone of a vanadium stabilised steel, with 79% ferrite in this zone, will be much higher (as expected) than that of a titanium stabilised steel. It may therefore be concluded that the FATT temperature of the HT HAZ of the vanadium stabilised steels will be higher than that of the titanium stabilised steels for any ferrite content in this zone although this is not suggested by the results in figure 3.12.

The effect of punch speed, within the range 2 mm/min. to 240 mm/min., on the FATT temperatures of the HT HAZ of steels A (3CR14Ti), C (3CR14Ti) and J (3CR14V) with respectively 3.5%, 19% and 48% ferrite in the HT HAZ, is summarized in figure 3.14. The FATT temperature were unchanged at punch speeds above about 133 mm/min., but increased considerably at punch speeds below 133 mm/min. The FATT temperatures of specimens tested by impact loading in a Charpy impact machine are very similar to the temperatures obtained in slow, three point bend testing at a punch speed of 133 mm/min. An increase of about 20°C was observed for steels C and J with a decrease in punch speed from 133 mm/min. to 7 mm/min.. These much higher FATT temperatures obtained at such extremely low punch speeds are not yet the true FATT temperatures of the HT HAZ. The HT HAZ still fractured in a completely brittle cleavage manner at the FATT temperature with ductile fracture in the weld metal adjacent to the fusion line.

It may be concluded at this stage that the HT HAZ FATT temperature of 14% chromium steels with less than 60% ferrite in the HT HAZ depends not only on the phase composition of this zone and the fusion line orientation relative to the plate surface but that it also depends on the punch speed during bend testing. The effect of fusion line orientation was controlled by careful selection of those specimens with a fusion line orientation within the specified range of 122 $\pm$ 3 degrees. The FATT of the HT HAZ of steels with more than 60% ferrite in this zone was not effected by the punch speed within the range 2 mm/min. to 400 mm/min.

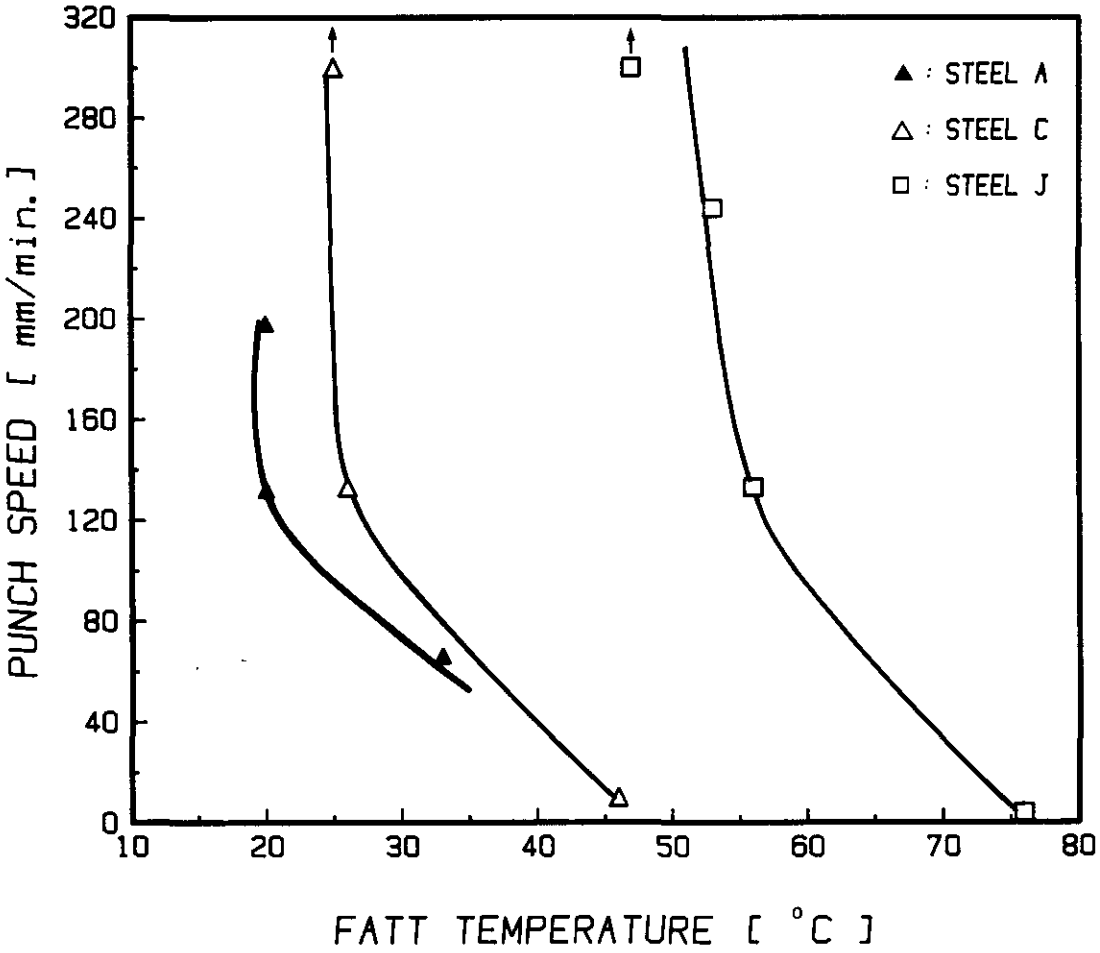

Figure 3.14: Punch speed for bend testing versus the FATT temperature of the HT HAZ of steels A, C and J with respectively 3.5%, 19% and 48% ferrite in the HT HAZ. The FATT temperatures indicated at a punch speed of 300 mm/min. were determined by impact loading of the specimens in a Charpy impact machine.

3.3.2 Weld metal properties

Another important aspect which has not yet been dealt with is the effect of the weld metal mechanical properties, i.e. yield strength, tensile and fracture stress, and the work hardening rate on the FATT of the HT HAZ of welds with less than 60% ferrite in the HT HAZ. According to Davidenkov's flow stress-fracture stress theory, the FATT temperature may be increased by increased weld metal strength properties relative to that of the HT HAZ. With the strength properties of the weld metal, especially the fracture stress (the fracture stress of the weld metal adjacent to the fusion line

is inter alia determined by the degree of constraint or stress triaxiality) much higher than that of the HT HAZ, within the temperature range 0°C to 100°C, it will be possible to determine the true FATT (with both cleavage and brittle fractures confined to the HT HAZ) of the HT HAZ.

The microhardness transverse across the fusion line of bead-on-plate AISI 316L welds on 6 mm hot rolled plate of steels E (3CR14 Ti) and G (3CR14V) with respectively 79% and 24% ferrite in the HT HAZ is shown in figure 3.15. The indicated hardness of the HT HAZ is the weighed average hardness of the martensite and ferrite in the HT HAZ. Both brittle and cleavage

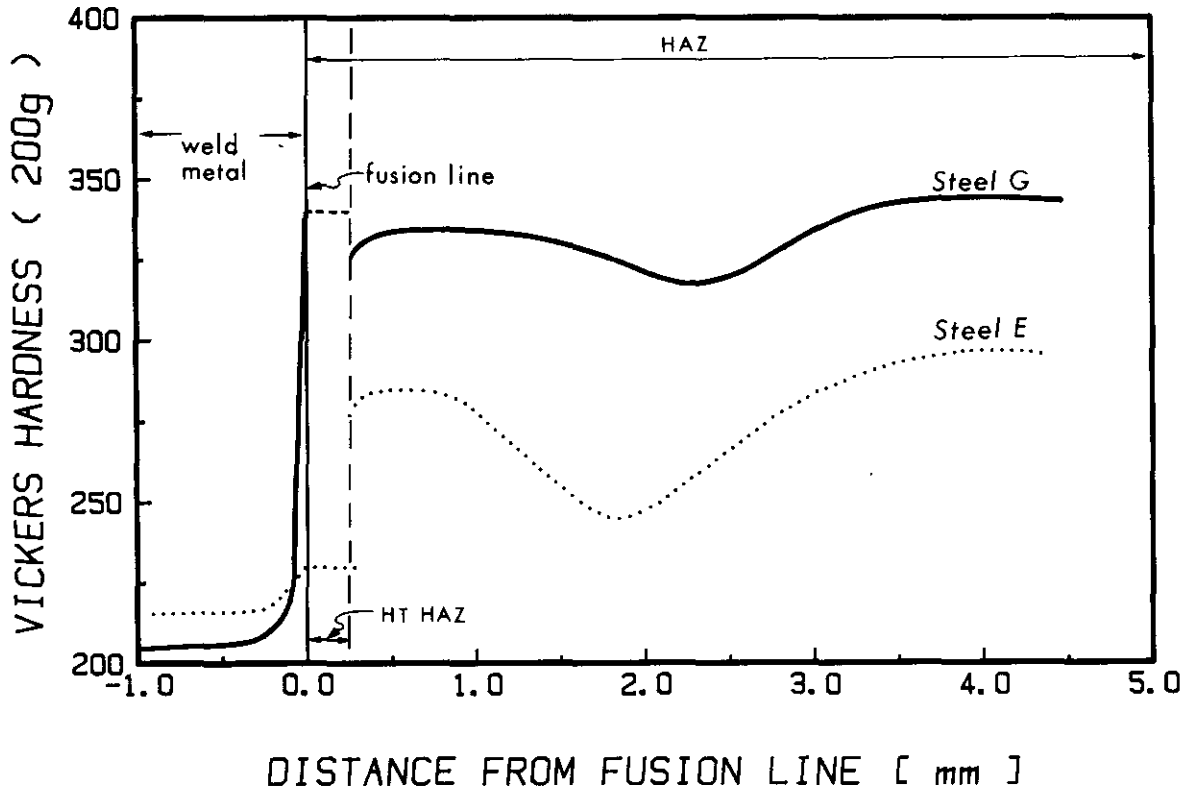

Figure 3.15: Microhardness transverse across the fusion line of bead-on-plate welds on 6 mm hot rolled plate of steel E and G with respectively 79% and 24% ferrite in the HT HAZ.

fractures occurred during bend testing in the HT HAZ of steel E due to the lower fracture stress of this zone compared to that of the adjacent weld metal and fine grained HAZ. The lower fracture stress may be attributed to the much larger grain size (ASTM No 1-2), the high ferrite content and the

higher work hardening rate of the austenitic weld metal. The hardness of this zone is also much lower than that of the adjacent fine grained HAZ and nearly equal to that of the weld metal (fig. 3.15).

At temperatures above the FATT temperatures of the HT HAZ of steels with less than 60% ferrite in this zone, ductile fractures occurred in the weld metal due to the higher fracture stress of the HT HAZ. The hardness of, e.g., the HT HAZ of steel G in figure 3.15 is much higher that that of the weld metal due to the presence of 76% martensite in this zone. The higher fracture stress of the HT HAZ, even with the much higher work hardening rate of the austenitic weld metal may therefore be attributed to the higher tensile strength (which is proportional to the hardness) and finer grain size compared to a zone with 79% ferrite.

In paragraph 3.1 it was specified that the bead-on-plate bend specimens were welded within the heat input range of 0.46 kJ/mm to 0.52 kJ/mm. Most specimens were welded at the lower end of this range. To study the effect of the weld metal mechanical properties on the FATT or fracture behaviour of the HT HAZ, an additional series of specimens of steels B, H and J were prepared by welding at the higher end of the heat input range in order to obtain a slightly higher dilution with the base metal, with improved weld metal strength properties.

The results which are summarized in table 3.3 show that the FATT temperature of the HT HAZ increased with a slight increase in weld metal hardness and therefore fracture stress. Figure 3.16 shows both effects of the weld metal strength and punch speed on the FATT of the HT HAZ of steel B with 96% martensite in this zone. This effect of the weld metal hardness seems to decrease with a decrease of punch speed from 133 mm/min. to 10 mm/min.

Table 3.3: FATT temperatures of the HT HAZ of steels B, H and J versus weld metal hardness. These values were determined at a punch speed of 133 mm/min.

Steel	Weld metal hardness (HV, 62.5kg)	FATT of HT HAZ (°C)
B	164	13
(4% ferrite in HT HAZ)	183	24
H	192	37
(32% ferrite in HT HAZ)	189	37
J	164	41
(48% ferrite in HT HAZ)	184	56

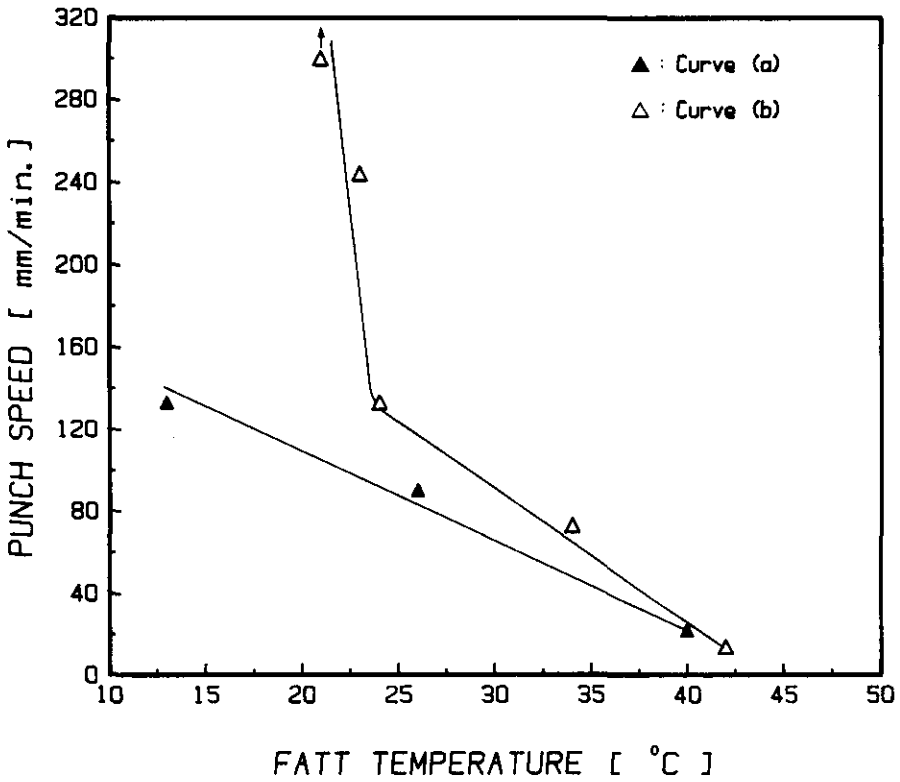

Figure 3.16: Punch speed for bend testing versus the FATT temperature of the HT HAZ of steel B.
Curve a: Weld metal hardness, 164 HV
Curve b: Weld metal hardness, 183 HV
(A FATT temperature of 21°C was obtained with impact loading in a Charpy impact machine)

4. DISCUSSION

The effects of the phase composition of the HT HAZ, of punch speed during bend testing, and of the weld metal mechanical properties on the fusion line fracture behaviour of bead-on-plate welds on 6 mm hot rolled 14% chromium steel plate may be explained by both Cottrell's and Davidenkov's flow stress-fracture stress theories.

In order to explain the experimental results by means of these theories the following assumptions have to be made:

a. The material at the notch tip (fig. 3.4) of a bead-on-plate bend specimen is modelled as a composite material consisting of the HT HAZ, the adjacent weld metal and fine grained HAZ.

b. The existance of a isostress field at the notch tip in the above-mentioned materials. The composite specimen at the notch tip is therefore assumed to be a series tensile specimen (fig. 3.17) with the composite materials in the specimen subjected to the same stress during bend testing or tensile loading.

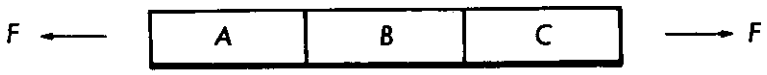

Figure 3.17: Series tensile composite specimen. The specimen consists of three different materials A, B and C.

4.1 Explanation of experimental results by means of the Cottrell-Petch fracture theory.

The Cottrell-Petch theory was discussed in detail in Chapter 2. Although this theory was originally developed for explaining only the ductile-brittle fracture mode transition in homogeneous materials, with decreasing temperature, grain size and loading rate, it may also be used to explain the fracture mode transition behaviour of a composite specimen, by superimposing the fracture stress and yield stress curves of the different

composite materials on the same figure. Since fracture was limited only to the weld metal adjacent to the fusion line and the HT HAZ of the 14% chromium steels in table 3.1, the curves for only the weld metal and HT HAZ of steel B, with 96% martensite in the HT HAZ, are superimposed on figure 3.18.

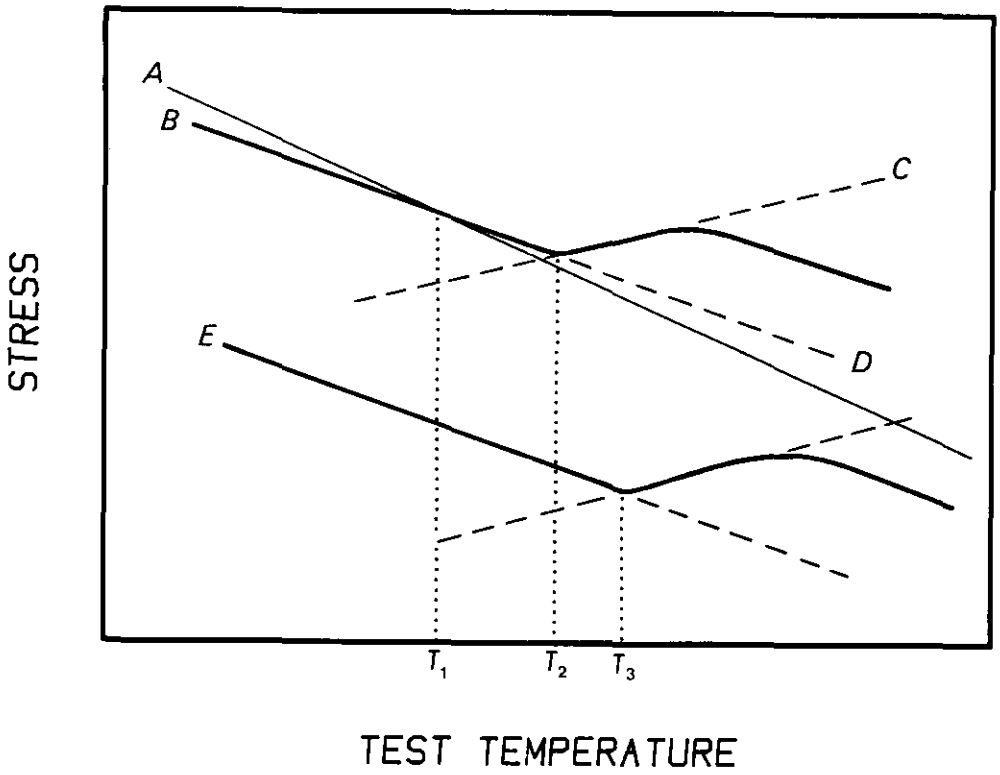

Figure 3.18: Fracture stress curves of the austenitic weld metal (A) and HT HAZ (B) of steel B with 96% martensite in the HT HAZ. The dotted curves C and D are respectively the theorectical fracture stress (σ_f according to Cottrell et al.) and yield stress (σ_{ys} according to Hall and Petch) curves of the HT HAZ. Curve E is the fracture stress curve for the HT HAZ of steel E with 79% ferrite in this zone.

Consider now only the fracture stress curve B for the HT HAZ. T_2 is then the true FATT temperature of this zone. At temperatures below and above T_2 the HT HAZ will fracture by respectively cleavage and ductile fracture at the fracture stresses indicated by curve B.

Only the ductile fracture stress curve A of the austenitic weld metal is indicated in figure 3.18 due to the fact that the FATT temperature of the

weld metal is much lower than that of the HT HAZ. The weld metal fracture stress curve A has a larger slope compared to the HT HAZ fracture stress curve B. This larger slope of curve A is derived from the fact that brittle cleavage fractures occurred in the HT HAZ at temperatures below the FATT temperature (lower HT HAZ fracture stress compared to the weld metal) while ductile fracture occurred in the weld metal adjacent to the fusion line at temperatures above the FATT temperature (lower weld metal fracture stress compared to HT HAZ).

The FATT temperature T_1 (fig. 3.18), which will be obtained for the composite specimen (this temperature is 13°C for steel B), is lower than the true FATT temperature T_2 for the HT HAZ.

The increase in the FATT temperature of the HT HAZ of e.g., steel B, from 13°C to 40°C (fig. 3.16) with a decrease in punch speed below 133 mm/min. may be explained as follows. With the much higher strain rate sensitivity of the yield strength and therefore the fracture strength of the BCC HT HAZ compared to the strain rate sensitivity of the FCC weld metal, the nett effect of a lower punch speed will be a displacement of the fracture stress curve B of the HT HAZ to lower stresses with the resultant intersection of curves A and B at the new FATT temperature which is higher than T_1 (fig. 3.18).

The increase in the FATT temperature of the HT HAZ of steel B from 13°C to 24°C with an increase in weld metal hardness from 164HV to 183HV may also be explained in a similar manner (table 3.3 and fig. 3.16). The fracture stress curve A of the weld metal in figure 3.18 is shifted to higher stresses with an increase in weld metal hardness with the intersection between curves A and B shifted to a higher FATT temperature.

Curve E in figure 3.18 represents the fracture stress curve for the HT HAZ of steel E with 79% ferrite in the HT HAZ. This curve is located at much lower stresses compared to curve B. This is due to the much larger grain size and lower martensite content of this zone compared to a zone with 96% martensite. The true FATT temperature T_3 of the HT HAZ with 79% ferrite may therefore be obtained since both the brittle and ductile fracture stresses are lower than the ductile fracture stress of the weld metal. Although curves B and E have the same slope, the slope of curve E may

actually be larger due to the larger grain size and smaller martensite content of the HT HAZ with 79% ferrite.

4.2 Explanation of experimental results by means of Davidenkov-Ludwik fracture theory

Although the Davidenkov-Ludwik fracture theory, which was discussed in chapter 2, was also originally developed for explaining the fracture mode transitional behaviour of notched tensile specimens, it may also be used to study the fracture behaviour of a series type composite specimen by superimposing the cleavage fracture stress, ductile fracture stress and flow stress curves of the different composite materials on the same figure.

Figure 3.19 shows such a superposition of the cleavage fracture- (curve A), ductile fracture- (curve B) and flow stress (curve D) curves of the HT HAZ of steel B with 96% martensite in this zone together with the ductile fracture- and flow stress curves of the weld metal. This figure applies to a test temperature of 13°C which is the FATT temperature of the HT HAZ of steel B at a punch speed of 133 mm/min. The curves in this figure therefore portrays the true stress-strain conditions at the notch tip of a bead-on-plate bend specimen which is being bent at a punch speed of 133 mm/min.

Consider now only the HT HAZ (curve D) and weld metal (curve E) flow stress curves. The yield strength of the HT HAZ at zero strain is much higher than that of the weld metal due to the high martensite content of this zone (fig. 3.15). The larger slope of curve E is due to the higher work hardening rate of the FCC austenitic weld metal.

Fracture will occur in the weld metal and/or HT HAZ when the flow stress curves intersect the fracture stress curves at $(\bar{\sigma}_2, \bar{\varepsilon}_2)$ and $(\bar{\sigma}_3\ \bar{\varepsilon}_3)$. With the present relative orientations of the curves in figure 3.19, the ductile weld metal fracture stress $\bar{\sigma}_2$ is less than the cleavage fracture stress $\bar{\sigma}_3$ of the HT HAZ. A ductile fracture will therefore initiate in the weld metal adjacent to the fusion line during bend testing. As the ductile crack propagates in the weld metal adjacent to the fusion line (it was found to propagate at a distance of 0.2-0.3 mm from the fusion line) the HT HAZ is subjected to increasingly higher stresses due to the

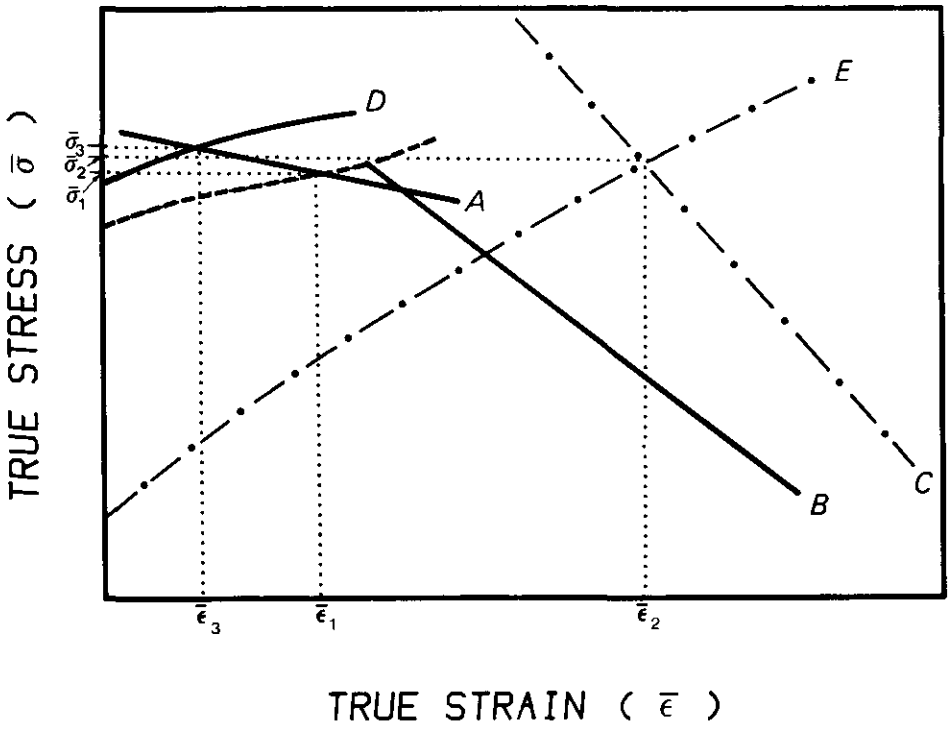

Figure 3.19: Fracture stress and flow stress curves for the weld metal and HT HAZ of steel B with 96% martensite in the HT HAZ. The curves describe the true stress-strain conditions at the notch tip of a bead-on-plate bend specimen which is being tested at 13°C at a punch speed of 133 mm/min.
Curve A : Cleavage fracture stress for the HT HAZ
Curve B : Ductile fracture stress for the HT HAZ
Curve C : Ductile fracture stress for the 316L weld metal
Curve D : Flow stress curve for the HT HAZ
Curve E : Flow stress curve for the 316L weld metal

fact that the fusion line is not oriented normal to the plate surface. The isostress conditions which were assumed originally are actually only valid as far as the fusion line notch tip fracture behaviour is concerned. Cleavage fracture initiation may therefore occur in the HT HAZ, after a ductile crack has propagated for a certain distance in the weld metal, when the cleavage fracture stress $\bar{\sigma}_3$ of this zone is exceeded. Bead-

on-plate bend specimens of steel B fractured in this manner at a FATT temperature of 13°C.

When the abovementioned bend specimens were tested at a lower punch speed of 10 mm/min., a cleavage crack initiated and propagated in the HT HAZ. This fracture made transition may be explained by the much higher strain rate sensitivity of the BCC HT HAZ. The nett effect of the lower punch speed is therefore a displacement of the flow stress and fracture stress curves of the HT HAZ to lower stresses relative to the curves for the weld metal. This displacement may be simplified by a shift of curve D to lower stress (dotted curve in fig. 3.19) with the cleavage fracture stress $\bar{\sigma}_1$, of the HT HAZ now lower than the ductile fracture stress $\bar{\sigma}_2$ of the weld metal. HT HAZ cleavage fracture initiation may also be caused by an increase of the weld metal strength and therefore an increase in weld metal fracture stress.

The notch tip true stress-strain conditions at the FATT temperature of 74°C for the HT HAZ of a bend-on-plate bend specimen of steel E with 79% ferrite in the HT HAZ is portrayed by the fracture and flow stress curves in figure 3.20.

The flow stress and fracture stress curves for the HT HAZ of steel E in figure 3.20 are located at lower stresses compared to the respective curves (dotted curves) for this zone with 96% martensite (fig. 3.19). This is due to the larger grain size and lower martensite content (fig. 3.1). Cleavage and ductile fractures will occur in the HT HAZ at stresses which are represented by the intersection of curve D with respectively curves A and B. A ductile weld metal fracture will occur at the intersection of curves E and C. Since the ductile fracture stress of the weld metal $\bar{\sigma}_1$ is much higher than both the cleavage and ductile fracture stresses of the HT HAZ, the true FATT temperature of the HT HAZ may therefore be determined. At temperatures lower than 74°C, curves A, B and D are shifted to higher stresses relative to curves C and E with the flow stress curve D intersecting the cleavage fracture stress curve A; a cleavage fracture will occur therefore in the HT HAZ. At temperatures above 74°C, curves A, B and D will be shifted to lower stresses relative to curves C and E with the flow stress curve D intersecting the ductile fracture stress curve B; a ductile fracture will occur therefore in the HT HAZ.

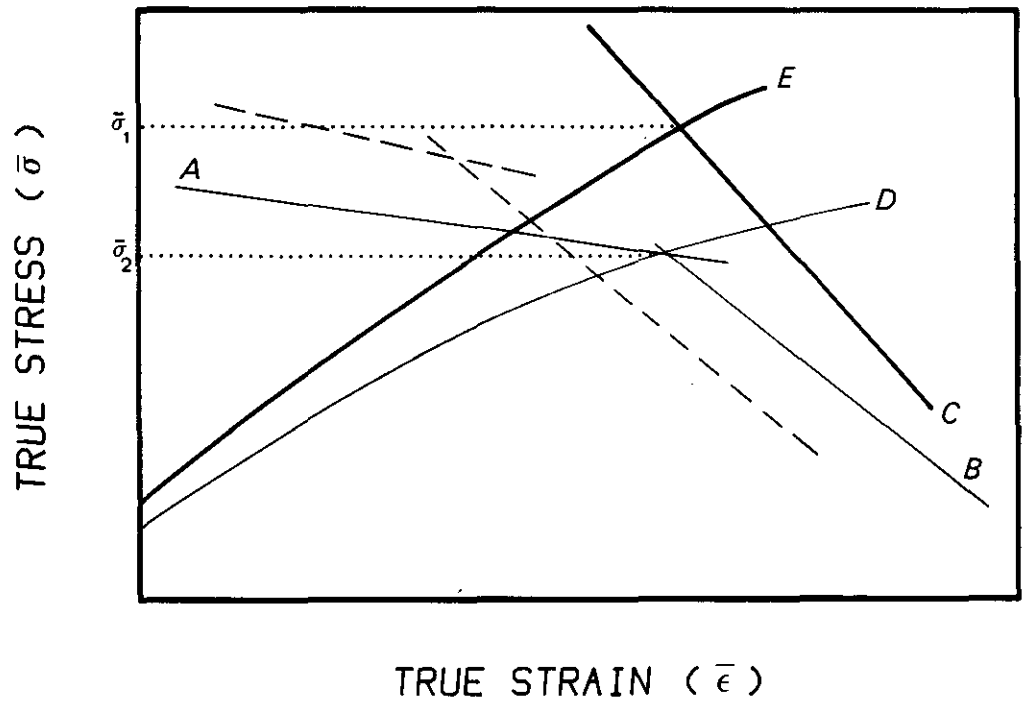

Figure 3.20: Fracture stress and flow stress curves for the weld metal and HT HAZ of steel E with 79% ferrite in the HT HAZ. The curves describe the true stress-strain conditions at the notch tip of a bead-on-plate bend specimen which is being tested at 74°C at a punch speed of 133 mm/min.
Curve A : Cleavage fracture stress for the HT HAZ
Curve B : Ductile fracture stress for the HT HAZ
Curve C : Ductile fracture stress for the 316L weld metal
Curve D : Flow stress curve for the HT HAZ
Curve E : Flow stress curve for the 316L weld metal
The dotted curves are the cleavage and ductile fracture stress curves for a HT HAZ with 96% martensite in this zone (fig. 3.19).

The fact that fracture was limited to only the weld metal adjacent to the fusion line and the HT HAZ, implies that both the cleavage and ductile fracture stresses of the fine grained HAZ are much higher than the corresponding stresses of both the weld metal and HT HAZ even with 96% martensite in the HT HAZ.

With reference to the explanations for the fusion line fracture behaviour of bead-on-plate AISI 316L welds on 6 mm hot rolled 14% chromium steel

plate in terms of Cottrell's and Davidenkov's flow stress-fracture stress theories, it may be concluded that the fusion line fracture behaviour is determined by the following factors:

a. Relative weld metal and HT HAZ mechanical properties: yield strength, work hardening rate, cleavage and ductile fracture stresses.

b. Relative strain rate sensitivities of the yield and fracture strength of the weld metal and HT HAZ.

c. Mechanical properties of the fine grained HAZ and base metal.

d. Fusion line orientation relative to the plate surface.

4.3 High temperature HAZ fracture toughness

The HT HAZ FATT temperatures which were obtained at punch speeds of respectively 10 mm/min. and 133 mm/min. for the 14% chromium steels in table 3.1 are summarized in figure 3.21. Superimposed on this figure are suggested curves for the minimum FATT temperatures of the HT HAZ (for a punch speed of 10 mm/min) for, respectively, the titanium and vanadium stabilised steels.

Curve B shows that the FATT temperatures of the HT HAZ of the titanium stabilised steels decreased by less than 32°C (from 74°C to 42°C) by an increase in the martensite content from 21% to 96% in the HT HAZ. These very high FATT temperatures of the HT HAZ, which are expected to be higher with impact loading, indicates that the fracture toughness of the HT HAZ of welds on 6 mm hot rolled 14% chromium steel plate is relatively low. Furthermore, the fact that the fracture toughness of this HT HAZ is not improved significantly by large fractions low carbon, titanium stabilised, grain boundary martensite, indicates that the fracture toughness is determined by another important factor or phenomenon which has not yet been identified. There is therefore no sense in substituting some of the titanium in the steel with vanadium as stabilising element, in order to limit the amount of coarse segregated titanium carbonitrides at the plate centre, since even the fracture toughness of the HT HAZ of steels stabilised with titanium only is unacceptably low.

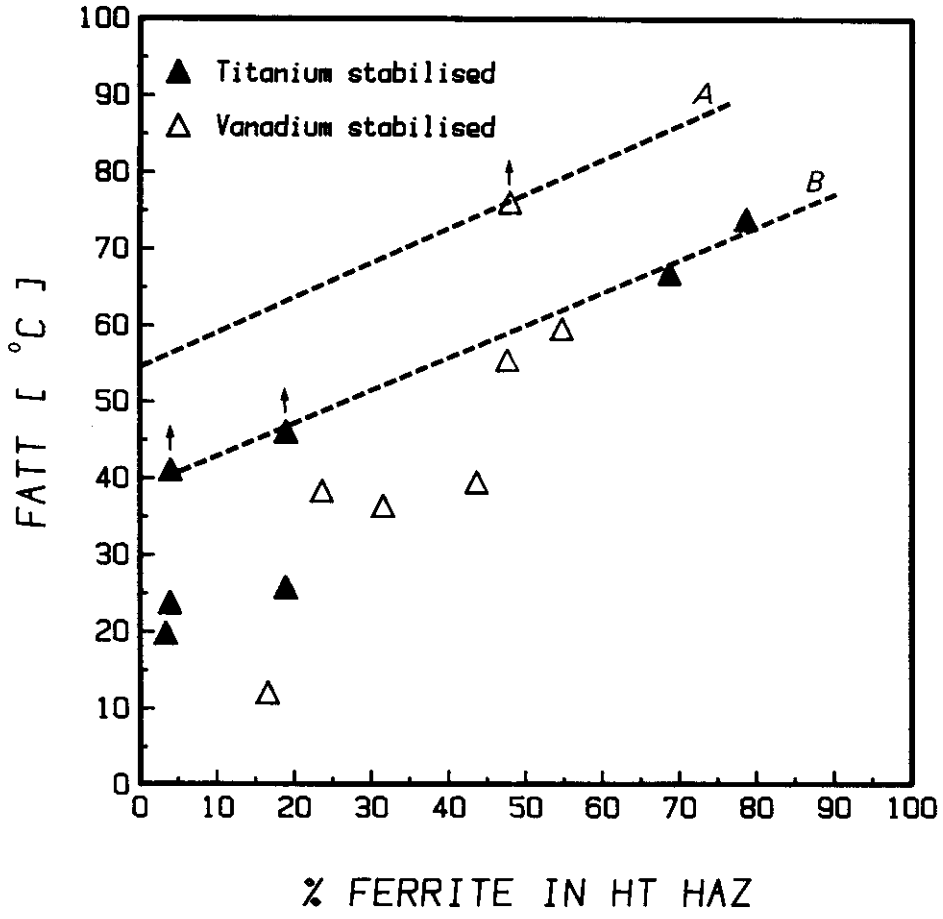

Figure 3.21: FATT temperature versus the ferrite content of the HT HAZ of bead-on-plate 316L welds on 6 mm hot rolled 14% chromium steel plate. The values indicated by arrows were obtained at a punch speed of 10 mm/min. with the other values obtained at a punch speed of 133 mm/min. (The fusion line orientation relative to the plate surface of the bead-on-plate specimens ranged from 120° to 124°)

Curve A: Minimum suggested FATT temperatures for the HT HAZ of vanadium stabilised 14% chromium steels

Curve B: Minimum suggested FATT temperatures for the HT HAZ of titanium stabilised 14% chromium steels

It may therefore be concluded that although the new notch-toughness test has certain practical limitations, valuable information has been obtained on the influence of the narrow coarse grained HT HAZ on the notch-toughness of welds on 6 mm 14% chromium steel plate. Due to the low fracture toughness of the HT HAZ, 14% chromium steel plate is not recommended for any structural applications. Brittle fracture may occur in welded

structures, especially in the as-welded condition, when high tensile residual stresses are present together with inevitable fusion line defects such as undercutting, lack of side-wall fusion, incomplete penetration and slag inclusions. In critrical applications, when a triaxial stress state develops in weld configurations offering a high degree of constraint the material is particulary susceptable to brittle fracture.

5. SUMMARY

a. A new test method has been developed which gives a reasonable indication of the influence of the narrow, coarse grained high temperature weld HAZ on the fusion line notch-toughness of bead-on-plate AISI 316L welds on respectively 6 mm hot rolled titanium and vanadium stabilised 14% chromium steels.

b. The FATT temperature of the HT HAZ of steels, with less than 60 percent ferrite in the HT HAZ, increased with decreasing punch speeds (during slow three point bend testing) below 133 mm/min. This phenomenon is explained in terms of Cottrell's and Davidenkov's fracture theories and the relative strain rate sensitivities of the yield and fracture strengths of the FCC austenitic weld metal and BCC HT HAZ.

c. The FATT temperatures increased with higher weld metal mechanical properties.

d. The actual or true FATT temperatures of the HT HAZ, for slow bend testing, of the two titanium stabilised steels with 69% and 79% ferrite in the HT HAZ, is 67°C and 74°C, respectively. The actual HT HAZ FATT temperatures of both the titanium and vanadium stabilised steels with less than 60% ferrite in the HT HAZ, are higher than the reported values. This is due to the fact that the fusion line notch-toughness of welds is enhanced by the ductile properties of the austenitic weld metal.

e. The HT HAZ FATT temperatures of the titanium stabilised steels are reduced by less than 32°C, during slow bend testing, as a result of an increase in martensite content from 21% to 96%. The HT

HAZ FATT temperatures of the vanadium stabilised steels are higher than that for the titanium stabilised steels.

f. It is concluded that the HT HAZ fracture toughness of 14% chromium steels is relatively low, even with high percentages of low carbon martensite.

CHAPTER 4

THE NOTCH-TOUGHNESS OF WELDED 3CR12 AND 3CR12Ni

SYNOPSIS

The newly developed bead-on-plate bend test was used to determine the influence of the narrow, coarse grained, high temperature weld heat affected zone (HT HAZ) on the fusion line fracture behaviour of bead-on-plate welds on 6.2 mm 3CR12 and 3CRNi plate. The weld fusion line fracture toughness is characterized in terms of a fracture appearance transition temperature (FATT). The influence of factors like the phase composition of the HT HAZ, base and weld metal strength, punch speed during bend testing and the weld fusion line orientation of the bead-on-plate bend specimens, on the fusion line fracture behaviour, was determined.

The actural FATT of the HT HAZ of bead-on-plate welds on 6.2 mm plate are higher than the maximum values of 106°C and 120°C which were obtained in this study for 3CR12 and 3CRNi, respectively. This is due to a fracture mode transition at the FATT from cleavage fracture in the HT HAZ to ductile tearing in the fine grained and low temperature HAZ. This transition is explained in terms of the Davidenkov-Ludwik fracture theory.

The HT HAZ fracture toughness of welds on 3CR12 and 3CR12Ni is lower than both the values reported in the literature for respectively the weld HAZ of 3CR12 and AISI 409. It was not improved significantly by a marked decrease in the grain size of this zone from ASTM No. 1-2 to a fine, low carbon, martensitic structure associated with an increase in the martensite content from 15 percent to 98 percent. The fracture toughness of the HT HAZ is therefore probably determined by other phenomena which has not yet been identified.

The effect of the weld heat input of bead-on-plate MMA welds on 11 mm thick 3CR12 plate, within the range of 0.64 - 1.81 kJ/mm, was to increase the width of the HT HAZ from 0.41 mm to 1.1 mm; the phase composition and grain size were unchanged. The phase composition of the HT HAZ is not only dependent on the ferrite factor but is also dependent on the Ti/(C+N) ratio and the thermomechanical history of the steel.

The influence of the base and weld metal strength on the fusion line fracture behaviour of bead-on-plate welds on 6.2 mm thick 3CR12 plate cannot be determined using the newly developed bead-on-plate bend test. This is attributed to the high constraint offered alone by the large welding bead.

THE NOTCH-TOUGHNESS OF WELDED 3CR12 AND 3CR12Ni

1. INTRODUCTION

The probability of the HT HAZ fracture toughness of 3CR12 being much lower than generally reported in the literature, has already been pointed out in the chapter one. The very low HT HAZ fracture toughness values which were obtained for the 14 percent chromium steels as well as the fact that these values were not significantly influenced by large fractions low carbon martensite and the fact that 3CR12 has a much lower nickel content (0.6%), strongly suggest that the HT HAZ fracture toughness of 3CR12 is not significantly higher than that of AISI 409.

The very low HT HAZ fracture toughness values which were obtained in the previous chapter can be attributed to the fact that the bead-on-plate bend test is a very severe test. The weld HAZ was subjected to very high levels of constraint during bend testing due to inter alia the high strength of the hot rolled base plate. It has also been shown that the weld fusion line fracture behaviour of the 14% chromium steels are strongly dependent on the weld metal mechanical properties. Recently, a new filler metal, designated E3CR12, became available on the market exclusively for welding of 3CR12.

With reference to the abovementioned aspects, it was decided to study the effects of the following factors on the fusion line fracture behaviour of welds on 3CR12 and 3CR12Ni. For this purpose the newly developed bead-on-plate bend test was used.

a. Phase composition of the HT HAZ
b. Base metal strength
c. Weld metal strength (AISI 316L weld metal vs E3CR12)
d. Loading rate or punch speed during bend testing
e. Orientation of the fusion line of bead-on-plate welds relative to the plate surface

2. EXPERIMENTAL PROCEDURE

2.1 Chemical compositions

In order to determine the effect of the phase composition on the fusion line fracture behaviour of welds on 3CR12, two experimental steels (Table 4.1) with respectively 45 (3CR12) and 100 percent martensite (3CR12Ni) in the HT HAZ were designed using Kaltenhauser's ferrite factor and the design curve in figure 4.1 which was determined in a previous study(1,23). Superimposed on this curve are also the curves which were obtained by Middelburg Steel and Alloys (Pty), Ltd. and Eckenrod and Kovach(24) for respectively 3CR12 and a 11.5 percent chromium, 0.85 nickel steel (Crucible E-4).

The experimental steels were supplied by Middelburg Steel and Alloys (Pty), Ltd. in two conditions, i.e. 6.2 mm hot rolled 3CR12 and 3CR12Ni plate and 6.2 mm tempered 3CR12 and 3CR12Ni plate. Final hot rolling was executed at 820-850°C followed by air cooling. Tempering was done at 780°C for 20 minutes.

Table 4.1: Chemical compositions (wt-%) of experimental 3CR12 and 3CR12Ni steels.

Steel	C	S	P	Mn	Si	Ti	Cr	Ni	N	F.F*
3CR12	0.027	0.008	0.020	1.32	0.44	0.32	11.34	0.60	0.022	9.54
3CR12Ni	0.025	0.011	0.027	0.94	0.49	0.22	11.53	1.19	0.018	7.87

*F.F.: Ferrite factor

2.2 Specimen preparation

The design of the bead-on-plate bend test specimen for evaluating the fusion line notch fracture toughness of welds on 3CR12 and 3CR14, has already been discussed in detail in chapter 3.

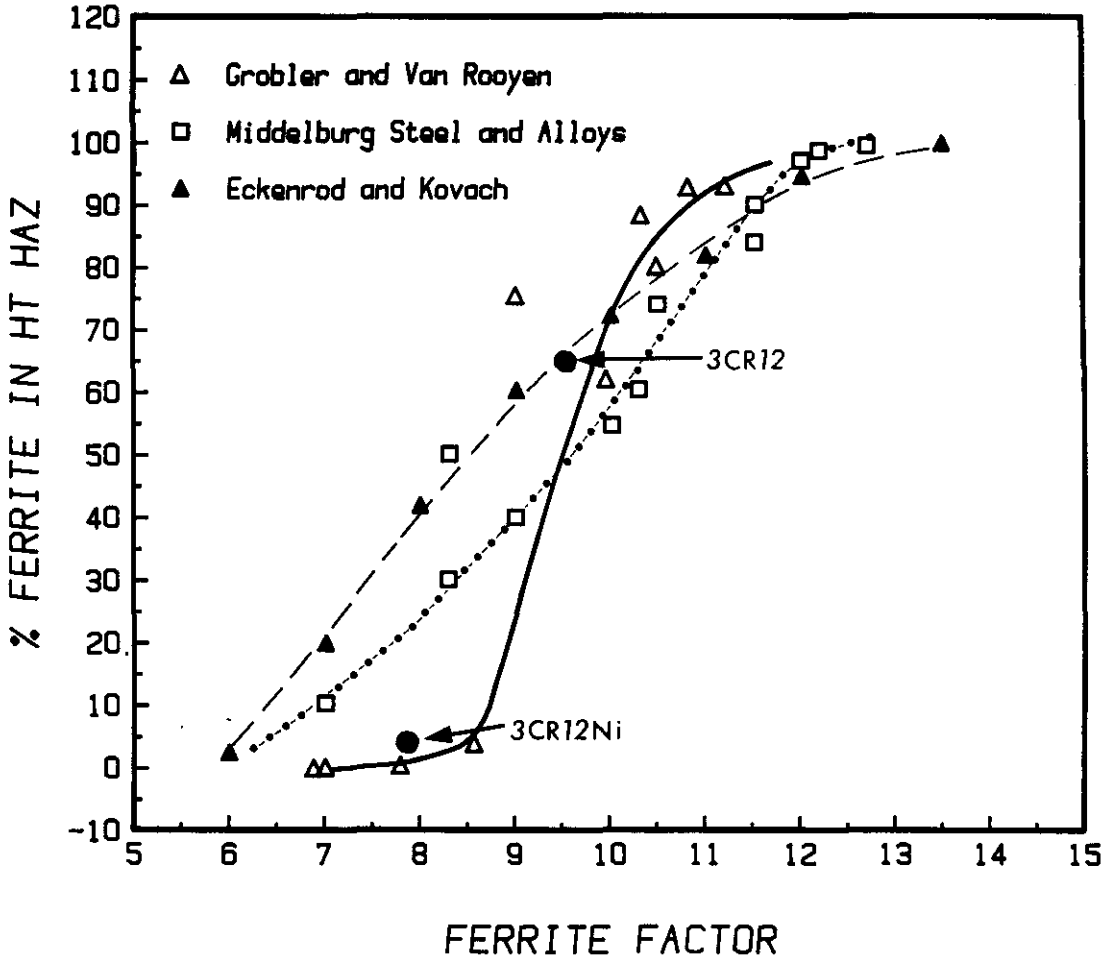

Figure 4.1: Percentage ferrite in the HT HAZ of 3CR12 and 3CR12Ni versus the ferrite factor. The HT HAZ phase composition of the experimental 3CR12Ni and 3CR12 steels are indicated.

Bead-on-plate bend specimens (fig. 3.2) were prepared from respectively 6.2 mm hot rolled and tempered plate, using two different filler metals, viz AISI 316L and E3CR12. The bead-on-plate welds were welded according to the following welding parameters:

Welding process	:	MIG
Welding position	:	Flat
Welding wire	:	1.6 mm dia. AISI 316L
	:	1.6 mm dia. flux cored E3CR12
Current (ampere)	:	370-380
Volts	:	20-21
Welding speed (cm/min.)	:	95 (316L)
	:	90 (E3CR12)
Welding gas	:	84% Ar, 13% CO_2 and 3% O_2.

In order to obtain the excessively large welding bead together with the deep penetration (fig. 3.3) a special shielding gas (84%Ar, 13%CO_2 and 3%O_2) was used. The weld metal carbon content increased slightly due to carbon pick-up from the CO_2 in the shielding gas. Table 4.2 show the weld metal chemical analysis of MIG welds which were welded with respectively the abovementioned shielding gas and a gas which contained only 98%Ar and 2%O_2. The increase in weld metal carbon content from 0.014% to 0.044% will result in an increase in the weld metal yield strength. The HT HAZ may therefore, as a result of this higher weld metal yield strength, be subjected to slightly higher constraints during bend testing.

Table 4.2: Weld metal (316L) chemical analysis of MIG welds (multi-layer cladded specimen), welded respectively with shielding gasses which contained (84%Ar, 13%CO_2, 3%O_2) and (98%Ar, 2%O_2).

Shielding gas	C	P	Mn	Ni	Cr	Mo	Si
84%Ar, 13%CO_2, 3%O_2	0.044	0.02	1.17	11.8	18.2	2.4	0.25
98%Ar, 2%O_2	0.014	0.02	1.35	11.9	18.6	2.5	0.28

3. EXPERIMENTAL RESULTS

3.1 Microstructures

Figure 4.2 shows the coarse grained, duplex ferrite-martensite microstructure of the HT HAZ of bead-on-plate welds on respectively hot rolled and tempered 6.2 mm 3CR12 plate. The HT HAZ of the tempered specimen exhibits a much higher martensite content compared to the hot rolled specimen. No significant differences were observed in the HT HAZ microstructures of the hot rolled and tempered 3CR12Ni specimens (fig. 4.3). The phase compositions of the HT HAZ's of the bead-on-plate bend test specimens, are summarized in table 4.3. It was determined by an area analysis from photographs which were prepared using both high contrast film and printing paper. The width of the HT HAZ ranged from 0.25 mm to 0.35 mm.

Table 4.3: Phase composition of the HT HAZ of bead-on-plate welds on 6.2 mm 3CR12 and 3CR12Ni plate.

Steel	Condition	% Martensite in HT HAZ
3CR12	Hot rolled	15
3CR12	Hot rolled and tempered	35
3CR12Ni	Hot rolled	97
3CR12Ni	Hot rolled and tempered	96

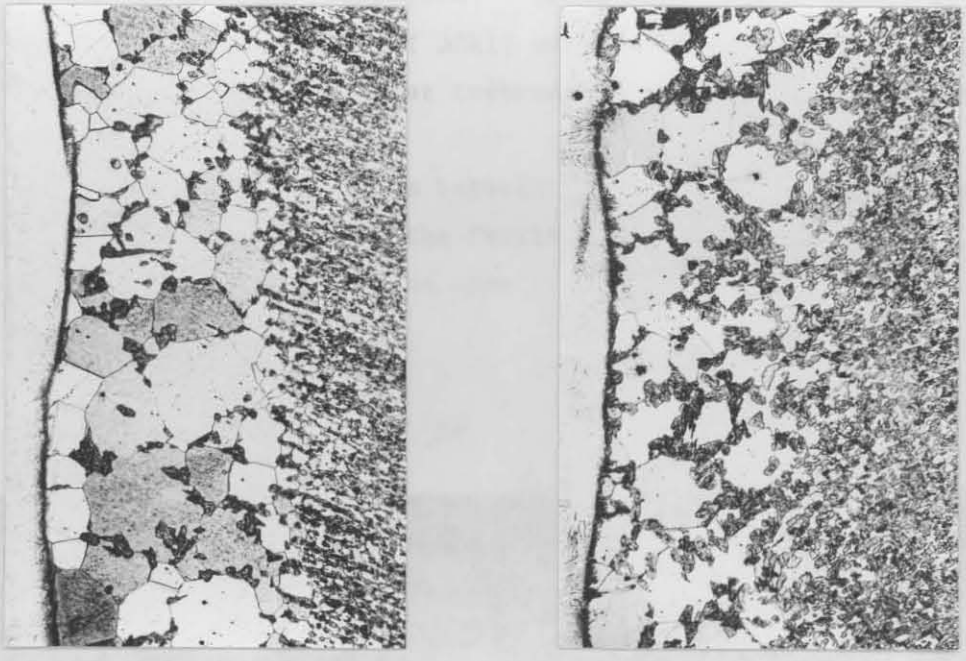

a. b.

Figure 4.2: Coarse grained, ferrite-martensite microstructure of the HT HAZ of bead-on-plate welds on 6.2 mm 3CR12 plate (160X).
a. Hot rolled plate
b. Hot rolled and tempered plate

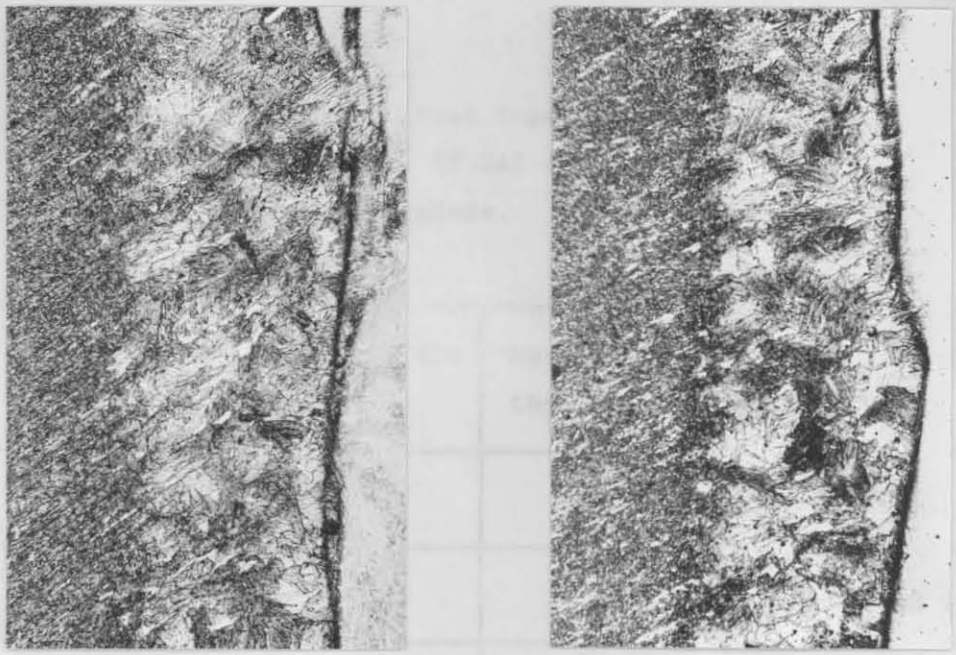

a. b.

Figure 4.3: Duplex ferrite-martensite microstructure of the HT HAZ of bead-on-plate welds on 6.2 mm 3CR12Ni plate (160X).
a. Hot rolled plate
b. Hot rolled and tempered plate

The phase compositions of the HT HAZ of the tempered 3CR12 and 3CRNi specimens are superimposed on figure 4.1. Figure 4.1 shows that the phase composition of the HT HAZ of MIG welds on 3CR12 may be accurately predicted using Grobler and Van Rooyen's design curve which was constructed using the MIG welding process. The other curves were constructed using both the MMA and MIG welding processes. The differences between the curves, especially at ferrite factors below 9.5 may be attributed partly to the fact that the steels which were used to determine these curves were not subjected to the same prior thermomechanical treatments. Table 4.3, e.g., shows that the martensite content of the HT HAZ of 3CR12 was increased from 15 percent to 35 percent by a prior tempering heat treatment subsequent to hot rolling.

Another reason for the differences between the curves in figure 4.1 may be the fact that the formula for the ferrite factor includes the total titanium, carbon and nitrogen in the steel, while the percentage ferrite in

the HT HAZ is determined by the dissolved titanium, carbon and nitrogen rather than by the total percentages. The dissolved titanium, carbon and nitrogen in the HT HAZ is determined by the Ti/(C+N) ratio which was not the same for the experimental steels which were used to construct the different curves in figure 4.1.

Since the microstructure of the HT HAZ originates during non-equilibrium heating and cooling cycles, the fraction δ-ferrite which will transform into austenite during the weld cooling cycle is determined, inter alia by the cooling rate. The cooling rate is determined by the welding process, the section thickness, joint design and the heat input during welding. The effect of heat input on the phase composition, width, and grain size, of the HT HAZ was determined in this study by preparing bead-on-plate MMA welded specimens from 10 mm commercial 3CR12 plate. The specimens were welded with a 3.25 mm diameter AISI 309L electrode at heat inputs ranging from 0.64 kJ/mm to 1.81 kJ/mm. The results are summarized in table 4.4 and figure 4.4.

Table 4.4: The effect of the weld heat input on the ferrite content, width and grain size of the HT HAZ of bead-on-plate welds on 10 mm thick commercial 3CR12 plate.

Weld heat input (kJ/mm)	% Ferrite in the HT HAZ	Max. width of the HT HAZ (mm)	ASTM grain size No.
0.64	81	0.406	2-3
0.97	82	0.742	1-2
1.25	80	0.802	1-2
1.36	77	0.902	1-2
1.51	78	1.043	1-2
1.81	79	1.063	1-2

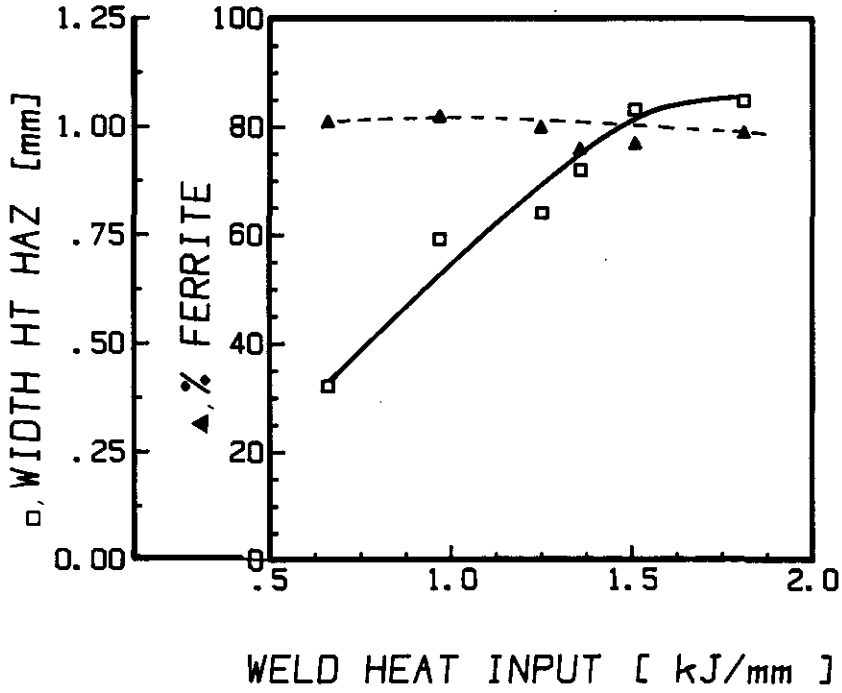

Figure 4.4: Phase composition and width of the HT HAZ of 3CR12 versus heat input for MMA welding.

Figure 4.4 shows that variation of the heat input only increases the size of the HT HAZ while the phase composition and grain size are unchanged. This may be explained as follows: Partial transformation of δ-ferrite to austenite occurs, during cooling from the solidus temperature, within the temperature range of about 1300°C to 1000°C (fig. 1.2). The resultant variations in thermal cycle which were obtained in this temperature range by welding within the heat input range of 0.64 to 1.81 kJ/mm had very little influence on the fraction δ-ferrite which transformed to austenite during cooling.

It may therefore be concluded that the phase composition of the HT HAZ of welds on 3CR12, over the range of heat inputs appropriate to manual welding (i.e. 0.6 to 1.6 kJ/mm), is determined mainly by the thermomechanical history, chemical composition and Ti/(C+N) ratio of the steel.

3.2 The influence of the phase composition of the HT HAZ, loading rate, the weld metal and base metal strength on the fusion line notch fracture toughness of 3CR12 and 3CR12Ni

The effect of the phase composition of the HT HAZ on the fusion line fracture behaviour was determined by comparing the bead-on-plate bend test results of specimens prepared from respectively 3CR12 and 3CR12Ni plate. The effect of weld metal strength was determined by comparing the test results of specimens welded respectively with a low strength AISI 316L filler metal and a high strength E3CR12 filler metal, while the effect of the base metal strength was determined by comparing test results of specimens prepared respectively from hot rolled and hot rolled-and-tempered plate.

The influences of the abovementioned variables on the fracture behaviour of welds were determined at a punch speed of 133 mm/min. during three point

Table 4.5: Bead-on-plate bend test results for 3CR12 and 3CR12Ni.

Steel	Condition A: Hot rolled B: & tempered	Filler metal	% martensite in HT HAZ	Bend testing (133mm/min)		Charpy impact loading		Vickers hardness	
				FATT (°C)	Frac. Mode*	FATT (°C)	Frac. Mode*	Weld metal	Base metal
3CR12Ni	A	316L	97	77	1	98	4	220	322
3CR12Ni	A	E3CR12	97	70	2	106	2	283	322
3CR12Ni	B	316L	96	69	2	36	2	282	196
3CR12	A	316L	15	92	3	104	2	277	246
3CR12	A	E3CR12	15	106	3	120	2	374	246
3CR12	B	316L	35	105	2	106	3	311	165

* Fracture mode transition at FATT:

1. Ductile - cleavage fracture in HT weld HAZ.
2. Cleavage fracture in HT weld HAZ at $T < FATT$.
   Ductile tearing in fine grained and low temperature HAZ at $T > FATT$.
3. Cleavage fracture in HT weld HAZ at $T < FATT$.
   90° bend without fracture at $T > FATT$.
4. Cleavage fracture in HT weld HAZ at $T < FATT$.
   Ductile fracture in HT weld HAZ and weld metal at $T > FATT$.

face bend testing. The effect of loading rate or punch speed was determined at punch speeds ranging from 2 mm/min. to 430 mm/min. Some specimens were also tested by impact loading in a Charpy impact machine. The results of this study is summarized in table 4.5.

3.2.1 3CR12Ni steel weld fracture behaviour

The hot rolled 3CR12Ni bend specimens welded with an AISI 316L filler metal, and which contained 97 percent martensite in the HT HAZ, fractured exclusively in the HT HAZ adjacent to the fusion line. Figure 4.5 shows a brittle cleavage fracture in this zone of a specimen tested at 50°C while figure 4.6 shows a ductile fracture in this zone of a specimen tested at 95°C.

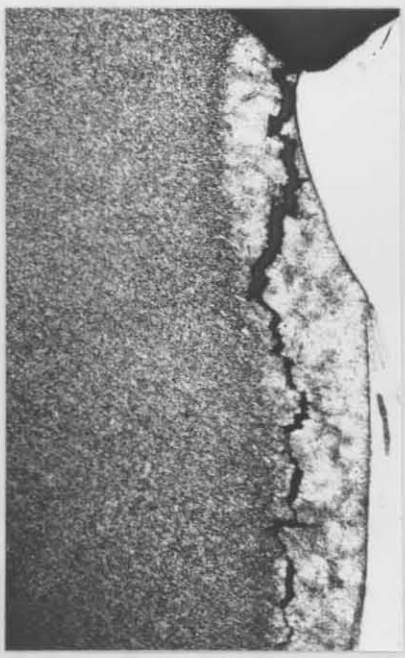

Figure 4.5: Brittle cleavage fracture in the HT HAZ of a bead-on-plate bent specimen, prepared from hot rolled 3CR12Ni plate and tested at 50°C (35X).

Figure 4.6: Ductile fracture in the HT HAZ of a bead-on-plate bent specimen, prepared from hot rolled 3CR12Ni plate and tested at 95°C (35X).

The FATT was determined by a fracture surface analysis of only that part of the fracture surface where the crack path was limited to the HT HAZ. The fracture surfaces of the bent specimens together with the FATT curve is shown in figure 4.7. A FATT of 77°C (at 50 percent ductile fracture surface) was obtained for the HT HAZ of hot rolled 3CR12Ni specimens welded with a AISI 316L filler metal.

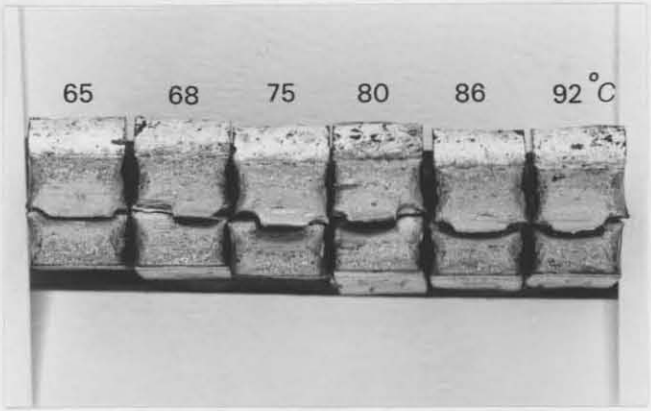

a.

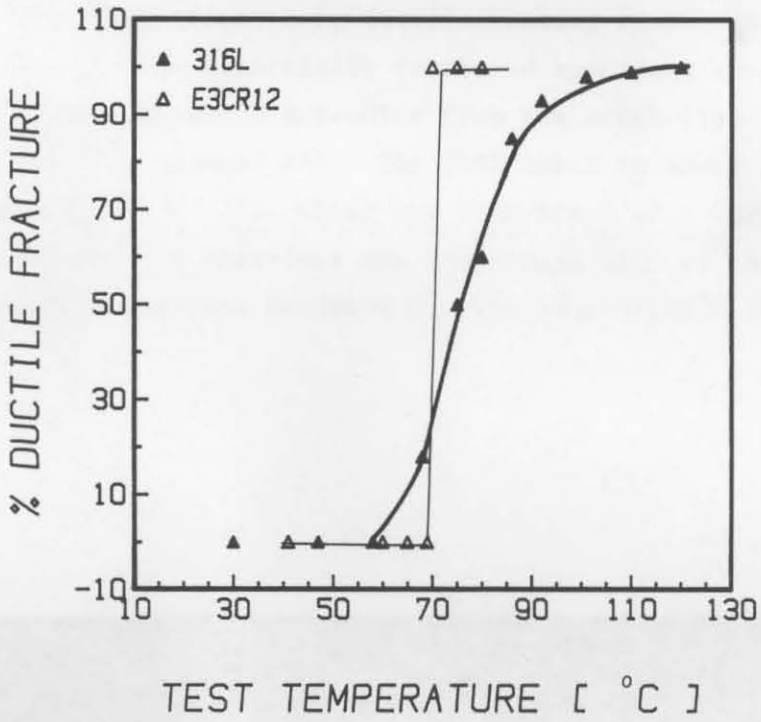

b.

Figure 4.7: a. Fracture surfaces of hot rolled 3CR12Ni bead-on-plate bent specimens welded with an AISI 316L filler metal. Test temperatures (°C) are indicated.

b. FATT curves for hot rolled 3CR12Ni specimens welded respectively with AISI 316L and E3CR12 filler metals.

In some of the bead-on-plate bend specimens the notch tip was not positioned exactly on the fusion line, but displaced slightly towards the weld metal (fig. 4.8). Even with the notch in this position, both brittle and ductile fractures were limited to the HT HAZ. Figure 4.8 shows a partially fractured specimen with a short ductile crack which propagated for a distance of only 0.15 mm in the weld metal. The possibility that this crack initiated in the HT HAZ rather than in the weld metal has already been discussed in the previous chapter.

Figure 4.8: Partially fractured bead-on-plate 3CR12Ni bent specimen with the notch tip located in the weld metal. Note the short ductile crack (specimen tested at 90°C) extending from the notch tip through the weld metal into the HT HAZ (75X).

The hot rolled 3CR12Ni specimens welded with the high strength E3CR12 filler metal fractured by cleavage fracture in the HT HAZ at temperatures below the FATT of 70°C (table 4.5). At temperatures above the FATT temperature fracture occurred by ductile tearing in the HAZ. Figure 4.9 shows a section through a partially fractured specimen, which was tested at 74°C, with a ductile crack extending from the notch tip, through the HT HAZ, into the fine grained HAZ. The FATT curve is shown in figure 4.7b. The FATT temperature of 70°C, which was determined at a very sharp ductile-brittle transition, is therefore not the actual FATT of the HT HAZ since a completely brittle fracture occurred in this zone at 69°C (fig. 4.7b).

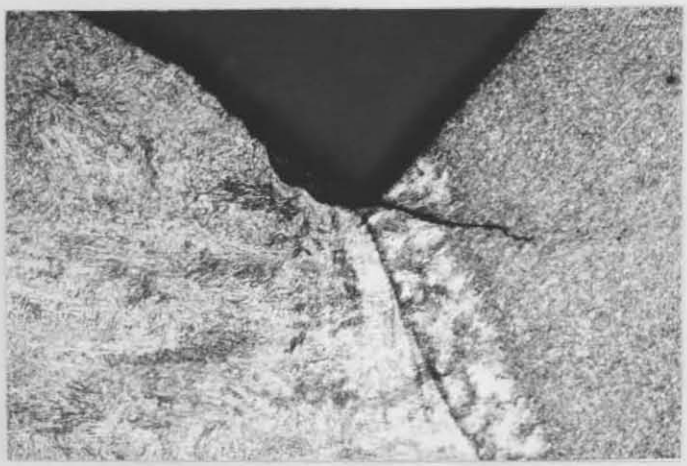

a.

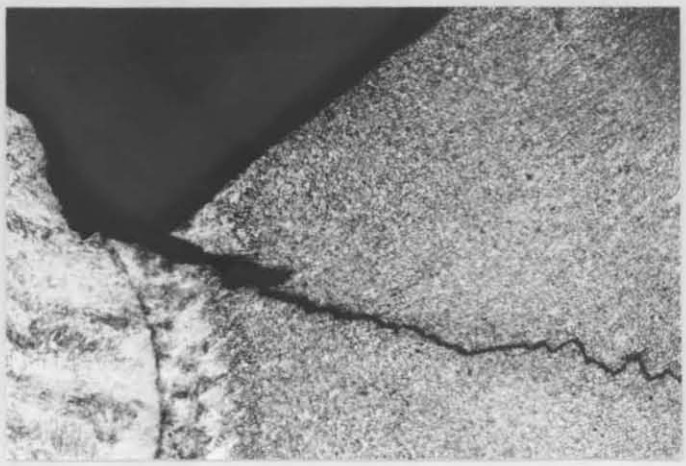

b.

Figure 4.9: Partially fractured hot rolled bead-on-plate 3CR12Ni bent specimens, welded with a E3CR12 filler metal and tested at 74°C.
a. Crack initiation
b. Crack propagation

The fracture mode transition at the FATT temperature of 69°C of the tempered 3CR12Ni specimens, welded with an AISI 316L weld metal, is similar to that of the hot rolled specimens welded with an E3CR12 filler metal (table 4.5). This may be attributed to the higher 316L weld metal strength (table 4.5) compared to that of the hot rolled specimens and the lower

strength and fracture stress of the fine grained HAZ of the tempered specimens compared to that of the the hot rolled specimens.

3.2.2 3CR12 weld fracture behaviour

The actual FATT of the HT HAZ of the hot rolled 3CR12 bead-on-plate bend specimens, welded respectively with AISI 316L and E3CR12 filler metals were not determined, since the specimens fractured at temperatures below the FATT temperature by cleavage fracture (fig. 4.10) in the HT HAZ while 90° bends were achieved at temperatures above the FATT temperature. Plastic deformation occurred mainly in the low temperature HAZ (table 4.5 and fig. 4.11). Although the fracture stress of the HT HAZ is expected to be much lower than that of the adjacent fine grained HAZ and weld metal, this stress was never reached during bending at temperatures above the FATT temperature.

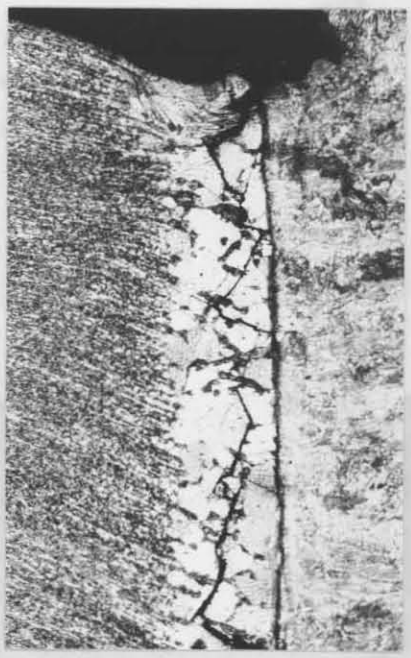

Figure 4.10: Partially fractured hot rolled bead-on-plate 3CR12 bent specimen welded with an E3CR12 filler metal. Specimen tested at 90°C. Note the plastic deformation lines at the notch tip preceding cleavage fracture (35X).

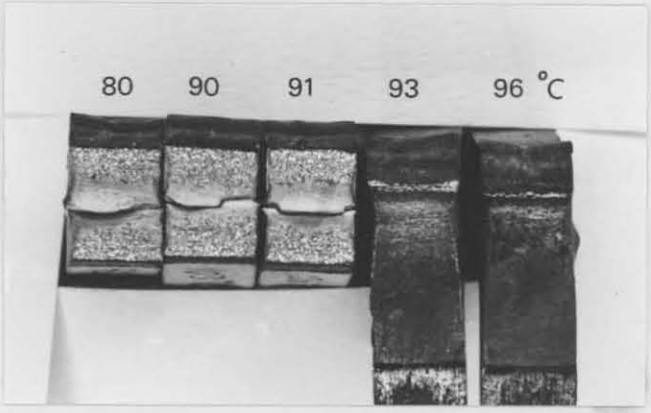

Figure 4.11: Fracture surfaces of hot rolled bead-on-plate 3CR12 bent specimens, welded with an AISI 316L filler metal. 90° bends were achieved at temperatures above the FATT while brittle cleavage fracture occurred in the HT HAZ at temperatures below 93°C. Test temperatures (°C) are also indicated.

A FATT of 105°C (table 4.5) was obtained for the tempered 3CR12 specimens, welded with a AISI 316L filler metal. This is again not the actual FATT of the HT HAZ since a fracture mode transition from cleavage fracture in the HT HAZ to ductile tearing in the low temperature HAZ occurred at the FATT temperature (fig. 4.12). The actual FATT will be much higher than 105°C even with the 35 percent martensite in this zone compared to the FATT of 92°C which was obtained for the hot rolled specimen with 15 percent martensite in the HT HAZ.

Two important observations can be made at this stage. First, the high FATT temperature or low fracture toughness which was obtained for the HT HAZ of 3CR12 even with 97 percent martensite in this zone and, secondly, the fact that the FATT temperatures, obtained with the bead-on-plate bend test, were not significantly influenced by the higher strength of both the hot rolled base metal or E3CR12 weld metal.

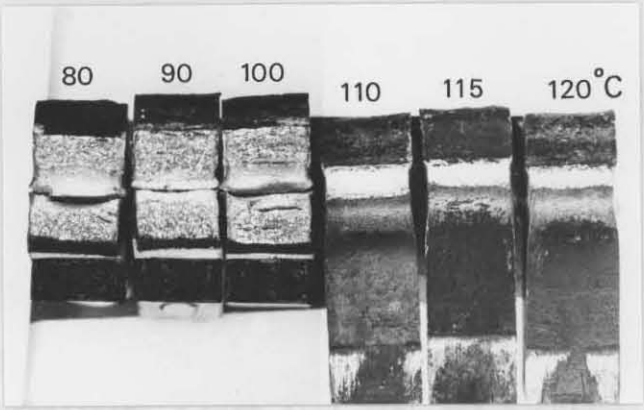

Figure 4.12: Fracture surfaces of tempered bead-on-plate 3CR12 bent specimens, welded with an AISI 316L filler metal. The test temperatures (°C) are indicated.

3.2.3 The influence of loading rate on the fusion line fracture behaviour behaviour of bead-on-plate welded 3CR12 and 3CR12Ni specimens

Figure 4.13 shows the influence of punch speed, ranging from 2 mm/min to 430 mm/min., on the FATT of the HT HAZ of bead-on-plate bend specimens which were prepared from hot rolled 3CR12 and 3CR12Ni plate, welded with AISI 316L and E3CR12 filler metals. The FATT temperatures obtained by impact loading in a Charpy impact machine are also indicated and summarized in table 4.5. Figure 4.13 shows that the FATT temperatures were not significantly influenced by punch speeds ranging from 2 mm/min to 430 mm/min. Higher FATT temperatures were obtained for the impact loaded specimens (table 4.5) except for the tempered 3CR12Ni specimens welded with an AISI 316L filler metal.

From the fracture mode transitions at the FATT indicated in table 4.5 it is evident that the actual FATT values of the HT HAZ were not determined with impact loading. The actual FATT of the HT HAZ of, e.g., tempered 3CR12 is therefore higher than the reported value of 106°C.

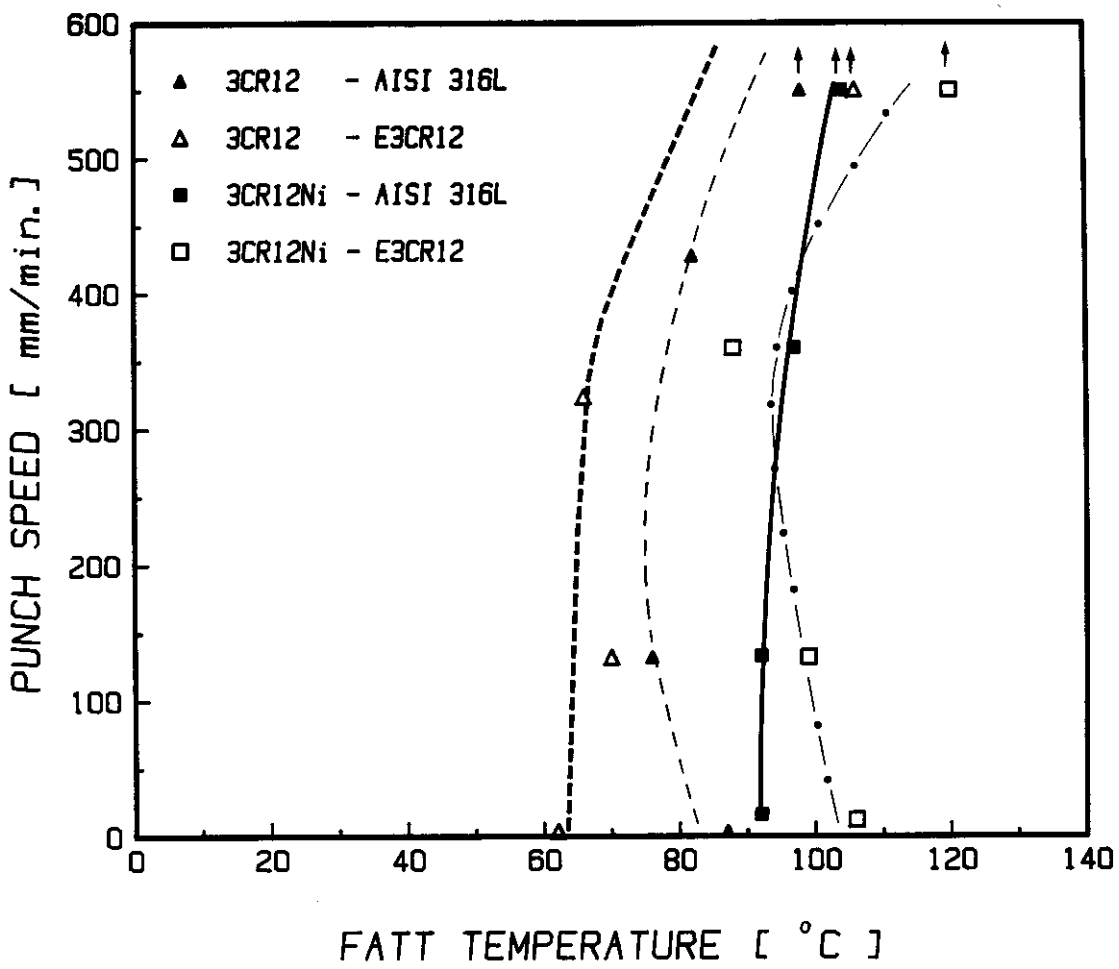

Figure 4.13: Loading rate (punch spead) versus FATT of the HT HAZ of hot rolled 3CR12 and 3CR12Ni bead-on-plate bent specimens, welded respectively with AISI 316L and E3CR12 filler metals. The FATT temperatures obtained by Charpy impact loading are indicated with arrows.

3.3 The influence of the fusion line orientation on the fracture behaviour of bead-on-plate bend specimens

Most of the FATT temperatures in table 4.5, which were obtained for welds on 6.2 mm 3CR12 and 3CR12Ni plate, are lower than the actual FATT temperatures of the HT HAZ since fracture occurred at temperatures above the FATT temperature by ductile tearing in the fine grained HAZ. This occurred among other factors as a result of the weld fusion line which is not oriented normal to the plate surface. The HT HAZ was therefore not

subjected to the maximum bending tensile stresses during bend testing. Higher FATT temperatures will be obtained with the fusion line oriented normal to the plate surface since the HT HAZ will then be subjected to the maximum principal stress during bending.

The influence of the fusion line orientation on the FATT temperature of the HT HAZ of bead-on-plate bend specimens prepared from hot rolled 3CR12Ni plate (welded with E3CR12 filler metal) was therefore determined, and the results of this study is summarized in figure 4.14. Figure 4.15 shows sections through the welds of two test specimens with fusion line orientations relative to the plate surface of respectively 122° and 136°. The actual FATT (77°C) of the HT HAZ of only the hot rolled 3CR12Ni specimens welded with AISI 316L was determined (table 4.5). If the fracture stress of the fine grained HAZ is higher than the fracture stress of the HT HAZ of 3CR12Ni bend specimens, welded with E3CR12, then a FATT of approximately 77°C will be obtained with the weld fusion line oriented normal to the plate surface (fig. 4.14).

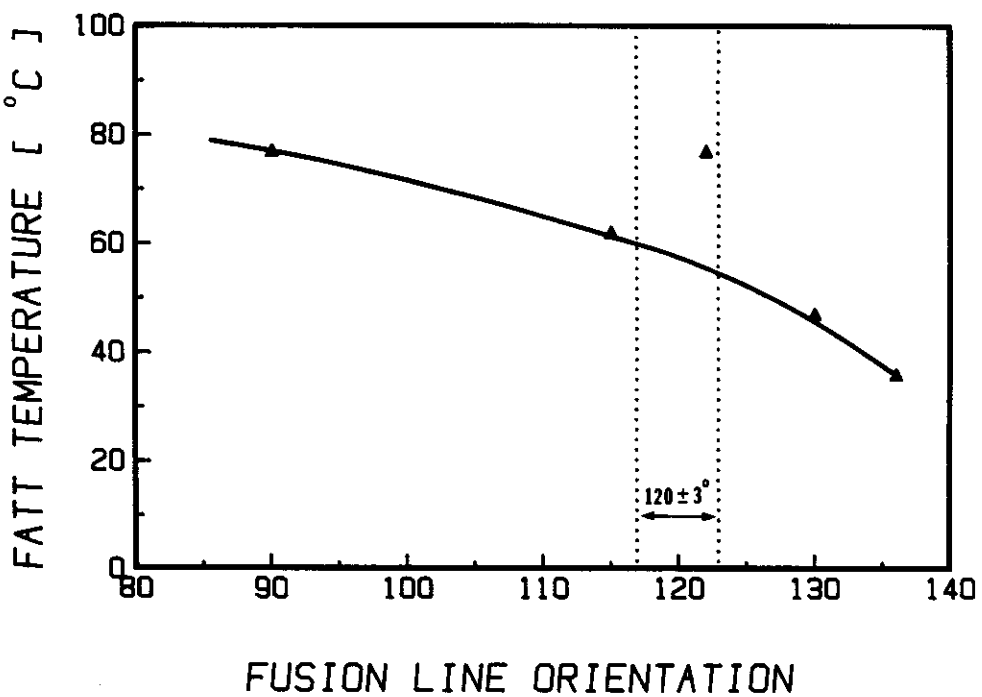

Figure 4.14: Fusion line FATT temperature versus fusion line orientation (θ in fig. 4.15) for hot rolled bead on plate 3CR12Ni specimens, welded with E3CR12. The FATT temperature at θ = 90° is an extrapolated value.

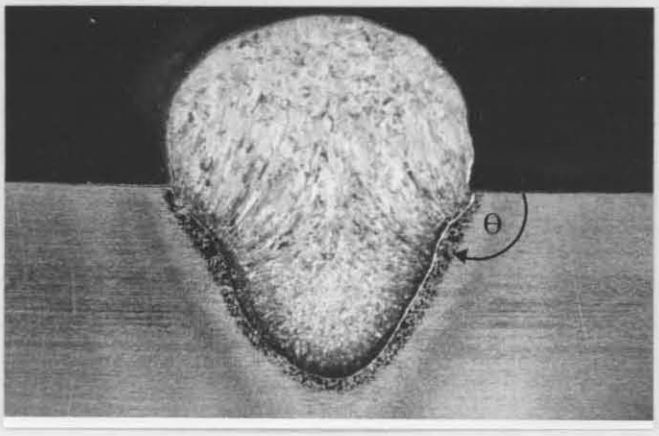

a.

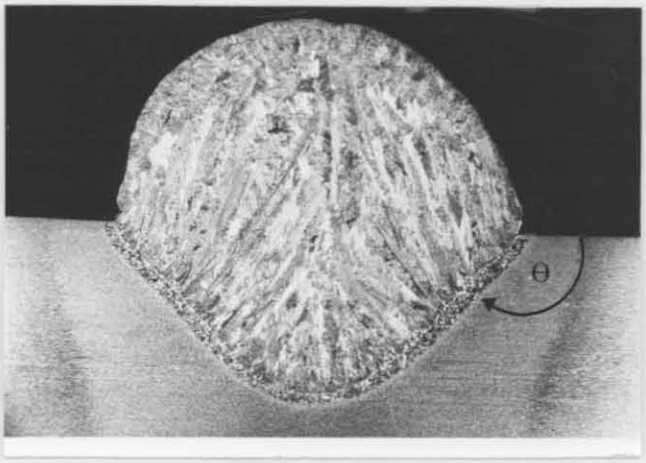

b.

Figure 4.15: Welds on bead-on-plate bend specimens with fusion line orientations relative to the plate surface of 122° (a) and 136° (b). Note the coarse grained HT HAZ adjacent to the fusion line.

Figure 4.14 shows that the fusion line FATT temperatures of bead-on-plate bend specimens is dependent on the fusion line orientation. The specimens which were used in this thesis to study the weld fusion line fracture behaviour of welds on 3CR12 and 3CR14 steels were therefore carefully selected, and only specimens with fusion line orientations within the range $120 \pm 3°$ were tested (fig. 4.14).

4. DISCUSSION

4.1 Fracture mode transition at the FATT

The fracture mode transitions which were observed at the FATT temperatures (table 4.5) of bead-on-plate welded 3CR12 and 3CR12Ni specimens may, be accounted for by using either the Cottrell-Petch or Davidenkov-Ludwik fracture theory. These theories are discussed in detail in chapter 2 and are used to explain the fracture mode transitions of welded 3CR14 steels in chapter 3.

Consider, e.g., the bead-on-plate bent specimens which were prepared from tempered 3CR12 plate (welded with a 316L filler metal) and which fractured by ductile tearing in the fine grained HAZ at temperatures above the FATT of 105°C, and by cleavage fracture in the HT HAZ at temperatures below 105°C (table 4.5). In order to explain this fracture mode transition in terms of the Davidenkov-Ludwik fracture theory, qualitative fracture and flow stress curves for respectively the fine grained HAZ, HT HAZ and weld metal are superimposed on the true stress-strain diagram in figure 4.16.

The relative positions of the different curves in figure 14.16 can be accounted for. The fracture stress curves E and A and the flow stress curve G for the fine grained HAZ is situated at higher stresses than the corresponding curves for the HT HAZ. This is due to the finer grain size and higher martensite content and hence higher fracture and flow stress for the fine grained HAZ compared to the HT HAZ. The weld metal flow stress curve H is situated at even higher stresses as a result of the relatively high weld metal strength (fig. 1.3 and table 4.5) and constraint offered by the large welding bead.

If the three different structures ahead of the notch tip of the bead-on-plate bend specimen represented in figure 4.16, are subjected to the same stress during bending at 90°C, a cleavage fracture will occur in the HT HAZ at a stress $\bar{\sigma}_1$, at the intersection of the curves D and F. The fracture stresses of the fine grained HAZ and weld metal are higher than this value. For any change in test temperature the relative shift of the different curves will always be such that the ductile fracture stress $\bar{\sigma}_2$ of the fine grained HAZ is higher than the cleavage fracture stress $\bar{\sigma}_1$ of

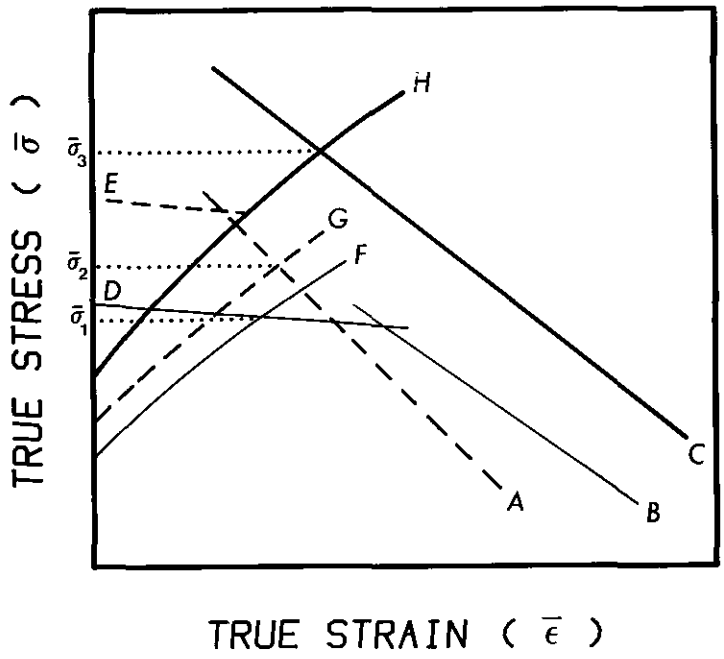

Figure 16: Fracture stress and flow stress curves for the fine grained HAZ, HT HAZ and weld metal at the notch tip of a bead-on-plate bend specimen, which was prepared from tempered 3CR12 plate welded with AISI 316L filler metal. The curves describe the crack tip stress-strain conditions of a specimen which is being bent at 90°C.

Curve A: Ductile fracture stress for the fine grained HAZ
Curve B: Ductile fracture stress for the HT HAZ
Curve C: Ductile fracture stress for the 316L weld metal
Curve D: Cleavage fracture stress for the HT HAZ
Curve E: Cleavage fracture stress for the fine grained HAZ
Curve F: Flow stress curve for the HT HAZ
Curve G: Flow stress curve for the fine grained HAZ
Curve H: Flow stress curve for the 316L weld metal

the HT HAZ. The fracture mode transition at the FATT of 105°C may then only be accounted for if the fine grained HAZ is subjected to higher stresses during bending than the HT HAZ and weld metal. With the weld fusion line of the bead-on-plate bend specimens not oriented normal to the plate surface and with the maximum principal stress developing a short distance ahead of the notch tip, due to plastic constraining, the fine

grained HAZ will in fact be subjected to higher stresses during bending. A fracture mode transition from ductile tearing in the fine grained HAZ at 110°C to cleavage fracture in the HT HAZ at 100°C will then occur when the cleavage fracture stress $\bar{\sigma}_1$ of the HT HAZ is reached prior to reaching the ductile fracture stress $\bar{\sigma}_2$ of the fine grained HAZ.

The true FATT of the HT HAZ can only be determined when the fusion line is oriented normal to the plate surface. The different materials at the notch tip will then be subjected to the same stress during bending, with fracture occurring at any temperature in the HT HAZ due to both the relatively low brittle and ductile fracture stresses of this zone.

The fracture mode transition at the FATT (table 4.5) of the tempered 3CR12Ni specimens can also be explained in a similar manner. The fracture and flow stress curves will only be situated at higher stresses relative to the curves in figure 4.16.

The fracture mode transition from cleavage fracture in the HT HAZ to ductile fracture in the weld metal adjacent to the fusion line, which was obtained for the welded 14 percent chromium steels in chapter 3, was not observed for 3CR12Ni. This is probably due to the much higher weld metal strength (Vickers Hardness : 282) and therefore weld metal fracture strength of the 3CR12 specimens (compared to the 3CR14 specimens with a weld metal Vickers Hardness of 180). The high weld metal strength resulted from the formation of some martensite in the weld metal.

4.2 The influence of the weld and base metal strength on the FATT

Since the actual FATT of the HT HAZ of 3CR12 and 3CR12Ni could not be determined, it was not possible to obtain any conclusive results on the influence of the weld metal and base metal strength on the fusion line fracture behaviour of welds. Some of the FATT values in table 4.5 do indicate a slight increase of the HT HAZ FATT at higher base and weld metal strengths.

Another reason why no significant influence of the base and weld metal strength was observed on the FATT temperature, is the fact that the large welding bead alone offers a very high constraint to the weld HAZ during

bending. In the next chapter the effects of the base and weld metal strength on the fracture behaviour of welds is demonstrated using bead-on-plate welded specimens with the large welding bead removed in order to eliminate the constraint associated with it.

It may be concluded therefore, that the newly developed bead-on-plate bend test is a very useful test for evaluating the influence of the narrow, coarse grained HT HAZ on the fusion line fracture toughness welds under conditions where the fracture behaviour of welds are primarily dependent on the fracture behaviour of the HT HAZ.

4.3 Fusion line FATT of 3CR12 and 3CR12Ni

Since 3CR12 was developed inter alia as a replacement for mild steel in various structural applications, the FATT of the HT HAZ of mild steel was also evaluated. Bead-on-plate bend specimens were prepared from 6.2 mm mild steel plate welded with an AISI 316L filler metal. Figure 4.17 shows the HT HAZ of a bead-on-plate weld on mild steel. A HT HAZ FATT

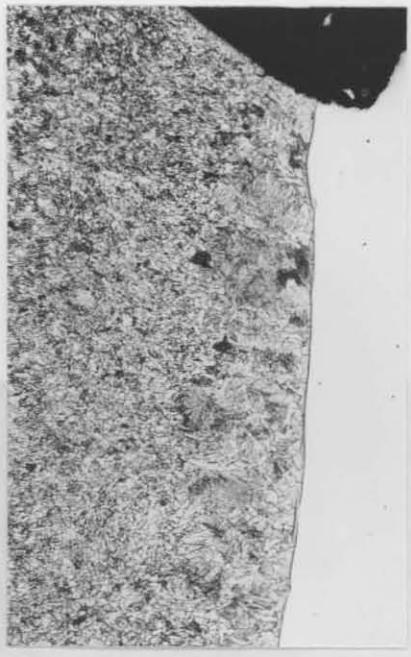

Figure 4.17: Weld HAZ microstructure of a bead-on-plate mild steel bend specimen. Note the fine grain size of the HT HAZ (35X).

of 0°C was obtained during slow bend testing with fracture occurring by ductile tearing in the low temperature HAZ at temperatures above 0°C.

The maximum fusion line FATT temperatures (table 4.5) which was obtained for 3CR12 and 3CR12Ni, are summarized in figure 4.18. Since a cleavage fracture occurred in the HT HAZ of both the 3CR12 and 3CR12Ni bead-on-plate bent specimens during impact loading at 100°C, it may be concluded that the Charpy ductile-brittle transition temperatures of the HT HAZ of both steels are probably higher than 100°C. These values are much higher than the transition temperatures of 0°C and 20°C which were reported for the HT HAZ of respectively 3CR12Ni and 3CR12 previously (8,9). This suggests that these low transition temperatures measured are in fact the transition temperatures for the tough fine grained HAZ adjacent to the HT HAZ. The most important observation at this stage is the fact that the HT HAZ FATT temperature of 3CR12 is higher than the value of 90-100°C which is reported for the HT HAZ of the ferritic stainless steel AISI 409, from which 3CR12 was developed(11).

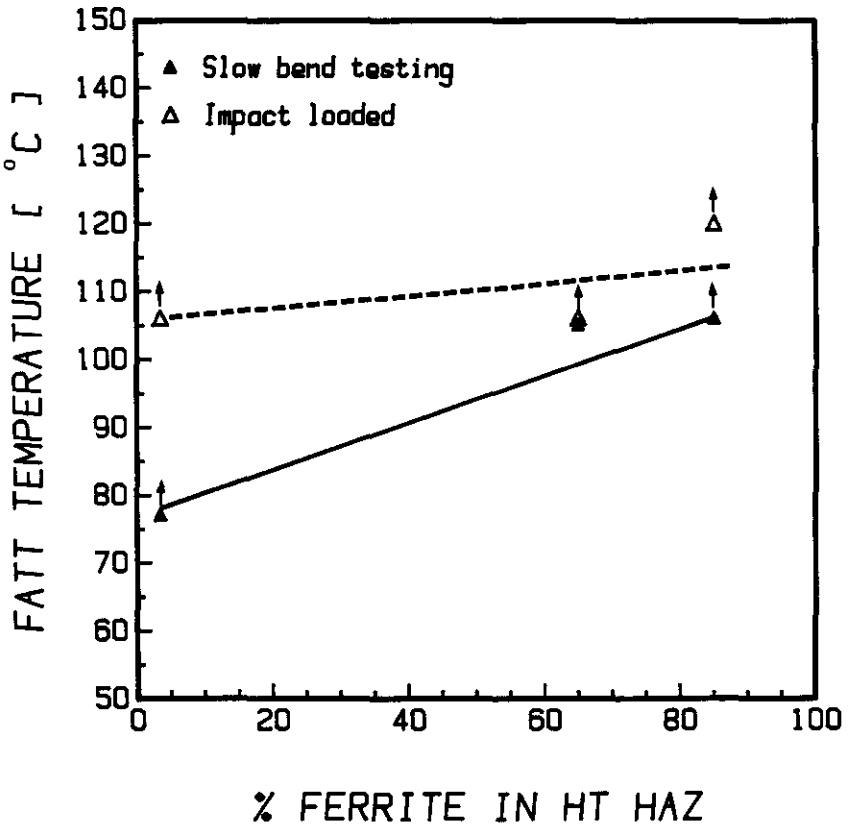

Figure 4.18: Maximum fusion line FATT temperatures obtained in this study for 3CR12 and 3CR12Ni bead-on-plate bend specimens.

Another important observation is the very small difference between the HT HAZ FATT values of the impact loaded 3CR12 and 3CR12Ni specimens (fig. 4.18). Although this difference is higher for the slow bend specimens, it is still relatively small. The toughness of the HT HAZ was therefore not improved to any significant extent by an increase in the martensite content from 15 percent to 98 percent. It seems to be insensitive to the marked reduction of the grain size from ASTM No. 1-2 to a fine grained, low carbon martensitic structure.

Therefore, it may finally be concluded that the toughness of the HT HAZ of 3CR12 is probably determined by other phenomena which have not yet been identified. The same effect was also observed in the previous chapter for the 14 percent chromium steels.

5. SUMMARY

a. The effect of the weld heat input of bead-on-plate welds on 11 mm 3CR12 plate, within the range 0.64 - 1.81 kJ/mm, was mainly to increase the width of the coarse grained HT HAZ from 0.41 mm to 1.10 mm; the phase composition and grain size are relatively unaffected.

b. The fusion line FATT of both 3CR12 and 3CR12Ni bead-on-plate bend specimens were not significantly changed by an increase of the punch speed during bending from 2 mm/min to 430 mm/min. Slightly higher transition temperatures resulted when the specimens were tested by impact loading in a Charpy machine.

c. The fusion line FATT of bead-on-plate bend specimens is dependent on the fusion line orientation relative to the plate surface. Only specimens with fusion line orientations within the range 120 $\pm$3° were tested.

d. The influence of the weld metal strength on the fusion line fracture behaviour of bead-on-plate welds on 6.2 mm 3CR12 plate may not be determined using the newly developed bead-on-plate bend test. This is attributed to the high constraint offered alone by the large welding bead.

e. The actual FATT of the HT HAZ of bead-on-plate MIG welds on 6.2 mm 3CR12 and 3CR12Ni plate could not be determined due to the fracture mode transition at the FATT from cleavage fracture in the HT HAZ to ductile tearing or bending in the fine grained and low temperature HAZ. This fracture mode transition is explained in terms of the Davidenkov-Ludwik fracture theory.

f. Maximum FATT temperatures of respectively 77°C and 106°C were obtained, during slow bend testing, for the HT HAZ of bead-on-plate welds on 3CR12Ni and 3CR12 plate. These temperatures increased to 106°C for 3CR12Ni and 120°C for 3CR12 when the bend specimens were impact loaded in a Charpy machine.

g. A FATT of 0°C was obtained for the HT HAZ of bead-on-plate welded mild steel specimens, prepared from 6.2 mm mild steel plate.

h. The fracture toughness of the HT HAZ of 3CR12 is much lower than either of the values reported in literature for the weld HAZ's of 3CR12 and AISI 409 from which 3CR12, was developed.

i. The fracture toughness of the HT HAZ of 3CR12 was not significantly improved by an increase in the martensite content from 15 percent to 98 percent.

j. It is finally concluded that since the fracture toughness of the HT HAZ of 3CR12 is not dependent on the martensite content and grain size, it is probably determined by other phenomena which have not yet been identified.

CHAPTER 5

FILLER METALS FOR WELDING 3CR12

SYNOPSIS

In the first part of this study the effect was studied of the base and weld metal mechanical properties on the susceptibility of defect-free bead-on-plate welds on 6 mm 3CR12 and 3CR12Ni plate, to brittle cleavage fracture in the HT HAZ. It is demonstrated that the recently developed E3CR12 weld metal has a detrimental effect on the fracture behaviour of defect-free welds.

In the second part of this study different filler metals (AISI 309L, 316L, 308L and E3CR12) were evaluated for welding of 3CR12 plate. The filler metals were compared on the basis of their relative effects on the fusion line notch fracture toughness of fillet welds on 12 mm 3CR12 plate. For this purpose a new test method was also developed for measuring the fusion line notch fracture toughness of fillet welds.

It is demonstrated that the fusion line fracture behaviour of welds on 3CR12 is critically dependent on the weld metal and base metal mechanical properties. A type AISI 309L filler metal is recommended for welding 3CR12. The E3CR12 filler metal is not recommended for welding 3CR12 due to its detrimental effect on the fusion line notch fracture toughness of welds.

FILLER METALS FOR WELDING 3CR12

1. INTRODUCTION

Two of the most important requirements for a filler metal for welding 3CR12 plate are the as-deposited properties that are to be both mechanically and electrochemically compatible with the base metal.

Gooch and Davey compared the suitability of different austenitic type AISI 309L, 309 and 310 filler metals for welding 3CR12(13). They found that all consumables gave crack-free welds with matched parent metal strength, adequate bend ductility and matched crossweld tensile properties. Although all filler metals gave satisfactory results a type AISI 309 was recommended due to the significant capacity for dilution without forming crack-sensitive microstructures. Hoffman recommended that any austenitic type filler metal may be used for welding 3CR12, but found the use of type AISI 308L, 309L and 309LMo to be preferable(8).

Both the abovementioned recommendations were based mainly on a weld metal with matching parent metal mechanical properties. Due to the cost of high alloy austenitic filler metals and the possibility of the occurrence of galvanic corrosion in the weld HAZ, Pagani has developed a lower alloy weld metal with as-deposited properties which, according to Pagani, are both electrochemically and mechanically compatible with the 3CR12 parent plate(15). In the present study the strength of this new weld metal, designated E3CR12, was found to be much higher than that of the parent metal. The hardness of the predominantly martensitic E3CR12 weld metal of both MIG and MMA welds ranged from 373 HV to 385 HV (50kg) in comparison with 170 to 190 HV for 12 mm 3CR12 plate. It appears that the main emphasis in Pagani's study was on the electrochemical and fatigue properties of the weld metal.

The mechanical tests which were mainly used in the abovementioned studies were the hardness test and the unnotched bend and crossweld tensile tests. It is of importance at this stage to consider the validity of the unnotched bend and crossweld tensile tests as criteria for evaluating the suitability of different filler metals in welding 3CR12.

The formation of the narrow, dual phase, coarse grained HT HAZ in the HAZ of 3CR12 is well documented. The very low fracture toughness of this zone was clearly demonstrated in the previous chapter. The bend and cross weld tensile tests, which were used by Gooch et al. and Hoffman, have not revealed any detrimental effect of this narrow coarse grained zone on the ductility and fracture behaviour of 3CR12, welded with different austenitic filler metals. The principal shortcoming of these mechanical tests is that they only evaluate the plane stress fracture behaviour of welds.

With an increasing degree of constraint, the narrow HT HAZ is expected to affect the fracture behaviour of welds significantly. In the case of fusion line type defects, this zone will be highly constrained and subjected to triaxial stresses in comparison with defect free bend and crossweld tensile tests. Due to the coarse grain size of the HT HAZ the fracture stress of this zone is expected to be much lower than that of the austenitic weld metal or that of the adjacent fine grained and low temperature HAZ. At increasing constraint and the development of a triaxial stress state, the fracture stress of the HT HAZ may be reached prematurely with subsequent brittle fracture. The level of constraint in this zone, and therefore the maximum stresses which may develop during loading, is not only dependent on the type, size and orientation of fusion line defects but also on the mechanical properties of the adjacent weld metal, fine grained HAZ, low temperature HAZ and base metal. The fusion line notch fracture toughness of welds on 3CR12 is thus expected to be critically dependent on, inter alia, both the weld metal fracture toughness and mechanical properties.

In the present study it was therefore decided to study and compare the suitability of some austenitic type AISI 309L, 316L and 308L and a dual phase martensitic-ferritic type E3CR12 filler metals for welding 3CR12 by comparing the effects of the different weld metals on the fusion line notch fracture toughness of welds. The fusion line notch fracture toughness is one of the crucial criteria in comparing different filler metals for welding 3CR12.

This study consists of two parts:

1. In the first part the influence of the base and weld metal

mechanical properties on the fracture behaviour of defect-free welds on 6 mm 3CR12 and 3CRNi plate were evaluated using a newly developed unnotched bead-on-plate face bend test.

2. In the second part a new test method was developed for measuring the fusion line notch fracture toughness (FLNFT) of fillet welds on 12 mm 3CR12 plate. The suitability of different filler metals (AISI 309L, 316L, 308 and E3CR12) for welding 3CR12 plate was also evaluated with the FLNFT test.

2. EXSPERIMENTAL RESULTS AND DISCUSSION

2.1 Bead-on-plate bend test

2.1.1 Introduction

The first part of the present study is mainly concerned with the effect of the base metal and weld metal mechanical properties on the fracture behaviour of defect-free bead-on-plate welds on 6.2 mm 3CR12 and 3CR12Ni plate. If the fracture stress of the coarse grained high temperature HAZ is less than the fracture stress of the austenitic weld metal, and the fine grained and low temperature HAZ, the plane stress fracture behaviour of defect-free welds is expected to be determined mainly by the fracture behaviour of the HT HAZ. The fracture behaviour of this coarse grained zone will again be determined by the maximum principal stress which will develop in this zone during, for example, bend or tensile loading. The satisfactory bend and crossweld tensile test results which were obtained by Gooch *et al.* and Hoffman can therefore be accounted for by the fact that the fracture stress of this zone was never reached during plane stress testing as a result of the low strength of both the austenitic weld metal and low temperature HAZ.

At increasing constraints and thus at an increase in stress triaxiality, the fracture toughness of this coarse grained HAZ decreases. The fracture stress increases with a decrease in fracture ductility as shown in figure 5.1. Figure 5.1 shows an increase of the flow stress curves with increasing constraint. The ductile (curve a) and brittle fracture (curve b)

stress curves, according to Ludwik and Davidenkov(19), are also included in figure 5.1. Depending on the fracture toughness and the test temperature a fracture mode transition from ductile fracture to brittle cleavage fracture may occur at increasing constraints as shown by the intersection of the fracture stress curves in figure 5.1.

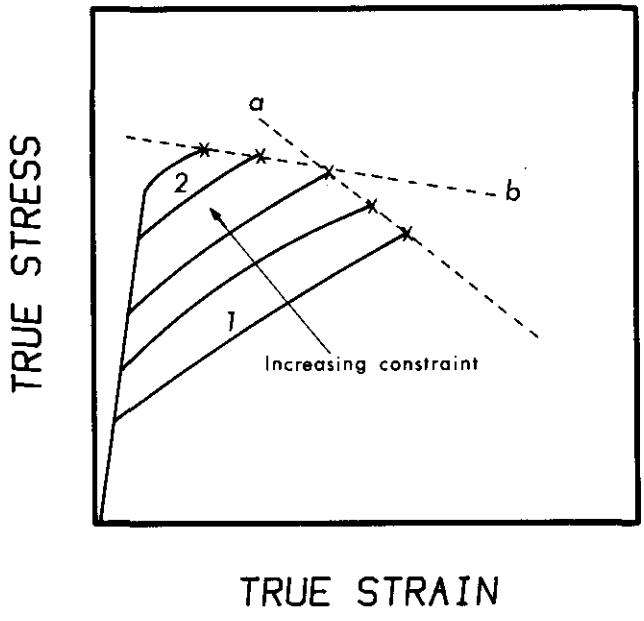

Figure 5.1: Flow stress curves for different constraint conditions.
Curve a. Ductile fracture stress curve
Curve b. Brittle cleavage fracture stress curve

The constraint in the narrow, coarse grained HAZ of a weld on 3CR12 depends not only on the size and notch tip radius (stress concentration factor) of fusion line defects, the section size and weld joint design, but also on the mechanical properties of the weld and parent metal. Consider the smooth composite tensile test specimen in figure 5.2 which is composed of two different materials (B and A), with mechanical properties similar to the HT HAZ of 3CR12, with 40 percent low carbon martensite, and an austenitic weld metal respectively. For similar mechanical properties for the composite materials of the composite tensile specimen in figure 5.2, the specimen will fracture by ductile fracture according to curve 1 in figure 5.1. By increasing the yield and tensile strength of the weld metal above that of the coarse grained HAZ, the centre part of the composite tensile specimen in figure 5.1 will be subjected to increasing constraints when the HAZ starts yielding. A triaxial stress field will develop in

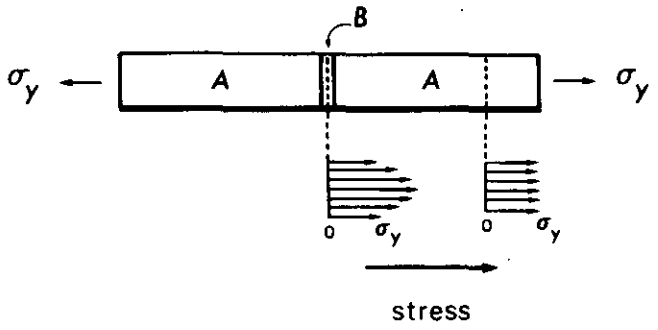

Figure 5.2: Composite tensile test specimen composed of two different materials. The narrow centre part (B) of the specimen has mechanical properties similar to the coarse grained HT HAZ in 3CR12 while both ends (A) have properties similar to that of an austenitic type weld metal. Note also the stress distribution in the different materials when the HAZ (B) starts yielding.

this narrow centre part of the test specimen during tensile loading as a result of local necking or deformation in this part and the high weld metal strength which plastically constrains it. At high constraints (higher weld metal mechanical properties) the composite tensile specimen may, therefore, fracture by brittle cleavage fracture in the centre part of the specimen as a result of the reduced fracture toughness of this part and the triaxial stress which reached the brittle fracture stress of this centre part according to curve 2 in figure 5.1.

2.1.2 Experimental Procedure

Bead-on-plate three point face bend specimens (fig. 5.3) were prepared from both hot rolled-and-tempered and hot rolled 6.2 mm 3CR12 plate and 3CR12Ni plate. The HT HAZ of welds on 3CR12Ni plate contains about 98 percent low carbon martensite (fig. 4.3) compared to the 15 to 35 percent martensite in this zone of welds on 3CR12 plate (fig. 4.2). The chemical compositions of 3CR12 and 3CR12Ni are shown in table 4.1.

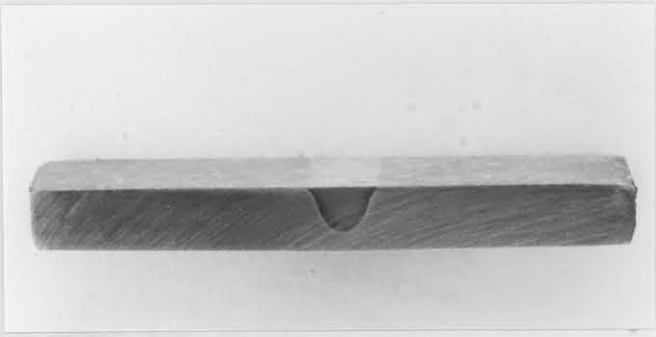

Figure 5.3: Bead-on-plate three point face bend specimen with the weld bead removed.

The bend specimens (6 mm x 10 mm x 60 mm) were machined from welded sections on which single beads were welded parallel to the rolling direction according to the following welding procedure:

Welding process	:	Gas metal-arc (MIG)
Welding wire	:	1.6 mm AISI 316L
	:	1.6 mm Flux cored E3CR12 (Philips)
Shielding gas	:	84%Ar, 13%CO_2, 3%O_2
Welding position	:	Flat
Current (amp)	:	360-380
Volts	:	20-21
Arc speed (cm/min.)	:	95 (316L)
	:	90 (E3CR12)

Bend specimens were prepared from both hot rolled and hot rolled-and-tempered 3CR12 and 3CR12Ni plate welded with a low strength austenitic type AISI 316L filler metal. Specimens which were welded with the high strength E3CR12 filler metal were only prepared from hot rolled 3CR12 and 3CR12Ni plate in which the customary tempering heat treatment was omitted. The weld bead was subsequently removed in order to eliminate any surface type defect.

The effect of the base metal strength on the fracture behaviour of the

HT HAZ was studied by comparing the bend test results of the hot rolled and the hot rolled-and-tempered specimens. The effect of weld metal strength was studied by comparing the bend test results of specimens welded respectively with AISI 316L and E3CR12 filler metals. The effect of the microstructure or phase composition of the HT HAZ on the fracture behaviour of the welds was studied by comparing the bend test results of 3CR12 and 3CR12Ni bent test specimens.

The deep penetrating welding variables were designed in order to obtain a fusion line and therefore a HT HAZ which ideally will be oriented normal to the plate surface. A very favourable orientation was obtained as shown in figure 5.3.

It is of some significance at this stage to consider the microstructure of the HAZ of MIG welded bead-on-plate welds on 6.2 mm 3CR12 and 3CR12Ni plate, as shown in figures 4.2 and 4.3, respectively. It has already been demonstrated in chapter 1 that the weld HAZ can be divided into three different zones:

1. A narrow coarse grained high temperature (HT) zone adjacent to the fusion line. The phase composition of this zone depends on the relative amounts of ferrite and austenite stabilizing elements in the steel, while the width depends on the heat input.

2. A much wider fine grained duplex zone, with ferrite and untempered martensite, right next to the coarse grained zone. The width of this zone, which was determined from the microhardness transverse of bead-on-plate welds on 3CR12 and 3CR12Ni in figures 5.4 and 5.5, respectively, ranges from 0.7 mm to 0.9 mm.

3. A third low temperature zone more distant from the fusion line. The width of this zone which was also determined from figures 5.4 and 5.5 ranges from 2.5 mm to 3 mm.

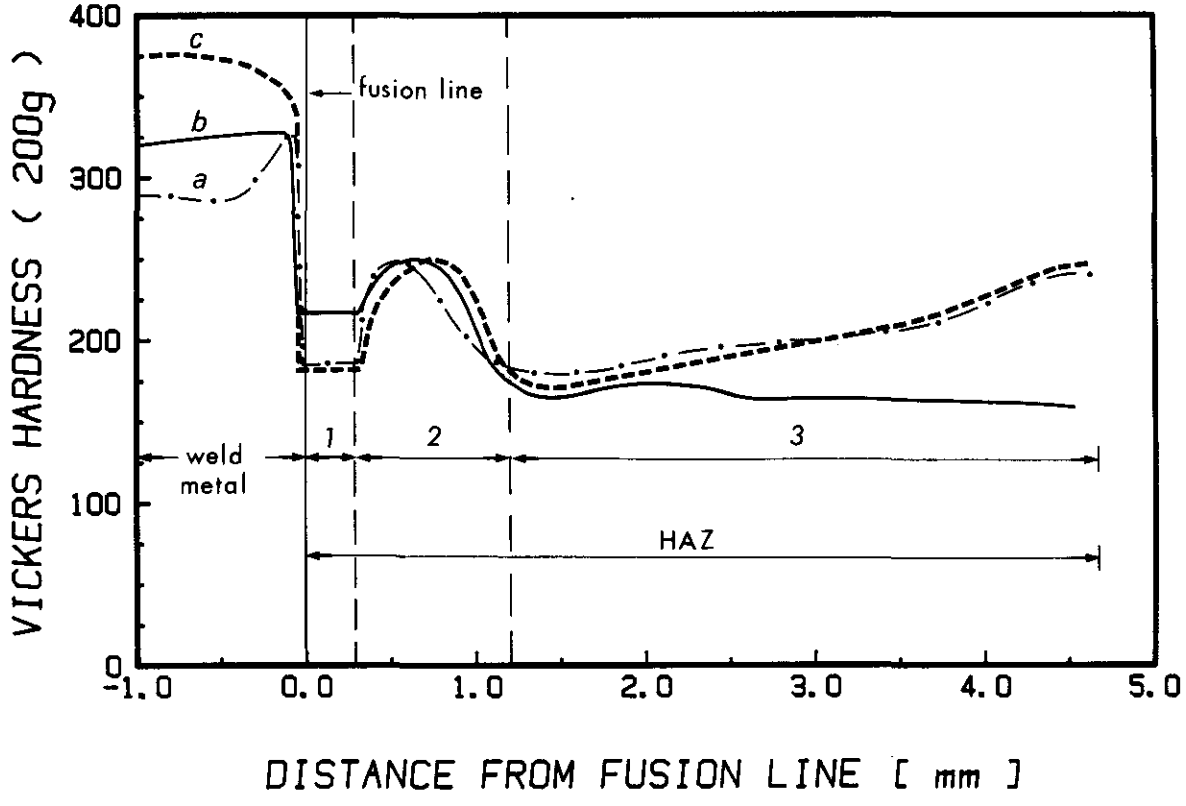

Figure 5.4: Microhardness transverse across the fusion line of bead-on-plate welds on 6.2 mm 3CR12 plate. The transverse was determined at a distance of 0.3 mm below the original plate surface.

Curve a: Hot rolled specimens welded with a 316L filler metal

Curve b: Hot rolled-and-tempered specimens welded with a 316L filler metal

Curve c: Hot rolled specimens welded with an E3CR12 filler metal

Zone 1: Narrow coarse grained HT HAZ. The weighed average hardness which is indicated in the figure was calculated from the microhardness of respectively the ferrite and martensite in this zone

Zone 2: Fine grained duplex HAZ

Zone 3: Low temperature HAZ

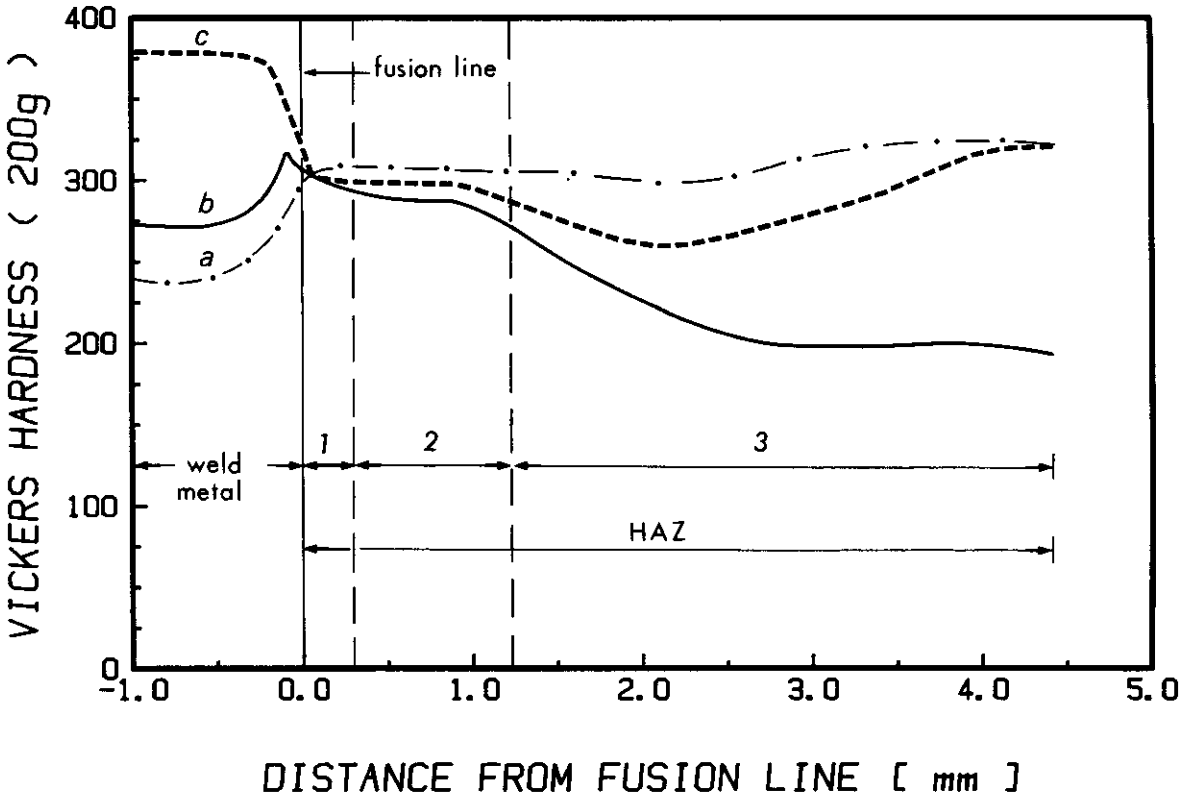

Figure 5.5: Microhardness transverse across the fusion line of bead-on-plate welds on 6.2 mm 3CR12Ni plate. This transverse was determined at a distance of 0.3 mm below the original plate surface.

Curve a. Hot rolled specimens welded with a 316L filler metal

Curve b. Hot rolled-and-tempered specimens welded with a 316L filter metal

Curve c. Hot rolled specimens welded with an E3CR12 filler metal

Zone 1. Narrow coarse grained HT HAZ

Zone 2. Fine grained duplex HAZ

Zone 3. Low temperature HAZ

The specimens were tested at room temperature in slow three point face bending with the bend radius equal to plate thickness. The weld bead was

therefore subjected to tensile stresses during bending. The maximum bend angle for cleavage fracture initiation in the narrow coarse grained HT HAZ was determined.

2.1.3 Experimental results

180° bends were successfully achieved for the hot rolled-and-tempered 3CR12 specimens welded with 316L. Figure 5.6 shows a close view of the weld bead surface of such a bent specimen. The three zones which have previously been identified in the weld HAZ are cleary evident as a result of the different amounts of deformation which occurred in the different zones during bend testing.

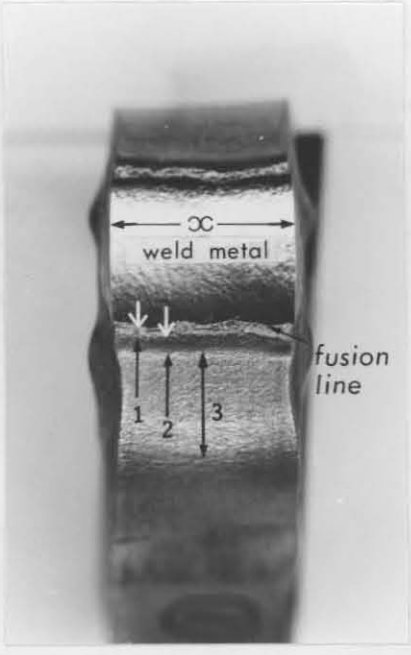

Figure 5.6: Surface view of a hot rolled-and-tempered 3CR12 bent specimen welded with AISI 316L. Note the different amounts of surface deformation which occurred in the coarse grained HT HAZ (zone 1), the fine grained HAZ (zone 2) and the low temperature HAZ (zone 3).

The bend test results are summarized in table 5.1. In each instance

the average of three tests is reported. The relative surface transverse strain of the weld metal and the high (zone 1) and low (zone 3) temperature HAZ, which was achieved at the maximum bend angle, is also shown in table 5.1 together with the parent and weld metal hardness values. The transverse strains are expressed on a ten point scale. These values were obtained by measuring the total transverse deformation ((10-x)/10) of the weld metal and low temperature HAZ (zone 3) together with the width of the coarse grained HAZ (zone 1) in figure 5.6. These values are then expressed on a relative scale with the deformation in that zone which exhibited the largest deformation equal to ten units. The transverse strain is expressed on a relative scale since it depends on the width of the bend specimen.

180° bends were successfully achieved with the hot rolled-and-tempered 3CR12 specimens, welded with AISI 316L. This is primarily due to the large amount of deformation which occurred in the low temperature HAZ (zone 1) as shown in table 5.1 and figure 5.6. Considerable deformation also occurred in the coarse grained HT HAZ (zone 1 in fig. 5.6) with less deformation in the fine grained HAZ (zone 2).

With a large fraction of the total deformation occurring in the low temperature HAZ during bending, the actual bend angle of the weld metal and zone 1 is less than 180° as indicated schematically by the dotted line in figure 5.7.

Table 5.1: Bend test results of bead-on-plate face bend test.

Steel	Condition	Filler metal	Bend angle	Relative deformation expressed on a ten point scale			Vickers Hardness 2.5kg	
				Weld metal	Zone 1 (Fig. 5.6)	Zone 3 (Fig. 5.6)	Weld metal	Parent metal
3CR12	Tempered	316L	180°	3.9	4.8	10	311	165
3CR12	Hot rolled	316L	133°	4.3	10	7	277	246
3CR12	Hot rolled	E3CR12	9°	0	2.5	0.5	374	246
3CR12Ni	Tempered	316L	180°	5.5	1	10	282	196
3CR12Ni	Hot rolled	316L	59°	10	0.2	1.5	220	322
3CR23Ni	Hot rolled	E3CR12	42°	5.2	0.2	1.5	383	322

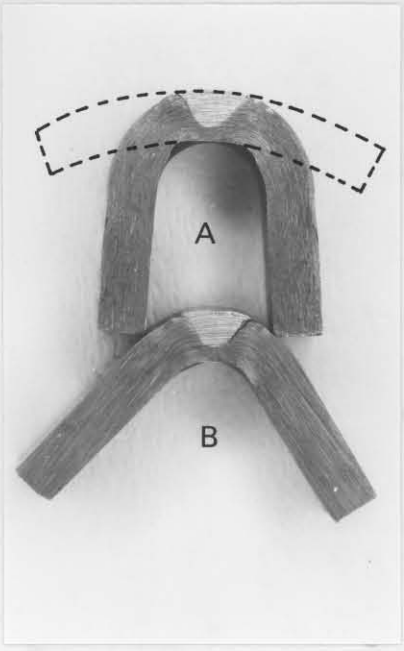

Figure 5.7: Hot rolled-and-tempered (A) and hot rolled (B) 3CR12 bead-on-plate bent specimens welded with 316L.

A maximum bend angle of 133° was obtained for the higher strength hot rolled bent specimens, welded with 316L (fig. 5.7B), before a cleavage fracture occurred in the narrow HT HAZ. A comparison of the surface appearance of such a bent specimen (fig. 5.8) with that of the annealed specimen in figure 5.6 shows that more deformation occurred in the HT HAZ with less deformation in zone 3 (table 5.1). This change in deformation mode in the hot rolled specimens, in comparison to the tempered specimens, occurred as a result of the higher strength of zone 3 with the strength of the HT HAZ unaffected. A brittle cleavage fracture occurred therefore in the narrow HT HAZ with the development of higher stresses during bend testing (the flow stress curve is raised in fig. 5.9) as a result of the higher degree of constraint which was imposed by the higher strength hot rolled low temperature HAZ and parent metal (fig. 5.4).

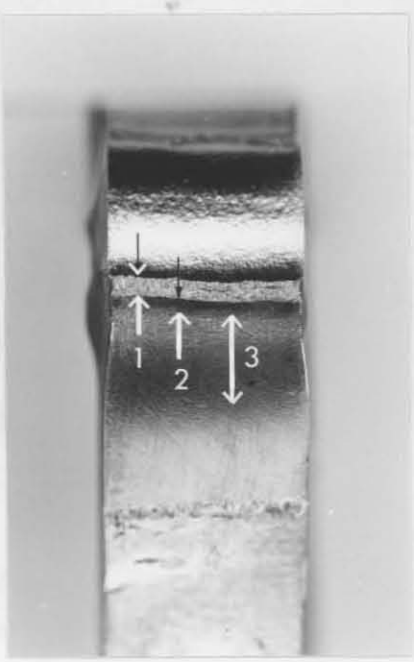

Figure 5.8: Surface view of a hot rolled 3CR12 bent specimen welded with 316L. A comparison with the bent specimen in figure 5.6 reveals that less deformation occurred in zone 3 with more deformation in the HT HAZ (zone 1).

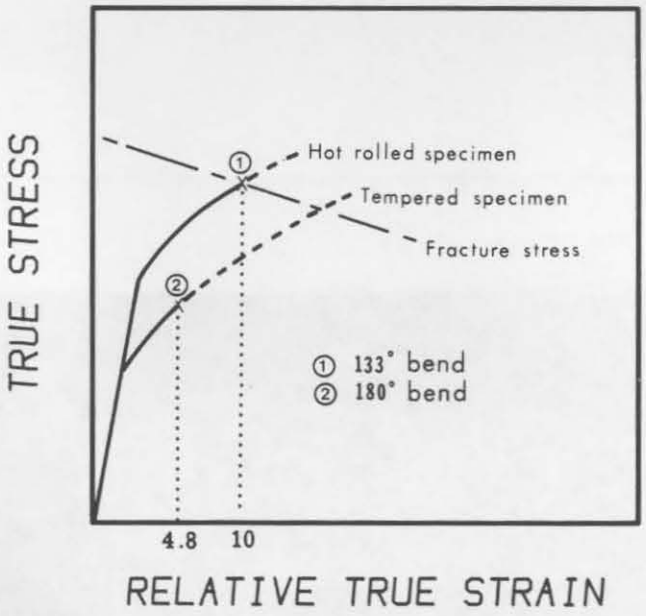

Figure 5.9: Flow stress curves for the HT HAZ (zone 1) of hot rolled and hot rolled-and-tempered 3CR12 bent specimens, respectively.

The unusual high hardness of the 316L weld metal in table 5.1 can be attributed to the high dilution of 40 to 45 percent which occurred during welding, with the subsequent formation of some low carbon martensite in the weld metal. At lower dilutions and consequently lower weld metal strengths, 180° bends may even be obtained with the higher strength hot rolled 3CR12 specimens.

A maximum bend angle of only 9° was achieved with hot rolled 3CR12 specimens welded with a high strength E3CR12 filler metal (fig. 5.4 and table 5.1). This very small bend angle in comparison with a bend angle of 133° for the specimens welded with a lower strength 316L filler metal (fig. 5.10) cleary demonstrates the detrimental effect of this high strength E3CR12 filler metal on the fracture behaviour of this very narrow coarse grained HT HAZ in 3CR12. The top view of a hot rolled 3CR12

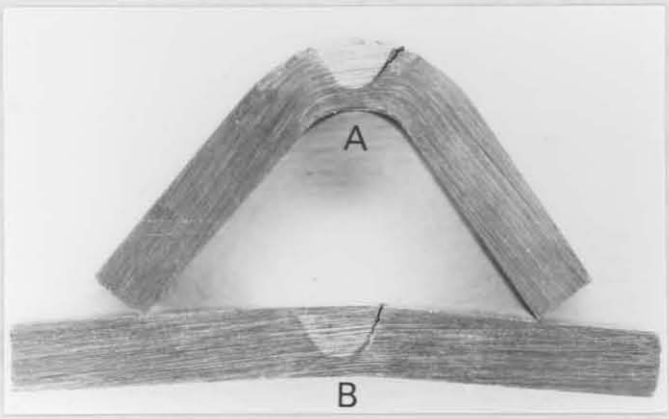

Figure 5.10: Hot rolled bead-on-plate 3CR12 bent specimens welded with a 316L (A) and E3CR12 (B) filler metal. Note the brittle cracks in the coarse grained HAZ adjacent to the fusion line.

bent specimen in figure 5.11 shows that most of the deformation occurred in the low strength HT HAZ. This is also indicated in table 5.1. The reduced fracture ductility of this zone, as a result of the large constraint imposed by the high strength E3CR12 weld metal (fig.5.1), is evident from a comparison of the amount of deformation in this zone shown in figures 5.8 and 5.11.

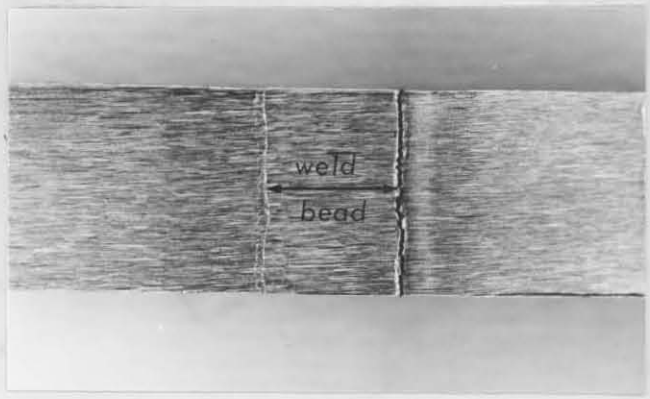

Figure 5.11: Top view of a hot rolled 3CR12 bent specimen welded with E3CR12. The brittle fracture which occurred in the HT HAZ is clearly evident together with the local plastic deformation in this zone on the left hand side of the weld bead.

With the strength of the fine grained HAZ (zone 2) higher than that of the adjacent HT HAZ (zone 1, fig. 5.4) this zone will also constrain the HT HAZ from plastic deformation during bend testing. This is also evident from figures 5.6 and 5.8 which show that less deformation occurred during bending in this zone in comparison with the HT HAZ and low temperature HAZ.

The microhardness transverse across the fusion line of bead-on-plate welds, welded respectively with 316L and E3CR12 filler metals, on 3CR12Ni plate, are compared in figure 5.5. The higher strength of the HT of 3CR12Ni in comparison with the same zone in 3CR12 (fig. 5.4) can be attributed to the finer grain size and higher content of low carbon martensite. This zone will therefore exhibit a higher fracture toughness as well as a higher fracture stress compared to the same zone in 3CR12. The higher toughness may also partly be attributed to the higher nickel content of 3CR12Ni. The fracture behaviour of this zone will also be determined by the mechanical properties of the adjacent weld metal, HAZ and parent metal. Figure 5.5 shows that the hardness of this zone is very similar to that of the adjacent fine grained HAZ (zone 2).

180° bends were successfully achieved with hot rolled-and-tempered 3CR12Ni specimens welded with a 316L filler metal (table 5.1). During bending most of the deformation occurred in the low strength low temperature HAZ (fig. 5.5) with some deformation in the weld metal. As a result of the relatively lower strength of the adjacent weld metal and low temperature HAZ, the fracture stress of the HT HAZ was therefore not exceeded during bending. The actual bend angle of this bend specimen is also, as shown in figure 5.7, less than 180°. This is due to the deformation which was concentrated mainly in the low temperature HAZ.

Figure 5.5 shows that for the hot rolled 3CR12Ni specimens, welded with a 316L filler metal, the hardness of the fine grained and low temperature HAZ is virtually similar to that of the HT HAZ with the hardness of the parent metal higher than that of this zone (table 5.1). A bend angle of only 59° was therefore obtained with this specimen before a cleavage fracture occurred in the HT HAZ. Most of the deformation occurred in the 316L weld metal (table 5.1). This smaller bend angle in comparison with that of the hot rolled-and-tempered specimen was obtained notwithstanding the lower weld metal hardness (220 HV against 282 HV, table 5.1). The weld metal and HT HAZ were subjected to higher stresses during bend testing as a result of the constraint imposed by the higher strength low temperature HAZ and that of the hot rolled parent plate. The flow stress of the austenitic weld metal increased, due to work hardening, to such an extent that at a bend angle of 59° the brittle fracture stress of the HT HAZ was exceeded. This indicates therefore that the fracture behaviour of the HT HAZ or the maximum bend angle is also dependent on the yield strength and work hardening rate of the weld metal. A larger bend angle may have been obtained with a ferritic weld metal with a similar yield stress but a lower rate of work hardening.

The hot rolled 3CR12Ni specimens which were welded with the high strength E3CR12 filler metal fractured by brittle cleavage fracture in the HT HAZ at a bend angle of 42° (table 5.1). The brittle behaviour of this zone in 3CR12Ni indicates that, although its fracture toughness is expected to be superior to that in 3CR12 as a result of its finer grain size and higher martensite and nickel content, the room temperature fracture toughness is still very low.

2.1.4 Discussion

One of the most important observations at this stage is the very low room temperature fracture toughness of the HT HAZ of defect free bead-on-plate welds on 6 mm 3CR12 and 3CR12Ni plate. Successfull 180° bends were achieved only when this zone was protected from high stresses by adjacent soft material (316L weld metal and tempered plate).

The results have clearly demonstrated the detrimental effect of the high strength E3CR12 weld metal on the fracture behaviour of defect-free bead-on-plate welded 3CR12 bend specimens. It has also been shown that the susceptibility of welds to brittle cleavage fracture in the HT HAZ increases with improved parent metal mechanical properties. The fracture behaviour of welds on 6 mm 3CR12 and 3CR12Ni plate is therefore critically dependent on the mechanical properties of the weld metal, base metal and that of the different zones in the weld HAZ.

In the developing filler metals for welding 3CR12 plate, the restrictions on the mechanical properties of the weld metal (yield stress, tensile stress, work-hardening rate) are as important as other requirements such as matching electrochemical, fatigue and fracture toughness properties. When the steel is considered for any high integrity structural type applications with highly restrained weld joints, the mechanical property requirements to insure fracture toughness are of even greater importance.

2.2 Fusion line notch-fracture toughness testing

2.2.1 Introduction

One disadvantage of the bead-on-plate face bend test is that although a qualitative indication is obtained of the effect of the weld and parent metal mechanical properties on the fracture behaviour of welds, the influence of typical 316L and E3CR12 weld metal compositions was not determined. This is due to the unusually high dilutions which occurred with the base metal during welding, with the formation of some low carbon martensite even in the 316L weld metal.

The combined effect of the base metal, HAZ and weld metal on the fracture behaviour of welds on 3CR12 and 3CR12Ni are determined with the bead-on-plate bend test. 180° bends were successfully achieved on annealed 6 mm 3CR12 plate, welded with a 316L filler metal. This is due to the fact that most of the deformation occurred in the low strength, low temperature HAZ during bending. With the presence of a notch type defect on the fusion line, the susceptibility of welds to brittle fracture in the HT HAZ, will be determined by the mechanical properties and fracture toughness of the weld metal rather than the properties of the low temperature HAZ and parent metal. The choice of the correct filler metal for welding 3CR12 therefore becomes even more important.

It was therefore decided that the fusion line notch fracture toughness is a better criterion for comparing different filler metals. In this second part of the present study the effect of different filler metals (AISI 309L, 316L, 308L and E3CR12) on the fusion line notch fracture toughness of welds on 12 mm hot rolled and annealed 3CR12 plate was studied with a newly developed fusion line notch fracture toughness (FLNFT) test.

2.2.2 Fusion line notch fracture toughness test specimen design and preparation

The introduction of a reproducible artificial notch type defect or crack on the weld fusion line has been one of the major design considerations in designing the FLNFT test specimen shown in figure 5.12. The specimen is machined from a welded cruciform test specimen shown in figure 5.13. The cruciform test specimen is prepared by welding 12 mm hot rolled-and-tempered 3CR12 plate sections (100 mm x 200 mm) to the machined top and bottom surfaces of a 200 mm x 200 mm x 12 mm 3CR12 plate section. The plates were tack welded prior to welding in order to prevent distortion during welding.

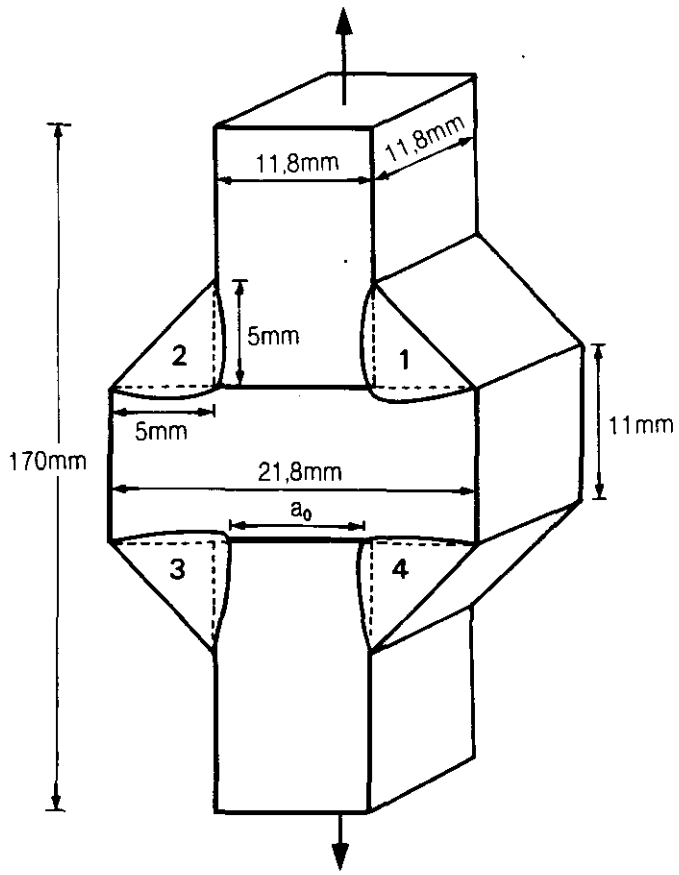

Figure 5.12: FLNFT test specimen design. a_0 is the artificial through-thickness crack length. The sequence of welding of the single bead fillet welds is also indicated.

The single bead fillet welds on the cruciform specimen were welded in the sequence shown in figure 5.12 according to the following welding procedure:

Welding process	:	Shielded metal arc
Filler metal	:	AISI 309L (3.25 mm dia.)
	:	AISI 316L (3.25 mm dia.)
	:	AISI 308L (3.25 mm dia.)
	:	E3CR12 (3.25 mm dia.)
Welding position	:	Flat
Heat input	:	1.4 kJ/mm (160amp, 23 volts)
	:	1.2 kJ/mm (110amp, 28 volts)

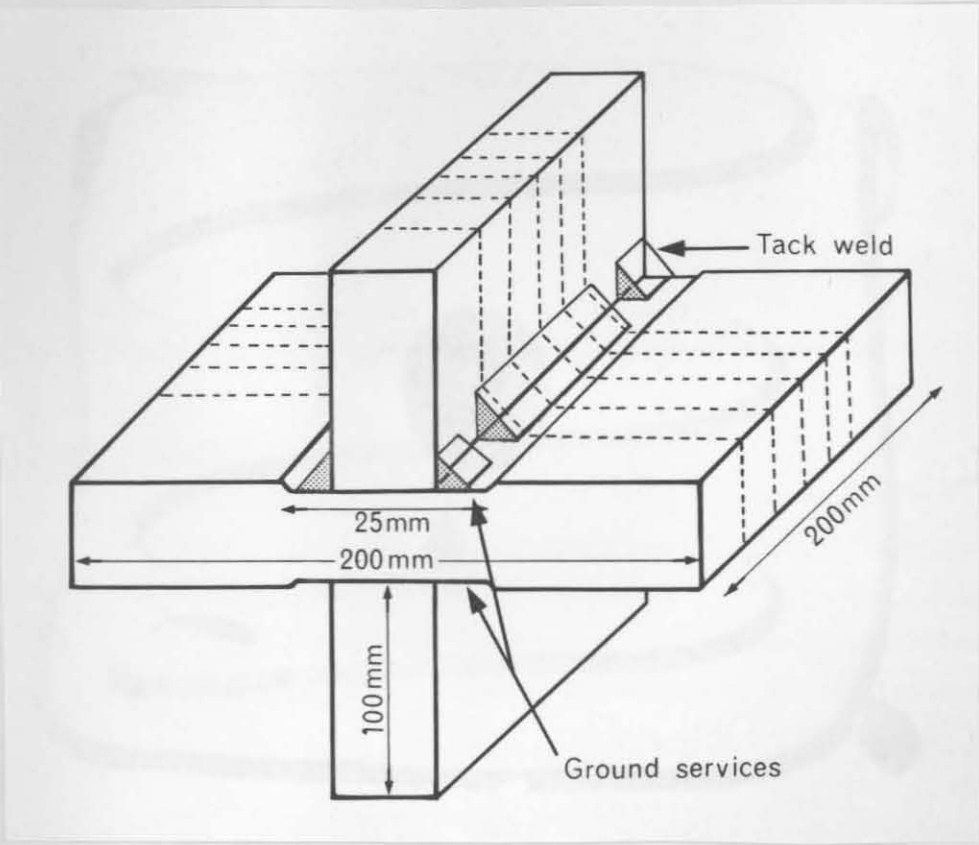

Figure 5.13: Cruciform test specimen.

Both high weld heat input (1.4 kJ/mm) and low weld heat input (1.2 kJ/mm) cruciform specimens were prepared with AISI 309L, 316L, 308L and E3CR12 filler metals, respectively. The cruciform specimens were allowed to cool to room temperature prior to welding subsequent fillet welds. Each subsequent fillet weld is subjected to a higher degree of constraint during cooling than the previous one, and if cracking occurred it was usually restricted to the fourth weld.

Four FLNFT test specimens were machined from the centre part of a cruciform specimen. One specimen was polished, etched and examined to establish whether any cracking has occurred in the weld or base metal.

Figure 5.14 shows a polished and etched section of a FLNFT test specimen which was welded with an E3CR12 filler metal at a heat input of 1.4 kJ/mm. The HT HAZ of each fillet weld together with the two artificial through-thickness cracks are clearly evident.

Figure 5.14: Polished and etched section of an FLNFT test specimen with the HT HAZ and two through-thickness cracks clearly evident. A clip gauge was attached to the specimen at the two small drilled holes during testing.

2.2.3 Experimental results and discussion

The FLNFT specimens were tested at room temperature by tensile testing. The load versus crack-opening-displacement (COD) curves were determined at a crosshead speed of 20 mm/min. The total crack-opening-displacement (δ) of the two through-thickness cracks were measured during testing with a clip gauge attached to the specimen at the small drilled holes shown in figure 5.14. The maximum load Pm together with the total crack-opening-displacement (δ_m) at maximum load were determined from the load-displacement curves as shown in figure 5.15. For the particular design of the FLNFT specimen (fig. 5.14) the measured crack-opening-displacement is equal to the crack-tip-opening displacement (δ =2CTOD) (17).

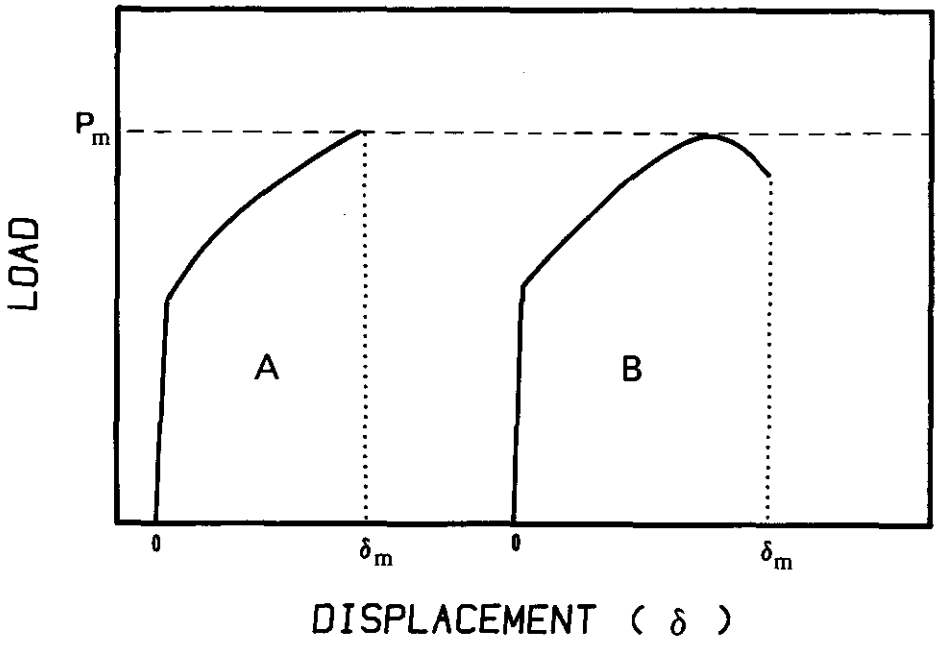

Figure 5.15: Typical load versus crack-opening displacement (δ) curves for the FLNFT test specimen.

Depending on the weld metal mechanical properties and the weld heat input, the FLNFT test specimens fractured in four possible different modes. The different failure modes are shown in figure 5.16. The load-displacement curves of specimens which fractured with modes 1 and 2 corresponded with curve A in figure 5.15 while specimens which fractured with modes 3 and 4 had load-displacement curves similar to curve B in figure 5.15.

The fusion line notch-toughness test results is summarized in table 5.2. In each instance the average result of three similar tests is reported.

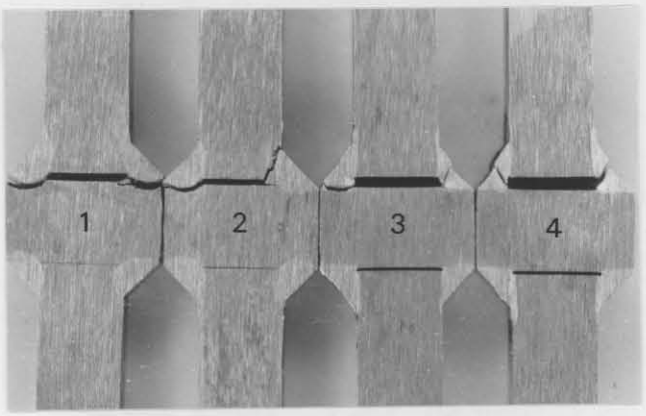

Fracture mode : 1. Cleavage fracture in HT HAZ of both fillet welds
2. Cleavage fracture in HT HAZ of both fillet welds
3. Cleavage fracture in HT HAZ of one fillet weld and ductile tearing in the weld metal of the second fillet weld
4. Ductile tearing in the weld metal of both fillet welds

Figure 5.16: Different fracture modes of FLNFT specimens. Note the increase in the COD with fracture mode transitions from mode 1 to 4.

Table 5.2: Fusion line notch fracture toughness test results.

Filler metal	Heat input (kJ/mm)	Hardness (HV) weld metal*	Crack length a_o (Fig. 5.12)	Max. load (MPa)	Displacement m(mm) (Fig. 5.15)	Fracture mode (Fig. 5.16)
Nicromax 309L	1.40	200	10.90	322	1.02	4
	1.21	184	11.90	291	1.45	3 and 4
Transarc 316L	1.40	207	11.35	315	0.76	4
	1.21	186	12.00	292	1.15	3 and 4
Transarc 308L	1.40	280	11.26	337	0.42	1
	1.21	185	11.94	295	0.98	3
Transarc E3CR12	1.40	373	8.90	456	0.15	1 and 2
	1.25	372	10.80	386	0.30	1 and 2

* The parent metal hardness of the hot rolled and tempered 3CR12 plate is 160HV.

2.2.3a High heat input (1.4 kJ/mm) test results

At a weld heat input of 1.4 kJ/mm, complete joint penetration of the fillet welds was achieved with each of the four filler metals (AISI 309L, 316L, 308L and E3CR12). Figure 5.14 shows an example of such a specimen welded with an E3CR12 filler metal. The crack tips of the through-thickness cracks were therefore successfully positioned on the weld fusion line of the fillet welds as shown for example in figures 5.17 and 5.18 for FLNFT specimens welded with E3CR12 and 316L filler metals, respectively. Figure 5.17 shows a smaller through-thickness crack tip radius for the specimen welded with an E3CR12 filler metal compared to the crack tip radius of the specimen in figure 5.18. This resulted from the higher constraint in the HAZ of the high strength E3CR12 fillet welds compared to the constraint in the HAZ of the lower strength austenitic fillet welds (table 5.2).

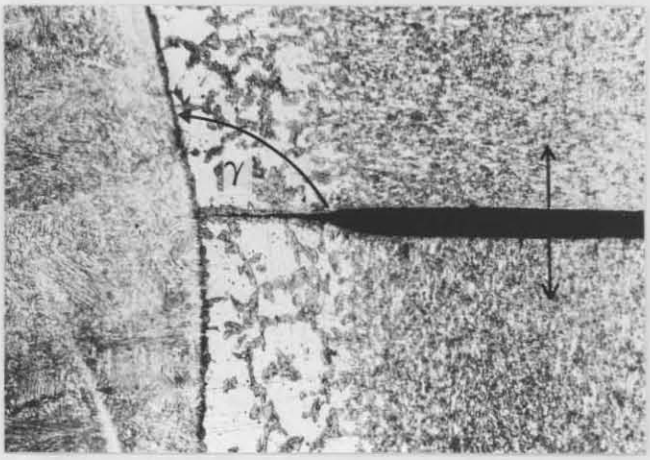

Figure 5.17: Through-thickness crack in a FLNFT test specimen with the crack tip on the fusion line of the E3CR12 weld metal. The direction of the principal load during tensile testing is indicated (35X).

The direction of the principal applied load during tensile testing is indicated in figure 5.17. A difference in the relative orientation (γ) between the through-thickness cracks and the fusion line of some of the E3CR12 welds (fig. 5.17) in comparison with the austenitic welds (fig. 5.18) was observed. The smaller angle (γ) in figure 5.17 is due to the

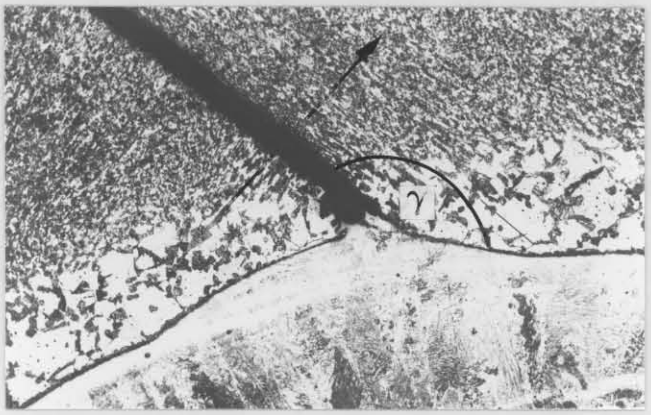

Figure 5.18: Through-thickness crack in an FLNFT test specimen with the crack tip on the fusion line of the 308L weld metal. The direction of the principal load during tensile testing is indicated (35X).

deeper penetration during welding with the thinner 3.15 mm diameter E3CR12 electrode (table 5.2). Although the angle (γ) is determined by the amount of weld bead penetration, roughly similar values were achieved for most of the fillet welds of the different austenitic filler metals.

A microscopic investigation of the FLNFT specimens, after welding and machining revealed that weld cracking occurred only in some fillet welds of the specimens welded with the E3CR12 filler metal. The cracking occurred in the fourth welded segment which was subjected to the highest degree of constraint. Figure 5.19 shows such a crack in the predominantly martensitic crack sensitive E3CR12 weld metal. The cracked specimens were not used for fracture toughness testing. These cracks are most probably hydrogen-induced cold cracks which developed as a result of inadequate drying of the welding electrodes. The electrodes were dried at 350°C for one hour prior to welding.

The bead-on-plate bend test results have shown that the cleavage fracture stress of the HT HAZ in 3CR12 is much lower than the ductile fracture stress of the predominantly austenitic 316L weld metal. The fracture stress, which also depends on the test temperature, usually increases with a decrease in grain size. With the crack tip on the fusion line (figs 5.17

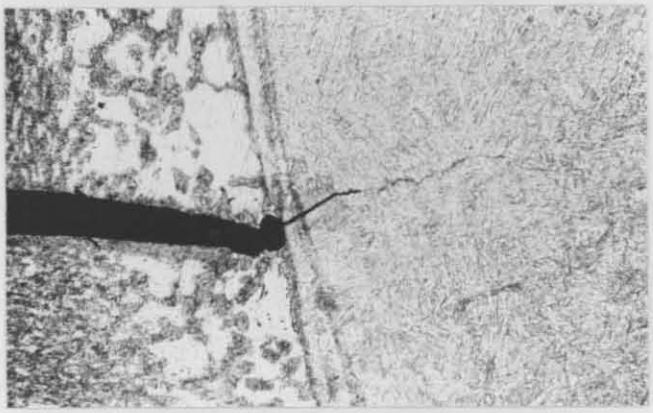

Figure 5.19: Weld metal crack in the fillet weld of a FLNFT test specimen welded with an E3CR12 filler metal. The crack initiated after some crack tip blunting of the through-thickness crack (35X).

and 5.18) the weld metal at the crack tip will be subjected to the maximum tensile stress during tensile loading. Since a smaller component of the principal stress is expected to result in fracture in the HT HAZ, a ductile fracture or tear may occur in the weld metal even with the fracture stress of the weld metal much higher than the fracture stress of the HT HAZ. A brittle fracture will therefore occur in the HT HAZ only when the component of the principal stress, which acts perpendicularly to the fusion line, exceeds the fracture stress of this zone before the principal stress exceeds the fracture stress of the weld metal.

The FLNFT specimens, which were welded with a heat input of 1.4kJ/mm and with AISI 309L and 316L filler metals respectively, fractured by ductile tearing in the weld metal (mode 4 in fig. 5.16). Sections through the two fillet welds on the side of fractured FLNFT specimens which did not fracture during testing, showed the crack tip state prior to fracture. Figure 5.20 shows crack tip blunting of a through-thickness crack in one of the fillet welds of a 309L welded and tested FLNFT specimen. Small voids have already developed at the crack tip indicating incipient tearing. Figure 5.21 shows that stable crack extension has occurred in the 309L weld metal of the second fillet weld prior to primary fracture. The results indicate that some stable crack extension occurred during tensile testing

when the maximum applied load was reached.

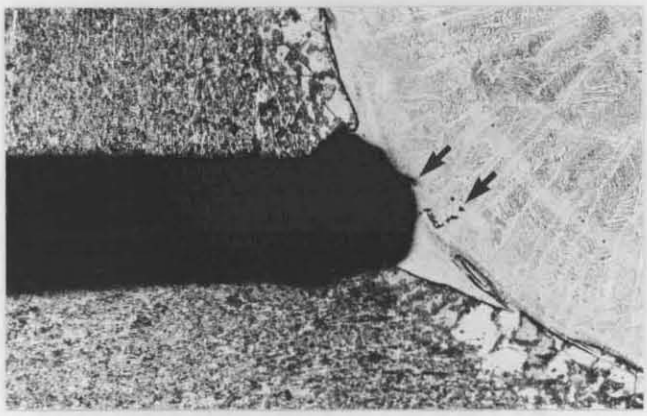

Figure 5.20: Crack tip blunting in the 309L weld metal of a fractured FLNFT specimens. Small voids have already initiated at the crack tip which shows incipient tearing (arrows) (35X).

Although the 309L and 316L welded FLNFT specimens have similar weld metal strengths and although similar maximum loads were applied during tensile testing, a larger total crack-opening-displacement (δm = 1.02 mm) was obtained for the 309L welded specimen than the δm value of 0.76 mm for the 316L welded specimen.

Figure 5.21: Stable crack extension in the 309L weld metal of a through-thickness crack in a fractured FLNFT specimen (35X).

Assuming that the δm value is a qualitative indication of the crack tip plastic zone size prior to fracture, a larger plastic zone developed in the 309L weld metal in comparison with that of the 316L weld metal. The larger plastic zone probably developed as a result of a lower yield stress which in turn can be attributed to a lower ferrite content. The weld metal hardness of different weld metals indicate the relative weld metal tensile strengths but does not necessarily indicate the relative yield stress values of the weld metal.

The FLNFT test specimens, welded with a 308L filler metal, fractured at an δm value of 0.42 mm by cleavage fracture in the coarse grained HT HAZ of both fillet welds (mode 1, fig. 5.16). Less crack tip blunting occurred and therefore a smaller crack tip plastic zone developed. This is due to the higher weld metal yield and tensile strength (table 5.2) in comparison with the plastic zone in for example the 316L welded specimen. The higher strength weld metal induces some plastic constraint at the crack tip, reducing plastic deformation or crack tip blunting. This results in the development of higher stresses in the HT HAZ. After a certain amount of crack tip blunting, transgranular cleavage cracks initiated in the HT HAZ prior to unstable brittle cleavage fracture in this zone (fig. 5.22).

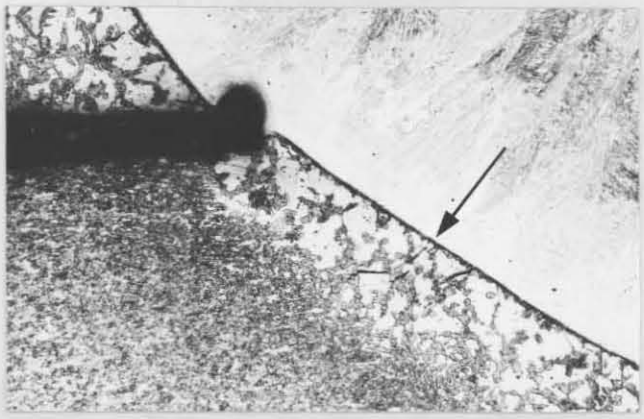

Figure 5.22: Crack tip blunting in the 308L weld metal of a FLNFT specimen during tensile loading. Small transgranular cleavage cracks have already initiated in the coarse grained HAZ. Compare crack tip blunting and δm value of this specimen with that of the 309L welded specimen in figure 5.20 (35X).

The FLNFT test specimens, welded with an E3CR12 weld metal, also fractured by cleavage in the HT HAZ of both fillet welds (modes 1 and 2, fig. 5.16). The high strength E3CR12 weld metal plastically constrained the crack tip from plastic deformation to a much greater extent in comparison with the 308L and 316L weld metals. Most of the crack tip blunting occurred in the lower strength, HT HAZ (fig. 5.12) before a cleavage fracture occurred. Table 5.2 shows that the δm value in this zone was only 0.15 mm.

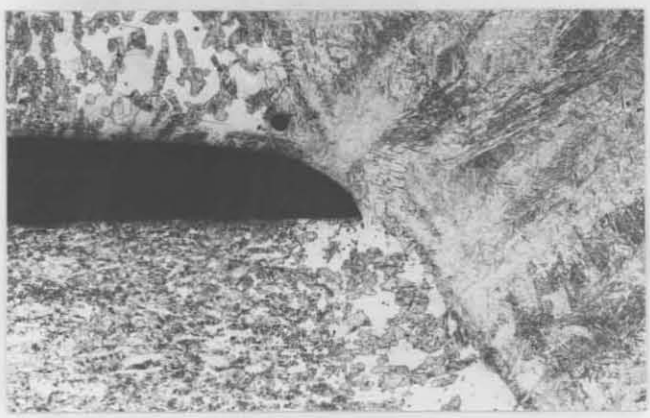

Figure 5.23: Crack tip blunting in an E3CR12 welded FLNFT test specimen during tensile loading. Incipient tearing has already occurred at the crack tip (270X).

Much higher maximum loads were reached with the E3CR12 welded specimens in comparison with the other specimens (table 5.2). This can be attributed partly to the shorter initial crack length of these specimens.

2.2.3b Low heat input (1.2 kJ/mm) test results

Complete joint penetration was not achieved at a weld heat input of 1.2 kJ/mm. A much larger initial crack tip radius resulted as shown in figure 5.24. Larger δm values were therefore measured for the FLNFT specimens welded at a low weld heat input (table 5.2). The largest δm value was again obtained with a 309L filler metal while the smallest δm value was again measured on the E3CR12 welded specimen.

Two of the three test specimens of both the 309L welded and 316L welded

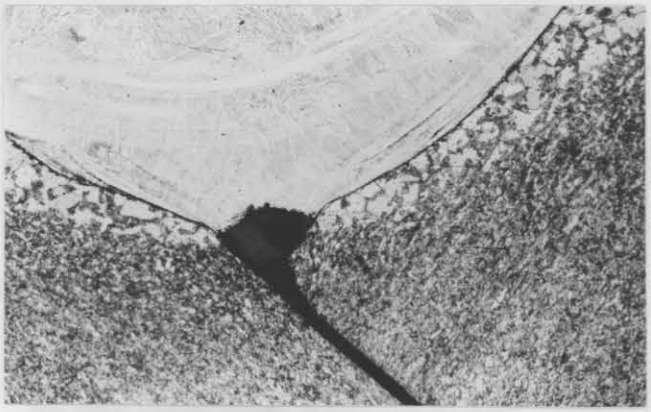

Figure 5.24: Through-thickness crack tip in an FLNFT test specimen welded with a 308L filler metal with a heat input of 1.2 kJ/mm. Note the incomplete joint penetration of the fillet weld (35X).

FLNFT test specimens fractured by tearing or ductile fracture in both fillet welds (mode 4, fig. 5.16). The third specimen fractured by ductile fracture in the one fillet weld and by cleavage fracture in the coarse grained HT HAZ of the second fillet weld (mode 3, fig. 5.16). The δ_m values for these specimens were smaller (0.91 mm for the 309L and 1.1 mm for the 316L welded specimen) than the average values reported in table 5.2. Sections of the fractured specimens (fig. 5.25) revealed that brittle

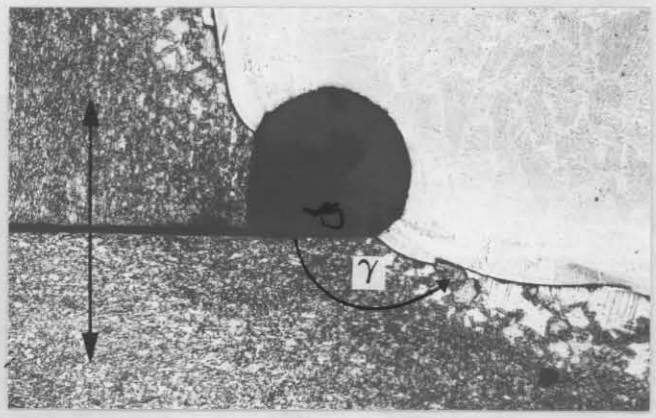

Figure 5.25: Incomplete joint penetration of a fillet weld in a FLNFT test specimen welded with a 309L filler metal. The direction of the principal stress during tensile loading is indicated (35X).

fracture occurred in the HT HAZ of fillet welds with even less joint penetration in comparison with the average joint penetration shown in figure 5.24.

In the case of incomplete weld joint penetration the relative orientation between the through-thickness crack and the fusion line (Υ in fig. 5.25) is such that the coarse grained HAZ is subjected to a larger tensile stress than the same zone in a full penetration joint shown in figure 5.18. Since the fracture stress of the austenitic weld metal is higher that that of the HT HAZ, the incompletely penetrated fillet weld will be more susceptible to brittle cleavage fracture in the HT HAZ.

Sections through both the 309L and 316L welded and fractured FLNFT specimens which fractured by cleavage fracture in the HT HAZ of one of the fillet welds (mode 3, fig. 5.16), revealed that a ductile crack has also initiated and propagated in the weld metal of this fillet weld. Some stable crack extension therefore occurred probably in the weld metal prior to cleavage fracture in the HT HAZ. The detection of stable crack growth prior to fracture is extremely difficult with a conventional COD bend test specimen(17). With two through-thickness cracks in the FLNFT test specimen, stable crack extension prior to fracture has been positively identified (figs. 5.21 and 5.26). The δm values reported were therefore determined at maximum load (fig. 5.15).

Figure 5.26: Section through the fillet weld of a 309L welded and fractured FLNFT specimen which fractured by cleavage fracture in the HT HAZ of one fillet weld. The direction of propagation of the cleavage crack is indicated by an arrow.
Note also the ductile tearing in the weld metal (35X).

Table 5.2 shows that different δm values were obtained for the specimens welded with 309L, 316L and 308L filler metals, respectively in spite of similar maximum loads during testing and although the weld metal hardness is the same for the different weld metal compositions. The different plastic zone sizes (δm) may be attributed to different weld metal yield strength and different weld metal work hardening rates. A larger crack tip plastic zone will result with a lower weld metal yield strength and a lower weld metal work hardening rate.

The FLNFT specimens, welded with an E3CR12 filler metal, fractured by brittle cleavage fracture in the coarse grained HT HAZ of two fillet welds. A larger δm value (0.3 mm) was obtained for the specimen welded with a low heat input (1.2 kJ/mm) than the value of 0.15 mm for the specimen welded with a heat input of 1.4 kJ/mm. The larger δm value may be attributed to the low heat input and the incomplete penetration.

Table 5.2 shows, apart from the incomplete penetration effect, significant differences, between the low and high weld heat input test results of 308L welded specimens. At the lower weld heat input a much lower weld metal strength was obtained and the maximum applied load dropped. A fracture mode transition occurred and δm increased with 0.56 mm. These differences can be attributed to the formation of some low carbon martensite in the weld metal of the high heat input welds. This is due to a large dilution with the base metal (fig. 5.27). The low heat input weld metal exhibited only austenite and some interdendritic δ-ferrite structures (fig. 5.28).

Figure 5.27: Weld metal microstructure of a FLNFT test specimen welded with a 308L filler metal with a heat input of 1.4 kJ/mm. The microstructure consists of austenite, martensite and interdentritic ferrite (250X).

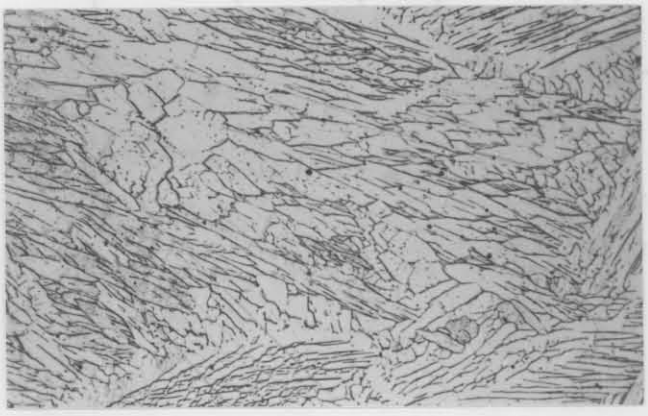

Figure 5.28: Weld metal microstructure of a FLNFT test specimen welded with a 308L filler metal with a heat input of 1.2 kJ/mm. The microstructure consists only of austenite and interdendritic δ-ferrite (250X).

The Schaeffler diagram in figure 5.29 was used to determine graphically the minimum percentage dilution which is required for the formation of martensite in 309L, 316L and 308L weld metals, respectively, during welding of 3CR12 (table 5.3). The chemical compositions of the different filler metals which were used to calculate the chromium and nickel equivalents are also shown in table 5.3.

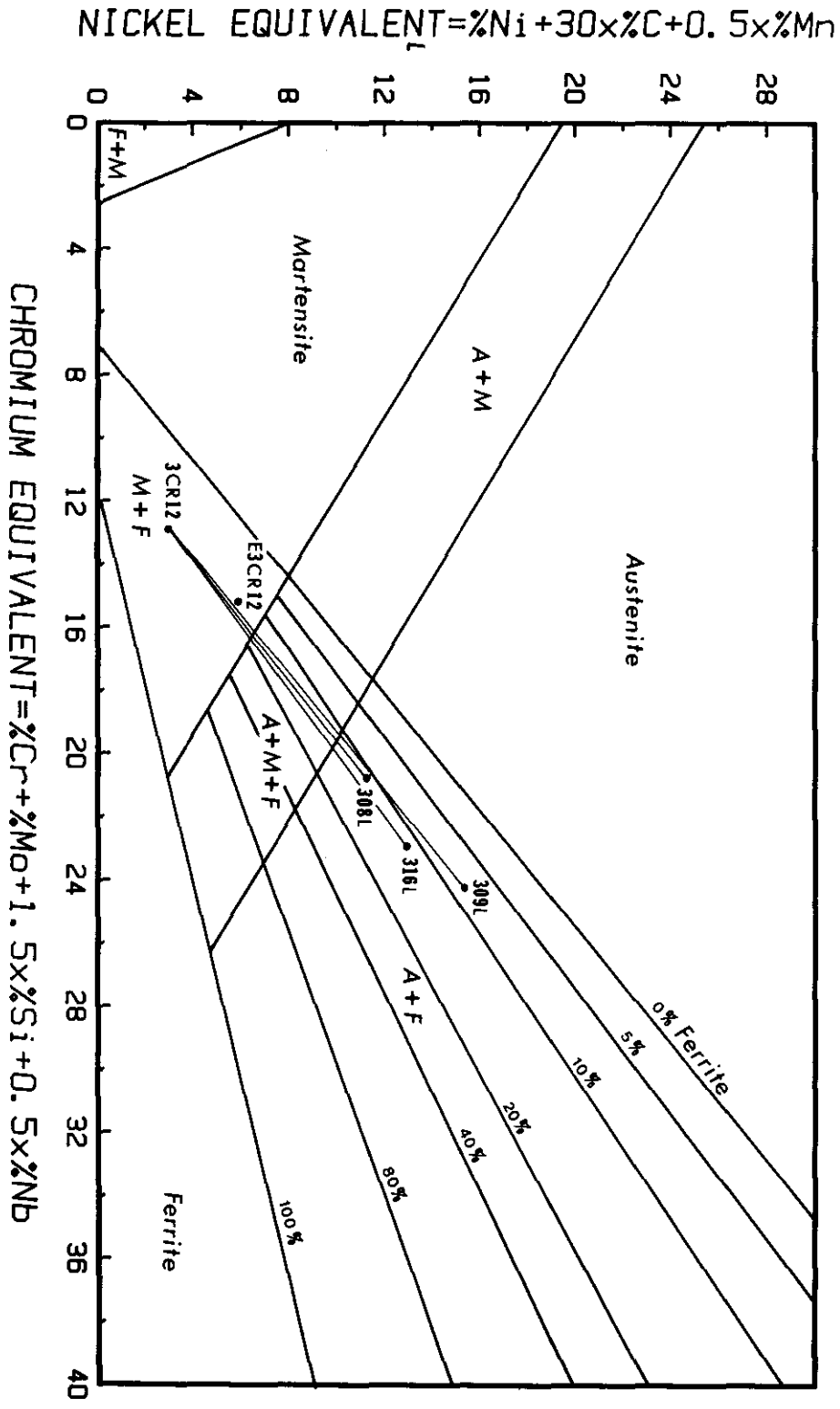

Figure 5.29: Schaeffler diagram. Superimposed on the diagram are the dilution lines for welding 3CR12 with 309L, 316L and 308L filler metals, respectively.

Table 5.3: Typical chemical compositions of AISI 309L, 316L and 308L filler metals. The critical dilution with 3CR12 base metal for martensite formation is also included.

Filler metal	%C	%Si	%Mn	%P	%S	%Cr	%Ni	%Mo	% dilution
309L	0.02	0.40	2.20	0.015	0.015	23.5	13.5	-	43
316L	0.02	0.40	1.80	0.015	0.015	19.0	11.5	2.2	27
308L	0.02	0.40	1.80	0.015	0.015	20.0	10.0	-	16
E3CR12*	0.03	0.67	0.87	0.013	0.012	13.6	4.9	0.5	0

*Chemical composition obtained by chemical analysis of an MIG welded multilayer cladded 3CR12 plate.

Table 5.3 shows that more than 16 percent dilution occurred during welding with a 308L filler metal at a heat input of 1.4 kJ/mm, while less than 16 percent dilution occurred during low heat input welding. The absence of any martensite in both the 309L and 316L weld metals indicates that less than 27 percent dilution (table 5.3) occurred with the base metal during welding at a high heat input.

The microstructure of the high strength E3CR12 weld metal consists of low carbon martensite with some interdendritic δ-ferrite (fig. 5.30). Superimposed on the Schaeffler diagram is also the composition of the E3CR12 filler metal which is situated in the martensite-ferrite dual phase field.

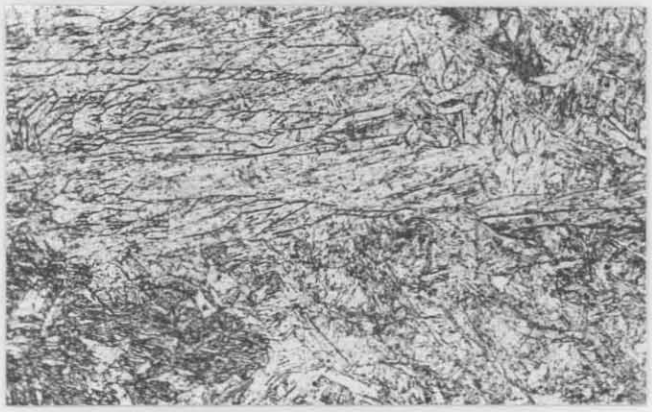

Figure 5.30: Weld metal microstructure of an FLNFT test specimens welded with an E3CR12 filler metal at a heat input of 1.2 kJ/mm. The microstructure consists of martensite and interdendritic δ-ferrite (250X).

3. GENERAL DISCUSSION

3.1 Filler metals for welding 3CR12

The bead-on-plate bend test results have clearly illustrated the cumulative effect of the base metal, weld metal and low temperature HAZ mechanical properties on the plane stress fracture behaviour of the narrow HT HAZ of welds on 3CR12 plate. In welds subjected to a high degree of restraint, the susceptibility of these welds to brittle cleavage fracture in the HT HAZ is primarily determined by the fracture toughness and mechanical properties of the weld metal. This fact was successfully confirmed with the FLNFT test. The susceptibility of welds to brittle fracture in the HT HAZ increased with higher weld metal yield-, tensile strength and work hardening rate.

The test results in table 5.2 indicate that the FLNFT test is a reliable test to compare different filler metals for welding 3CR12 plate. The choice of a certain filler metal will therefore determine the fusion line notch fracture toughness of welds on 3CR12. Although the E3CR12 weld metal meets the requirements on the electrochemical, fatigue and fracture

toughness properties, this high strength weld metal has a detrimental effect on the fusion line fracture toughness of welds on 3CR12(15). It is therefore not recommended for welding 3CR12 in any critical structural type application.

Both the low and high weld heat input FLNFT test results in table 5.2 show that the highest fusion line fracture toughness (δ m) for fillet welds on 12 mm 3CR12 plate was obtained with a 309L weld metal. Due to the high dilution capacity of this filler metal (table 5.3), satisfactory results are expected for dilutions up to 43%. At higher dilutions the fusion line fracture toughness will be reduced with the formation of some weld metal martensite. This filler metal is therefore recommended for welding 3CR12 for high integrity structural applications.

Satisfactory results were also obtained with both the low and high weld heat input specimens, welded with a 316L filler metal, although the fusion line fracture toughness of these welds are lower than the toughness values of the 309L welds (table 5.2). The mechanical properties of the 316L weld metal shown in table 5.2 indicate that the maximum dilution with the base metal did not exceed 27% during welding (table 5.3). At dilutions higher than 27% the fusion line fracture toughness will also be reduced as a result of the formation of martensite in the weld metal. In practice dilutions higher than 27% are common, depending on the weld joint design, the welding process and the weld heat input during welding. The following dilutions can occur with manual metal-arc welding:

a. Root run or square butt with gap : 30-40%
b. Single run fillet or normal cladding : 20-30%

TIG dilution varies from 20-35% for butt and fillet welds. MIG welds usually give 20-45% dilution, while submerged arc gives 30-50%. Fill passes of multirun welds can range from 0-45% depending upon the process and the exact position of the run. Careful control should therefore be exercised when welding 3CR12 with a 316L filler metal in order to limit the dilution during welding.

A type 308L filler metal is not recommended for welding 3CR12 due to the formation of martensite in the weld metal at dilutions exceeding 16%. The

results in table 5.2 clearly show the detrimental effect of martensite formation in the 308L weld metal on the fusion line fracture toughness.

At this stage 309L filler metal appears to be the best filler metal for welding 3CR12. The major disadvantages of this filler metal is its high cost and the possibility of galvanic corrosion in certain environments. Neither the E3CR12 nor 309L filler metals, therefore meet both the mechanical (fusion line notch fracture toughness) and electrochemical requirements as a filler metal for welding 3CR12. In practice the specific application will dictate the choice of one of these filler metals.

The higher mechanical properties of the E3CR12 weld metal compared to those of annealed 3CR12 plate may be predicted from the Schaeffler diagram. The composition of any weld metal with matching electrochemical properties with the 3CR12 base metal will probably be situated in the martensite-ferrite dual phase field of the Scheffler diagram (fig. 5.29). Superimposed on the Schaeffler diagram in figure 5.29 is the composition of E3CR12. The mechanical properties of such an as-deposited weld metal will always be higher than that of the tempered 3CR12 base metal as a result of the relatively large amount of untempered martensite in such a weld metal.

3.2 Fusion line-defect orientation

It has been shown that the fusion line fracture toughness of the fillet welds of the FLNFT specimen is not only dependent on the weld metal mechanical properties but that it is also dependent on the relative orientation (Υ in fig. 5.25) between the through-thickness crack (simulated fusion line defect) and the fusion line or HT HAZ. The relative orientation between a through-thickness crack and the fusion line is determined by the weld joint penetration and the welding process. Figure 5.31 shows a section through the fillet welds of an FLNFT specimen which was welded with the MIG process with a 1.6 mm diameter 316L filler metal and a heat input of 0.41 kJ/mm. The two simulated through-thickness cracks are indicated with arrows. The angle Υ for the MIG welds in figure 5.31 is much smaller than that of MMA welds in figure 5.14. For similar weld metal mechanical properties the MIG fillet welds will be less susceptible (larger δm value) to brittle cleavage fracture in the HT HAZ than MMA fillet welds.

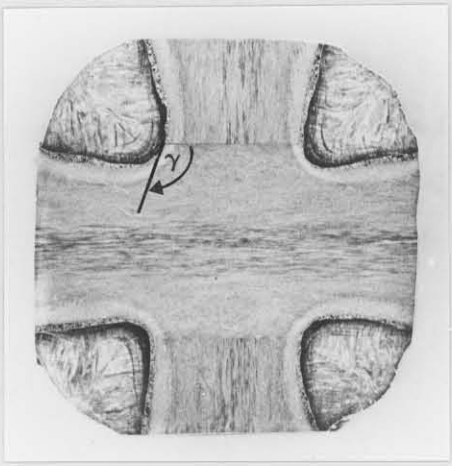

Figure 5.31: Section through the fillet welds of a MIG welded FLNFT test specimen.

The HT HAZ will be subjected to the maximum tensile stresses which develop at the through-thickness crack tip during tensile loading of the FLNFT specimen when the angle γ is equal to 180°. In practice this condition may occur with some fusion line defects such as incomplete joint and root penetration, lack of side-wall fusion, undercutting, slag inclusions, etc. A brittle cleavage fracture in the HT HAZ will then be inevitable during tensile loading since the fracture stress of the HT HAZ with 40% martensite is lower than the fracture stress of the austenitic weld metal. The weld metal mechanical properties will again determine whether a cleavage fracture will initiate from such a fusion line defect at the maximum design stress of the joint. The amount of crack tip blunting (δm value) which may occur at a certain design stress and which thus limits the maximum stress at the crack tip, is mainly determined by the weld metal yield strength and work hardening rate. For a particular design stress the susceptibility of a weld to cleavage fracture in the HT HAZ, with γ equal to 180° is increased by a higher weld metal yield strength.

As a result of the much finer grain size, the fracture stress of an austenitic weld metal, e.g. AISI 316L, with a yield stress similar to that of tempered 3CR12 plate, is much higher than the fracture stress of the coarse grained HT HAZ which contains for example 40% martensite. It therefore appears impossible to develop a weld metal with a yield stress matching that of 3CR12 base metal but with a fracture stress which is lower

than that of the HT HAZ. This is only possible if the yield and fracture stress of the HT HAZ is increased by increasing the martensite content of this zone with the resultant reduction in grain size. The fusion line notch fracture toughness of a 316L weld on 3CR12Ni plate will thus be higher than that on 3CR12 plate due to the higher martensite content and fracture stress of the HT HAZ in 3CR12Ni.

3.3 Conclusion

It can be concluded that the FLNFT test is a more reliable test than the conventional bend and crossweld tensile tests for evaluating different filler metals for welding 3CR12. Although a 309L weld metal on 3CR12 greatly enhances the fusion line fracture toughness of welds, the very low fracture toughness of the HT HAZ is evident from the test results. It is therefore doubtful whether 3CR12 steel should be specified for any critical structural applications.

4. SUMMARY

a. The room temperature fracture toughness of the high temperature coarse grained HAZ of welds on both 3CR12 and 3CR12Ni steels is relatively low.

b. The fracture behaviour of the HT HAZ of defect-free bead-on-plate welds on 3CR12 and 3CR12Ni plate is dependent on the degree of restraint in this zone. The susceptibility of welds to brittle fracture in this zone increases at a higher constraint which is associated with a higher base metal and weld metal yield strength and work hardening rate.

c. A new test method has been developed for measuring the fusion line notch fracture toughness of fillet welds on 3CR12. Different filler metals for welding 3CR12 were characterised by evaluating the fusion line notch fracture toughness of welds. The susceptibility of welds to brittle cleavage fracture initiation, in the HT HAZ, from fusion line defects increases with a higher weld metal yield stress and work hardening rate.

d. A type AISI 309L weld metal is recommended for welding 3CR12 plate, especially for high integrity structural applications.

e. The maximum dilution should be limited when welding 3CR12 with a type AISI 316L weld metal.

f. Types E3CR12 and AISI 308L filler metals are not recommended for welding 3CR12 for any structural type applications.

g. The reliability and integrity of as-welded 3CR12 structures welded with even a 309L filler metal is questioned due to the very low fracture toughness of the HT HAZ adjacent to the fusion line.

CHAPTER 6

THE RELATIONSHIP BETWEEN SPLITTING IN TRANSVERSE CHARPY SPECIMENS AND LAMELLAR TEARING DURING WELDING OF 3CR12 PLATE

SYNOPSIS

In the first part of this study the mechanisms which are responsible for splitting in Charpy and edge-sheared specimens were identified. In the second part an attempt was made to establish the relationship between splitting and the ferrite factor and splitting and the susceptibility of 3CR12 to lamellar tearing during and after welding.

Planar oriented splits, parallel to the rolling plane, which develop during transverse impact testing and shearing, result in a decrease of the impact shelf energy as well as the ductile-brittle transition temperature. Transverse Charpy ductile-brittle transition (30J) temperatures within the range of -57°C to -68°C were measured for three experimental 3CR12 steels. The degree of planar splitting is mainly controlled by the degree of dimensional anisotropy of the grain structure. It was shown that splitting cannot be attributed to a single microstructural feature alone, but that it is governed by different mechanisms which depend on both the microstructure and the stress distribution at the crack tip. Splitting at sheared edges, which are subject to intense shear deformation, are nucleated by planar oriented inclusions. Splitting in Charpy specimens occurred by transgranular cleavage as well as by decohesion of ferrite-ferrite and ferrite-martensite grain boundaries and is not related to the presence of inclusions in the microstructure. The excellent toughness of 3CR12 arises from its fine grained microstructure and the fact that the splitting phenomenon is not related to the occurrence of inclusions in the microstructure.

The tendency for splitting to occur in transverse Charpy specimens was affected to a limited extent by normalising from 1000°C followed by tempering at 750°C. This resulted in a considerable increase in the transverse ductile-brittle transition temperature.

A direct relationship between the ferrite factor and the occurrence of

splitting in transverse Charpy specimens could not be established. Although the through-thickness ductile-brittle transition temperatures ranged from 107°C to 116°C, through-thickness tensile tests indicated the absence of a correlation between splitting observed in transverse Charpy specimens and the through-thickness ductility. It is concluded that splitting in transverse Charpy specimens is not expected to result in lamellar tearing, in the absence of planar oriented defects or inclusions, during welding.

THE RELATIONSHIP BETWEEN SPLITTING IN TRANSVERSE CHARPY SPECIMENS AND LAMELLAR TEARING DURING WELDING OF 3CR12 PLATE

1. INTRODUCTION

Splitting or laminated type fractures in Charpy, tensile, bend and sheared-edge specimens have been reported in the literature as a phenomenon which manifests itgself in high-strength low alloy steels(24, 25, 26, 27), some ferritic stainless steels(28, 29), ausformed(30, 31), marformed(30) and low carbon(32) steels. Lamellar type fractures (or splits), occur parallel to the rolling plane in the plate when hot rolling is terminated below the A_3 temperature. Splitting or lamellar fractures have also been found in Charpy, tensile and edge-sheared specimens of 3CR12. These fractures occurred when hot rolling was terminated at temperatures low in the duplex ferrite-austenite phase field. An example of this type of fracturing in transverse 3CR12 Charpy specimens is shown in figure 6.1, in which secondary splitting occurred, in the rolling plane, at right angles to the main fracture surface.

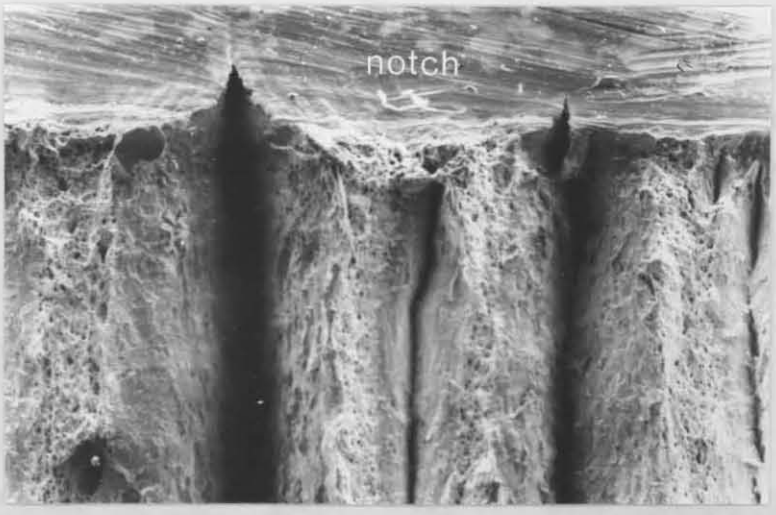

Figure 6.1: Splitting in a fractured transverse 3CR12 Charpy specimen. The splits are oriented in the rolling plane.

Although Hoffman does not consider these splits to have an adverse effect on the properties of 3CR12, the possibility of a correlation between splitting and the susceptibility of 3CR12 to lamellar tearing during and after welding has not yet been investigated(8). With 3CR12 being used in

more and more higher strength structural applications this aspect of the weldability of 3CR12 becomes even more important.

3CR12 is currently produced with ferrite factors ranging from 7.8 to 11.5. It has already been shown in Chapter 4 that the phase compositions of both wrought 3CR12 plate and the HT HAZ are among other factors dependent on the ferrite factor. The ferrite factor may also influence the susceptibility of the steel to splitting. Before any correlation between splitting and the phenomenon of lamellar tearing during and after welding can be established it is of importance, first, to identify the mechanism which is responsible for splitting, and, secondly, to establish whether the susceptibility of the steel to splitting is influenced to any extent by the ferrite factor.

This study consists of two parts:

1. In the first part the mechanisms which are responsible for splitting in Charpy and edge-sheared specimens were identified. The influence of a normalising and tempering heat treatment on splitting was also assessed. Normalising and tempering was also used to simulate the effect of the weld HAZ thermal cycles on the occurrence of splitting.

2. In the second part an attempt was made to establish the relationship between splitting and the ferrite factor and splitting and the susceptibility to lamellar tearing during and after welding.

2. EXPERIMENTAL RESULTS AND DISCUSSION

2.1 A study of the mechanism by which splitting occurs along sheared edges and in transverse Charpy specimens of 3CR12

2.1.1 Introduction

A considerable amount of work was carried out in recent years in order to investigate the origin of splits or fissures. Many investigators have attributed the phenomenon of lamellar fracture in HSLA type steels either to the distribution and morphology of carbides(24,27), the dimensional anisotropy of the microstructural unit which controls fracture(25,27),

polygonal or acicular ferrite structures resulting in transgranular cleavage, or to intergranular failure along prior austenite grain boundaries. Ausformed steels appear to split by decohesion along grain-boundaries as a result of fine alloy carbides dispersed along austenite grain boundaries while marforming seem to promote some kind of texture-banding which leads to splitting. Bramfitt and Marder attributed splitting in a high-purity single phase Fe-1%Mn alloy, which was hot rolled below the A_1 temperature, to decohesion along grain boundaries, independent of the texture of the material(32).

For ferritic stainless steels different mechanisms of laminar decohesion have been suggested. Mintz has shown that grain boundary shape, rather than texture, is the important factor controlling lamellar type fractures in a ferritic stainless steel containing 13% Cr(28). Hung-Chi Chao suggested that in the case of AISI type 430 ferritic stainless steel sheet, the banded cube-on-face texture component imbedded in other matrix orientations, tends to cause lamellar fracture of the sheet at low temperatures or high strain rates(29). Although splitting appears to be associated with microstructures exhibiting a high degree of dimensional anisotropy, there appears to be no single consistent metallographic or crystallographic feature uniquely responsible for splitting.

The purpose of this first part of this study as a component of a broader assessment of the weldability of 3CR12 was to:

a. identify the mechanisms responsible for splitting in Charpy and edge-sheared specimens;

b. assess the effectiveness of a normalising heat treatment to decrease splitting tendencies.

2.1.2 Materials and experimental techniques

2.1.2a Composition and mechanical properties

The chemical composition of the experimental 3CR12 steel is given in table 6.1. The steel was hot rolled by the producer into plate 12 mm thick, at a temperature within the two phase ferrite-austenite field, air cooled and

finally subcritically annealed (750-780°C) to obtain the mechanical properties shown in table 6.2.

Table 6.1: Chemical composition of experimental 3CR12 steel , wt-%.

	C	N	Mn	Si	Cr	Ni	S	Ti
Specification	0.03 max	0.03 max	1.5 max	1.0 max	11-12	1.5 max	0.03 max	4(C+N) min 0.6 max
Experimental steel	0.023	0.016	1.22	0.33	11.23	0.57	0.008	0.45

Table 6.2: Mechanical properties of experimental 3CR12 steel.

Proof stress 0.2% offset (MPa)	Tensile Strength (MPa)	Elongation %	Hardness as received (BHN)	Hardness* heat treated (BHN)
345	512	36	164	157

* Normalised from 1000°C followed by tempering at 750°C for 1h.

2.1.2b Heat treatment

The steel was tested in the as-received hot rolled-and-tempered condition as well as after a heat treatment consisting of normalising after heating for a period of 1h at 1000°C followed by subcritical annealing (tempering) for 1h at 750°C and subsequent air cooling. The Brinell hardness values of the steels in the hot rolled-and-tempered and the heat treated conditions are compared in table 6.2.

2.1.2c Specimen preparation

Standard 10 mm x 10 mm Charpy V-notch specimens were prepared according to ASTM E23 from both the conventional transverse (RW), the RT and through-thickness (TR) orientations shown in figure 6.2. The through-thickness impact specimens were prepared by electron-beam welding of extensions of the same material to the top and bottom surfaces of a transverse section of the plate shown in figure 6.2. Figure 6.3 shows an electron-beam welded through-thickness Charpy specimen.

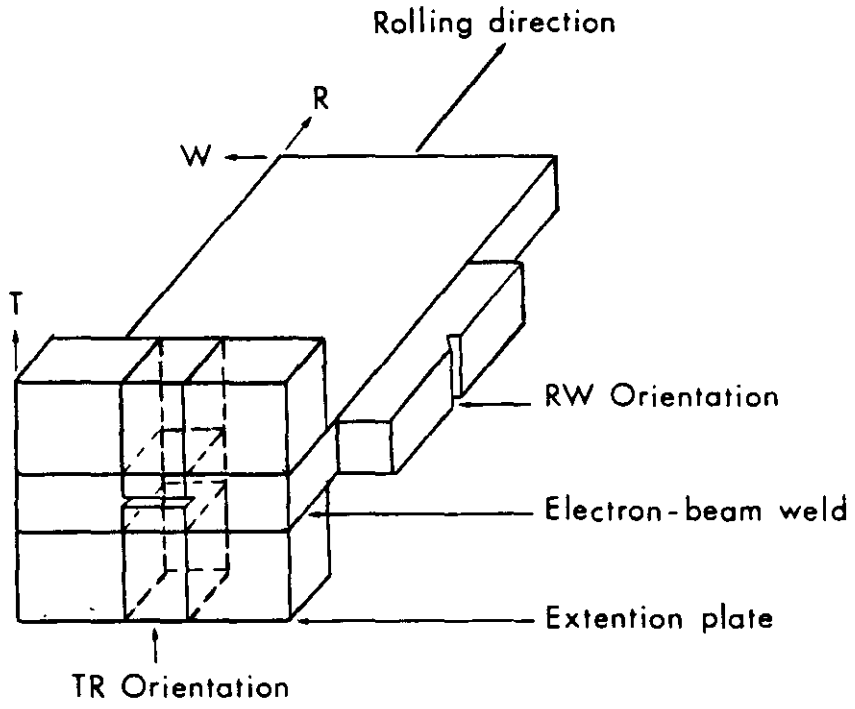

R = rolling direction; W = width direction; T = through-thickness direction

Figure 6.2: Charpy specimen orientation and notation. The first letter refers to the axis of the specimen and the second to the direction in which the fracture propagates.

The 12 mm thick plate was supplied by the producer in 30 cm x 15 cm sheared sections, and sheared surfaces of the sections were evaluated in the as received condition.

2.1.2d Metallographic preparation

Following final metallographical polishing using 0.3 μm alpha alumina abrasive, optical microstructural studies were conducted on specimens etched with Kalling's reagent (5g $CuCl_2$ + 100 HCl + 100ml Ethyl alcohol + 100ml H_2O). It was found that a pseudo-structure, resulting from the presence of a surface layer of disturbed metal, is revealed on the first etch. However, by alternatively polishing and etching several times, the true structure of the specimen was revealed.

Figure 6.3: Electron-beam welded through-thickness Charpy impact specimen (TR orientation).

2.1.3 Results and discussion

2.1.3a Microstructures

The banded grain structure of 3CR12, in the hot rolled-and-tempered condition, as it appears in the TR-plane, parallel to the rolling direction (fig. 6.2) is shown in figure 6.4a. Figure 6.4b, on the other hand, shows the grain structure as it appears in the TW-plane, perpendicular to the rolling direction. The microstructure of the steel consists of narrow bands of small recrystalised ferrite grains and pancake shaped tempered martensite grains.

The change in microstructure induced by normalising from 1000°C followed by subcritical annealing at 750°C for 1h is shown by a comparison of the microstructure in figure 6.4a with the microstructure in figure 6.5. It is evident that the dimensional anisotropy of the ferrite-martensite grain structure has not been completely eliminated by this particular heat treatment. The retention of anisotropy is probably due to the low solubility of titanium carbo-nitrides at 1000°C and their ability to act as grain boundary precipitates to effectively restrict the movement of the ferrite-austenite grain boundaries(33). The most striking change that occurs on normalising is the change in the ferrite-martensite grain boundary from straight to undulating.

a.(300X)

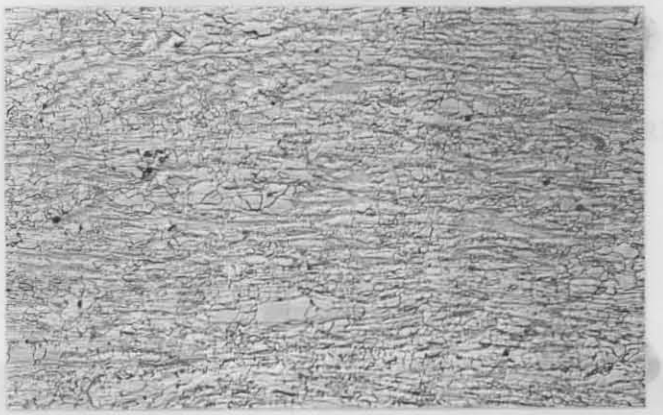

b.(150X)

Figure 6.4: Microstructures of 12 mm hot rolled and tempered 3CR12 plate.
a. in plane TR (fig. 6.2) parallel to the rolling direction
b. in plane TW perpendicular to the rolling direction

Figure 6.5: Microstructure of 12 mm 3CR12 plate, in plane TR (fig. 6.2) parallel to the rolling direction, after normalising from 1000°C with subsequent tempering at 750°C for 1h (150X).

2.3.3b Splitting in edge sheared specimens

Visual examination of the sheared surfaces of 12 mm thick plate sections revealed two types of fracture surfaces. Figure 6.6 shows a sheared surface with scaly appearance as well as a smooth sheared surface. Transverse sections through the different sheared surfaces indicated that the scales shown in figure 6.6 were in effect small splits. Figure 6.7 seems to indicate that the fine splits are nucleated by voids which develop around individual coarse TiCN inclusions in the vicinity of the sheared interface. The sheared surface of most steels becomes rougher with an increase in the clearance between the edges of the shear. An increase in the clearance results in an increase of the volume subjected to intense

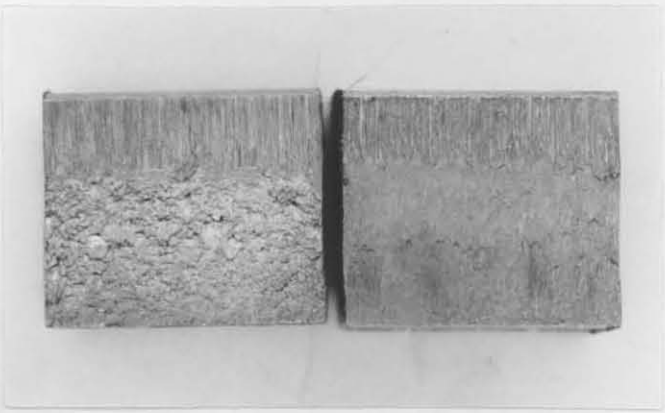

Figure 6.6: Scaly and smooth sheared surfaces of 12 mm 3CR12 plate.

shear strain. In 3CR12 this allows shear cracks which nucleate in the rolling plane to propagate to a greater extent.

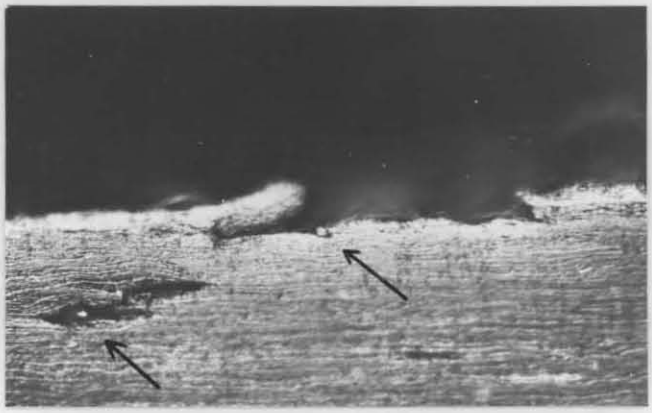

Figure 6.7: Section through the scaly sheared surface in figure 6.6. Arrows indicate voids around TiCN inclusions and a split which nucleated from a void on the sheared surface (270X).

The development and growth of voids around TiCN inclusions can be controlled by decreasing the clearance between the edges of the shear and maintaining sharp cutting edges. With a small clearance, the voids which develop around TiCN inclusions will usually not result in splitting on the shear surface, but internal shear cracks can develop from these voids just below the sheared surface as shown in figure 6.8.

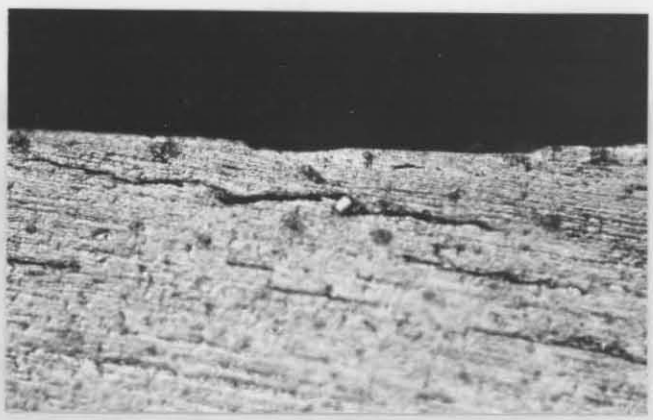

Figure 6.8: Section through the smooth sheared surface in figure 6.6. Internal shear cracks which originated from TiCN inclusions are evident (270X).

A third type of fracture surface was identified in specimens sheared in the laboratory with an excessive clearance of 2.4 mm between the edges of a blunt shear. Figure 6.9 shows the longitudinal sheared surface (parallel to the rolling direction) containing fine parallel splits which extend into the plate parallel to the rolling plane. A scanning electron microscope

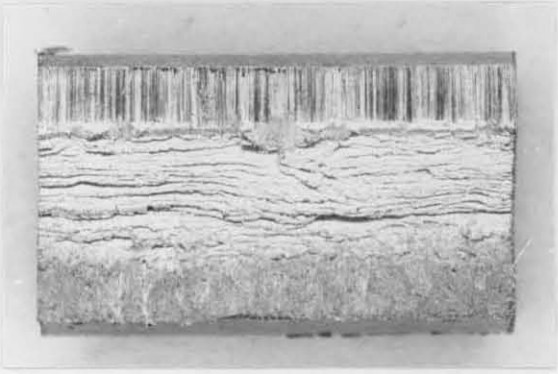

Figure 6.9: Longitudinal sheared surface with fine parallel splits. The specimen was sheared with a clearance of 2.4 mm between the edges of the shear.

(SEM) analysis of the sheared surfaces revealed that the splits propagated mainly by transgranular cleavage, while a section through the sheared surface also showed that the splits were not associated with TiCN inclusions. The splits were possibly caused in this particular case by the propagation by cleavage of micro shear cracks as a result of high secondary tensile stresses which developed in the through-thickness direction during shearing.

It may be concluded that fine splitting of 3CR12 plate, which manifests itself as scales on the sheared surface, occurs by different mechanisms depending on the clearance between the edges of the shear. The quality of the sheared surface can be improved and controlled by close control of the clearance between the edges of the shear.

2.1.3c Splitting or delamination behaviour of Charpy V-notch specimens

Transverse Charpy test

Transverse Charpy specimens (RW orientation shown in figure 6.2) were tested in the as-received as well as in the heat treated condition. The fracture surfaces of the specimens exhibited a characteristic appearance with small transverse splits running parallel to the rolling plane. Figures 6.10 and 6.11 show the Charpy transition curves for the experimental steel and the fracture surfaces of Charpy specimens fractured at different temperatures, respectively. Transverse splits or fissures, which tend to divide the fracture area, occurred at all test temperatures. The number of splits increased as the test temperature was decreased(32).

The curves in figure 6.10 show that the 30J ductile-brittle transition temperature and upper shelf energy were increased by normalising from 1000°C, followed by subcritical tempering. Splitting still occurred after this heat treatment but there was a significant decrease in the number of splits. The development of splits in the heat treated steel is probably due to the dimensional anisotropy of the grain structure which was retained (fig. 6.5). Some proof of this conclusion is to be found in the observation that the hardness was not significantly changed by this heat treatment (table 6.2).

The very low ductile-brittle transition temperature (-64°C) of 3CR12 in the hot rolled-and-tempered condition can primarily be attributed to the development of small transverse plits which effectively release the high triaxial stress condition in the plastic zone at the root of the notch. The ductile-brittle transition temperature and, to a lesser extent, the shelf energy, shift to lower values when fracture is associated with transverse splits. The impact specimen tends to behave like a set of thinner samples(34). In effect these transverse splits resulted in brittle cleavage fracture occurring at lower temperatures(32).

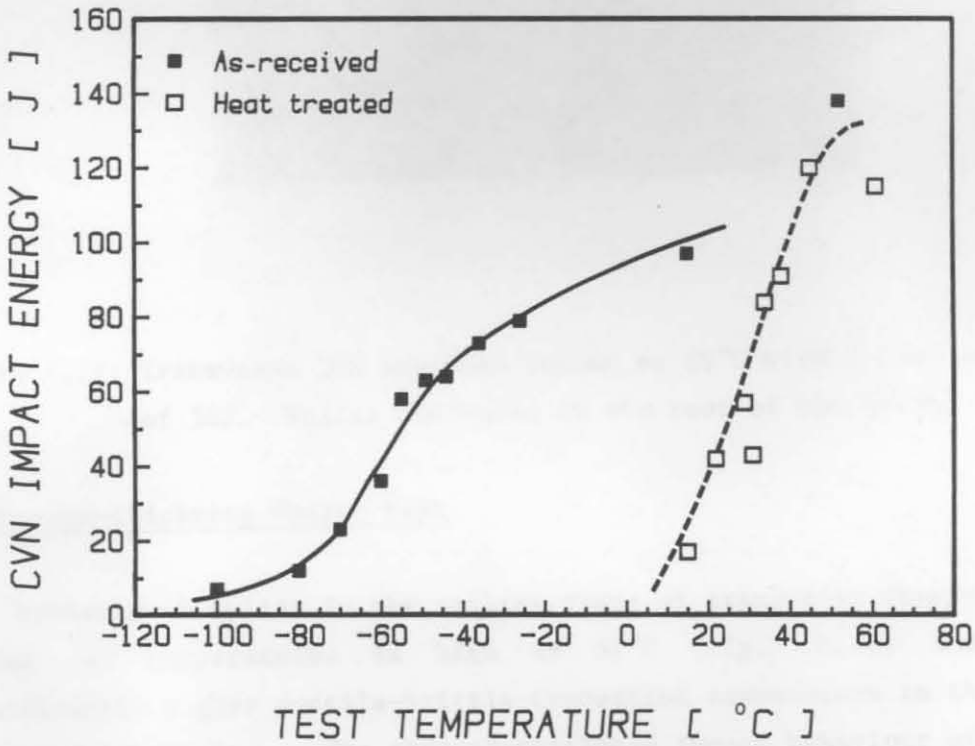

Figure 6.10: Transverse Charpy curves for 3CR12 tested in the as-received and heat treated conditions.

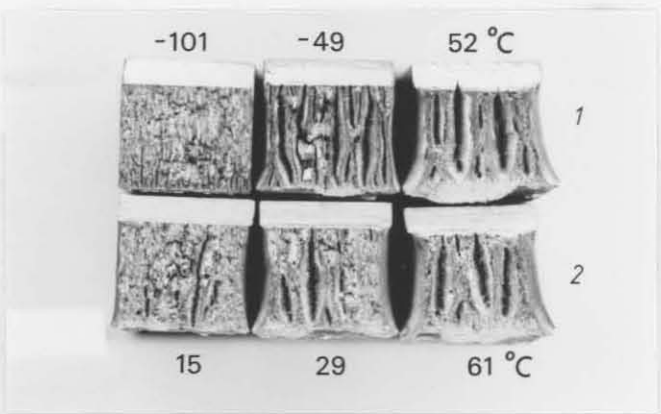

Figure 6.11: Fracture surface of transverse Charpy specimens tested in the as-received (1) and heat treated conditions (2). The test temperatures (°C) are included in the photograph.

Dabkowski suggested that splits may nucleate and propagate ahead of the principal propagating crack during impact testing of high-strength steels used for pipe lines(26). In order to determine whether the splits in 3CR12 steel occur before, after or concurrently with the passage of the principal propagating crack, an impact specimen was tested at 20°C in an impact machine by limiting the energy of the blow to 30J. The specimen was bent slightly and figure 6.12 shows that the root of the notch contains three small splits. These splits had already propagated to some extent without any transverse fracturing taking place. Splitting or laminated fractures in 3CR12 are therefore initiated ahead of the principal propagating crack. The principal fracture occurs by ductile failure of smaller subsized specimens created by splitting. The actual fracture appearance of the split surface will therefore be altered as a result of the large amount of plastic deformation which preceeds ductile failure of the material between the splits.

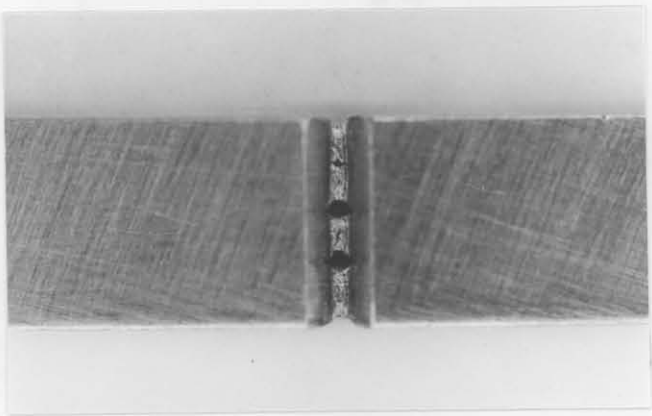

Figure 6.12: Transverse CVN specimen tested at 20°C with a low energy blow of 30J. Splits nucleated at the root of the notch.

Through-thickness Charpy test

The presence of splits in the rolling plane of transverse Charpy specimens tested at temperatures as high as 52°C (fig. 6.11) indicates a significantly higher ductile-brittle transition temperature in the through-thickness direction. The through-thickness impact behaviour of 3CR12 was therefore studied in order to determine the ductile-brittle transition temperature in the through-thickness direction and to characterize the appearance of the fracture surface parallel to the rolling plane.

Figure 6.13 shows the through-thickness Charpy curves for the 3CR12 steel tested in the as-received and heat treated conditions, respectively, while figure 6.14 shows the fracture surfaces of specimens fractured at different temperatures. The 30J through-thickness ductile-brittle transition temperatures are 112°C and 116°C for 3CR12 specimens tested in the as-received and heat treated conditions, respectively. The through-thickness transition temperatures are significantly higher than in the transverse direction (compare figures 6.10 and 6.13). A normalising heat treatment from 1000°C, followed by tempering at 750°C, caused a significant increase in the shelf energy with the ductile-brittle transition temperature being unchanged (fig. 6.13). The increase in shelf energy resulted from a transition from a ductile fibrous fracture to a conventional ductile fracture by micro-void coalescence (fig. 6.14). A notable feature shown in figure 6.13 is the virtual absence of any lower shelf energy for specimens tested at temperatures slightly below the ductile brittle-transitional temperature. The large difference between the transverse (20°C) and through-thickness (116°C) ductile-brittle transition temperatures after heat treatment is a feature which is associated with the dimensional anisotropy of the grain structure (fig. 6.5).

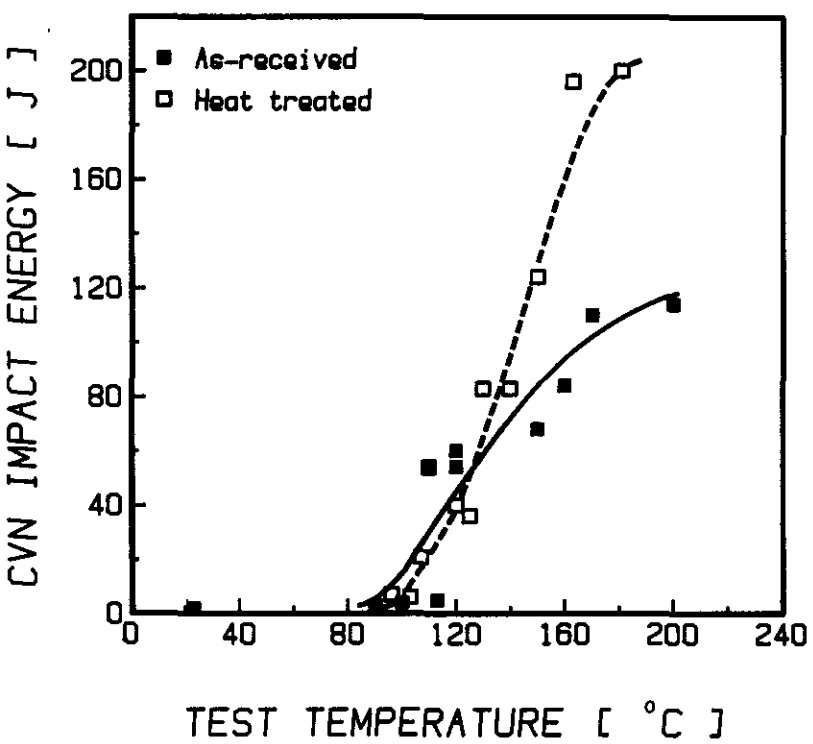

Figure 6.13: Through-thickness Charpy curves for 3CR12 tested as-received and heat treated.

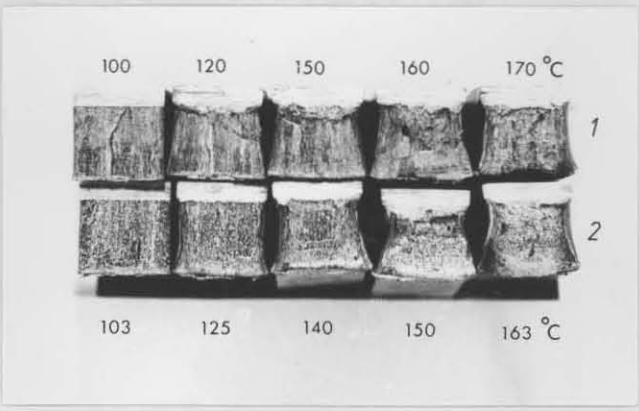

Figure 6.14: Fracture surfaces of through-thickness Charpy specimens tested in the as-received(1) and heat treated conditions(2). The temperatures (°C) at which the tests were conducted are are included in the photograph.

2.1.3d Metallographic and micro fractographic analysis of the splitting behaviour of Charpy specimens.

Splitting which preceeds the fracture of transverse Charpy specimens shown in figure 6.11 results in the subdivision of the fracture surface into an assembly of thinner specimens. Each sub-unit fractures in a ductile manner. This behaviour will result in a relatively high toughness of the steel even at very low test temperatures. In effect the transverse splitting ahead of the principal propagating crack changes the stress condition in the notch from plane strain to plane stress. Figure 6.15 shows the appearance of a fracture surface resulting from splitting. A portion of the fracture surface was relatively smooth and undulating adjoining a cleavage fracture surface with small cleavage steps. The appearance of the undulated fracture surface matches the pancake-shaped grain structure of the steel and probably arose as a result of intergranular decohesion. The undulating surface developed its characteristic appearance as a result of the subsequent tensile-elongation of each subunit prior to ductile fracture.

The original fracture appearance of the split surface has thus been altered by the subsequent large amount plastic deformation. Although Bramfitt and Marder(32) showed similar smooth undulating split surfaces in transverse

Figure 6.15: SEM micrograph of the split surface of a Charpy specimen showing a smooth undulating fracture surface (left) adjacent to a cleavage fracture (right) (1260X).

Charpy specimens of a high-purity Fe-1%Mn alloy and suggested that splitting occurred by decohesion of grain boundaries, the fracture characteristics of the split surface shown in figure 6.15 seems to indicate that splits may occur virtually simultaneously by grain boundary decohesion as well as by transgranular cleavage.

Polished and etched transverse sections through splits of a transverse Charpy specimen (fig. 6.11) tested at -100°C, revealed that the split crack propagated by decohesion of the ferrite-ferrite and ferrite-martensite grain boundaries as well as by transgranular cleavage through the ferrite grains (fig. 6.16). The transverse splits only gradually disappeared with the onset of cleavage fracture. Careful examination of the split surface and sections through splits showed that splitting in transverse Charpy specimens is not related to TiCN inclusions in the steels.

A visual examination of the through-thickness Charpy fracture surfaces of specimens machined from as-received plate and tested at 100°C and 120°C respectively, revealed two different fracture appearances on the same specimen (figs. 6.14 and 6.17A). The first 50% fracture surface adjacent to the notch, exhibited a dull appearance while the rest of the fracture surface had a brighter appearance. The fracture surface of the heat

Figure 6.16: Microstructure showing the propagation of a split by grain boundary decohesion of the ferrite-ferrite and ferrite martensite grain boundaries together with transgranular cleavage through the ferrite grains. Tested at -100°C (270X).

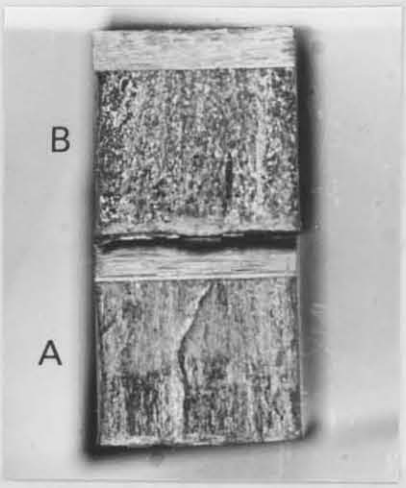

Figure 6.17: Through-thickness Charpy fracture surfaces of 3CR12.
A. Tested as-received at 100°C. Different fracture appearances on the same specimen are evident
B. Tested in the heat treated condition at 100°C. A shiny brittle fracture appearance is evident

treated specimens tested at 103°C and 125°C, respectively, exhibited the characteristic shiny appearance associated with a brittle cleavage fracture (figs. 6.14 and 6.17B).

Fractographic examination with the SEM indicated that the dull fracture surface, adjacent to the notch of the specimen machined from as received material and tested at 100°C was, of an intergranular nature. From a comparison of the equi-axed grains of this fracture surface with the microstructure of the steel shown in figure 6.4a, which contained pancake shaped tempered martensite grains (recrystalised), separated by small recrystalised ferrite grains, it can be inferred that fracture occurred mainly by decohesion along ferrite-ferrite grain boundaries. The grain diameter measured by both SEM and light micrographs are comparable. The other half of the fracture surface exhibited a combination of intergranular and transgranular cleavage fractures. The change in the fracture appearance was therefore associated with a change in the mechanism from intergranular decohesion to a combination of intergranular decohesion and transgranular cleavage. Brittle fracture of the heat treated through-thickness Charpy specimens occurred exclusively by transgranular cleavage in the rolling plane. The cleavage cracks are probably limited to the ferrite grains which are separated by tougher pancake shaped tempered martensite grains.

It can therefore be concluded that the mechanism of splitting or brittle crack propagation in the rolling plane of through-thickness Charpy specimens is dependent on the microstructure (heat treatment) and the stress state at the crack tip.

2.2 A study of the relationship between splitting and the ferrite factor and lamellar tearing during and after welding .

2.2.1 Introduction

A prerequisite for splitting is a large component of stress acting in the short transverse or through-thickness direction. Splitting in transverse Charpy, tensile and edge-sheared specimens occurs frequently in various low alloy and stainless steels including 12% chromium duplex ferrite-martensite steels. The degree of planar splitting in 12% chromium steels is mainly controlled by the degree of dimensional anisotropy of the grain structure. Splitting cannot be attributed to a single microstructural feature alone, but is attributed to different mechanisms which depend on the crack tip stress state as well as the microstructure. The type of lamellar tearing

which occurs in transverse Charpy specimens is not related to inclusions and will be referred to as splitting.

In order to obtain the required properties, the chemical composition of 3CR12 is adjusted by carefully balancing the ferrite and austenite stabilising elements. For this purpose the ferrite factor proposed by Kaltenhauser is used(1).

$$\text{Ferrite Factor (F.F.)} = Cr + 6Si + 8Ti - 40(C + N) - 2Mn - 4Ni + 4MO + 2Al$$

Although the Kaltenhauser relationship was initially derived to calculate the phase composition of ferritic stainless steel weld metal, it can also be used as a qualitative parameter to predict the relative balance between the ferrite and austenite phase stabilisers in wrought steel. The phase composition of 3CR12 which depends on the thermomechanical treatment is therefore characterized by the ferrite factor. A low ferrite factor will yield a higher martensite content and vice versa. Duplex ferite-martensite structures are obtained in 3CR12 when the values of the ferrite factor range from 7.8 to 11.5.

The mechanical properties of flat-rolled products which traditionally have been of interest, are those in which stress is applied in the rolling plane. The short transverse properties in which stress is applied in the thickness direction are of particular interest during welding in weld configurations susceptible to lamellar tearing. This applies especially in thick plate with high through-thickness restraint(28). Lamellar tearing is sometimes also referred to as splitting. Lamellar tearing, however, is usually related to the planar orientation of highly segregated inclusions. The splitting encountered in transverse Charpy specimens of 3CR12 suggests a susceptibility to lamellar tearing not related to inclusions. De Ardo studied the influence of splitting, in high strength low alloy steels, on the susceptibility to lamellar tearing(28). He concluded that the occurrence of splitting in impact specimens is neither related to, nor a good indication of, the probability of lamellar tearing during welding.

The purpose of this second part is to report on results of a study in which an attempt was made to establish, first the relationship between the ferrite factor and the phenomenon of splitting in transverse Charpy

specimens of hot rolled-and-tempered 12mm thick 3CR12 plate, and, secondly, the contribution of splitting to the susceptibility to lamellar tearing during welding.

2.2.2 Materials and experimental techniques

The compositions of the three 3CR12 steels used in this study are shown in table 6.3. The ferrite factors of these steels span the range of 12 mm thick 3CR12 plate currently produced. The plate was produced by completing hot rolling at a temperature of about 800°C. Subsequently the plate was subcritically annealed or tempered at 750°C-760°C. The mechanical properties of the steels so produced are given in table 6.4. All the tests were performed on the steel in the as-received condition.

Standard 10 mm x 10 mm Charpy V-notch specimens, with the longitudinal direction in the rolling direction, were prepared with the notch in the short transverse direction. Also Charpy V-notch specimens with the notch oriented to result in a fracture path parallel to the rolling plane, were prepared by electron beam welding extensions to the top and bottom plate surfaces.

Through-thickness tensile specimens were specially prepared from a composite which was manufactured by furnace brazing mild steel extensions to the top and bottom surfaces of square sections cut from the rolled plate. (The maximum temperature during brazing was 650°C while the time at temperature varied between 1-3 seconds). Miniature tensile specimens with a 9 mm gauge length and 3.8 mm diameter were prepared from this composite as shown in figure 6.18. The through-thickness ductility was determined by measuring the total percentage reduction in area.

Table 6.3: Chemical analysis of 12 mm 3CR12 plate, wt-%.

Steel	C	N	S	P	Mn	Si	Ti	Cr	Ni	F.F.
A	0.027	0.022	0.008	0.020	1.32	0.44	0.32	11.34	0.61	9.70
B	0.023	0.016	0.008	0.017	1.22	0.33	0.45	11.23	0.57	10.75
C	0.021	0.010	0.013	0.017	1.22	0.48	0.36	11.20	0.53	11.26

Table 6.4: Mechanical properties of 12 mm 3CR12 plate material.

Steel	Proof stress (0.2%) MPa	Tensile Strength MPa	Elongation, Percentage	Brinell Hardness HBN
A	336	509	30	169
B	345	512	36	164
C	390	526	29	164

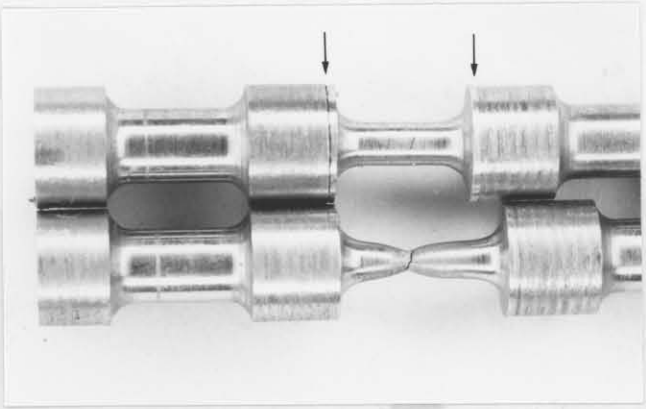

Figure 6.18: Composite through-thickness tensile specimen. Brazed joints are indicated by arrows.

2.2.3 Results and Discussion

2.2.3a Microstructures

The microstructures of steels A and C (table 6.3) with ferrite factors 9.70 and 11.26 respectively are shown in figures 6.19 and 6.20. The

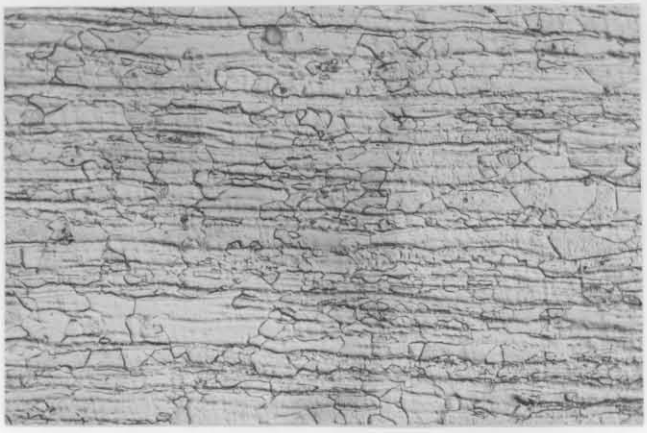

Figure 6.19: Microstructure of steel A (F.F. = 9.70), in the as-received condition. The banded structure consists of pancake shaped tempered martensite grains separated by recrystalised ferrite bands which lie in the rolling plane (300X).

Figure 6.20: Microstructure of steel C (F.F. = 11.26). The higher percentage ferrite is evident when this microstructure is compared to the microstructure in figure 6.19. The ferrite bands are also slightly thicker due to the higher percentage ferrite (300X).

microstructures of the steels consist of narrow bands of recrystalised ferrite and pancake shaped tempered martensite grains. It is evident from figures 6.19 and 6.20 that an increase in the ferrite factor results in an increase in the average width of the recrystalised ferrite bands (with a concurrent decrease in the percentage tempered martensite). The pancake shaped ferrite and martensite grains are oriented in the rolling plane.

2.2.3b Charpy impact testing

Charpy impact tests were conducted at various temperatures on the experimental steels in the as-received condition. The results of the impact tests are summarized in figure 6.21. Splitting occurred in all of the specimens tested in the temperature range -100°C to 55°C. Some of the Charpy fracture surfaces are shown in figure 6.22. The number of splits increases with a decrease in test temperature and the onset of cleavage fracture is suppressed to temperatures below -60°C. In specimens tested below -20°C the number of splits which developed was the same for all three steels. Specimens of steel B tested at temperatures above -20°C exhibit a smaller number of splits than steels A and C. This is reflected by the slightly higher impact energy in figure 6.21. The 30J ductile-brittle transition temperatures of the three steels are shown in table 6.5. Although the ductile-brittle transition temperature decreases slightly with a decrease in the ferrite factor, this does not necessarily indicate a correlation between the ferrite factor and splitting. It has already been shown that the transverse toughness of 3CR12 is greatly enhanced by the occurrence of splitting. The very low transition temperatures of the three 3CR12 steels are at least partially due to splitting which releases the high triaxial stress state at the root of the notch. Figure 6.23 shows a comparison of the impact energy, testing temperature relationship for steel B with the fracture plane in the long and short transverse planes, respectively.

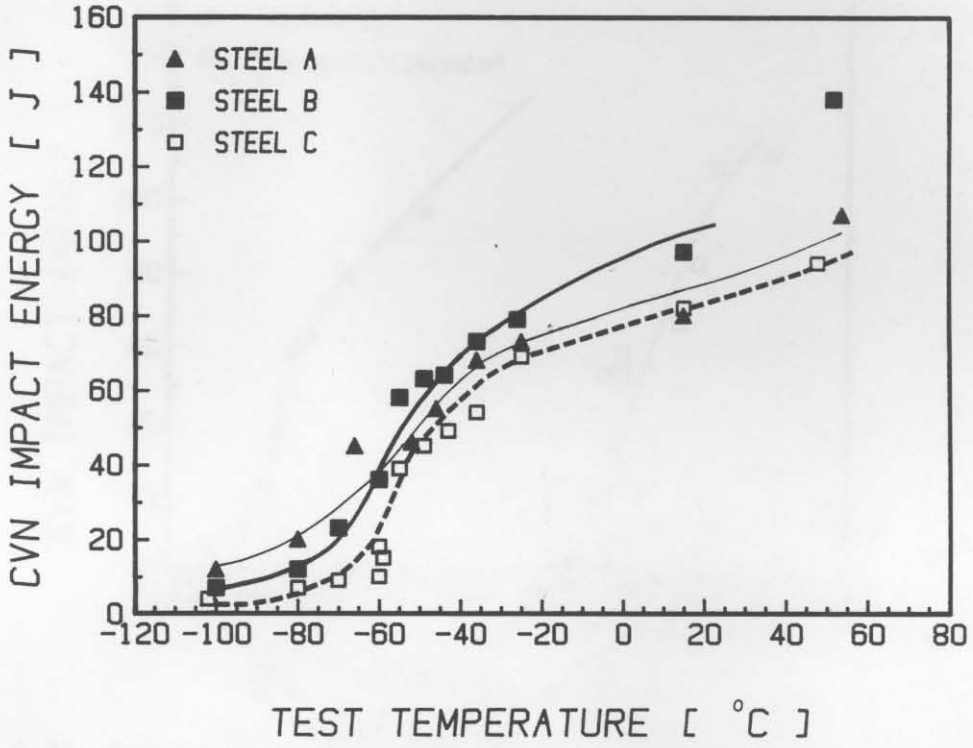

Figure 6.21: Transverse CVN impact curves for steels A (F.F. = 9.70), B (F.F. = 10.75) and C (F.F. = 11.26) tested as-received.

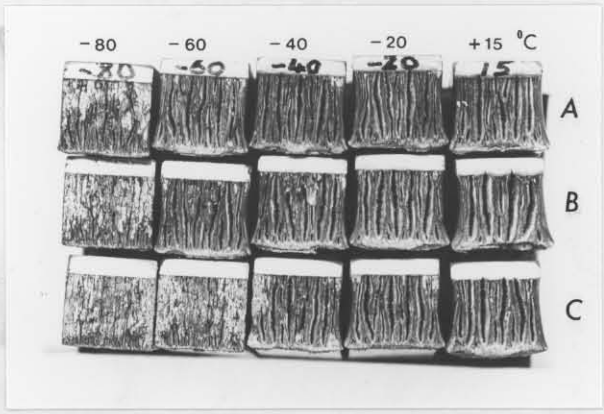

Figure 6.22: Charpy fracture surfaces of 3CR12 steels A, B, and C tested at different temperatures (°C).

Table 6.5: Transverse ductile-brittle transition temperatures (°C) at 30J for 3CR12 steels tested in the as-received condition

Steel	Ferrite Factor (F. F.)	Transition Temperature (°C)
A	9.70	-68
B	10.75	-64
C	11.26	-57

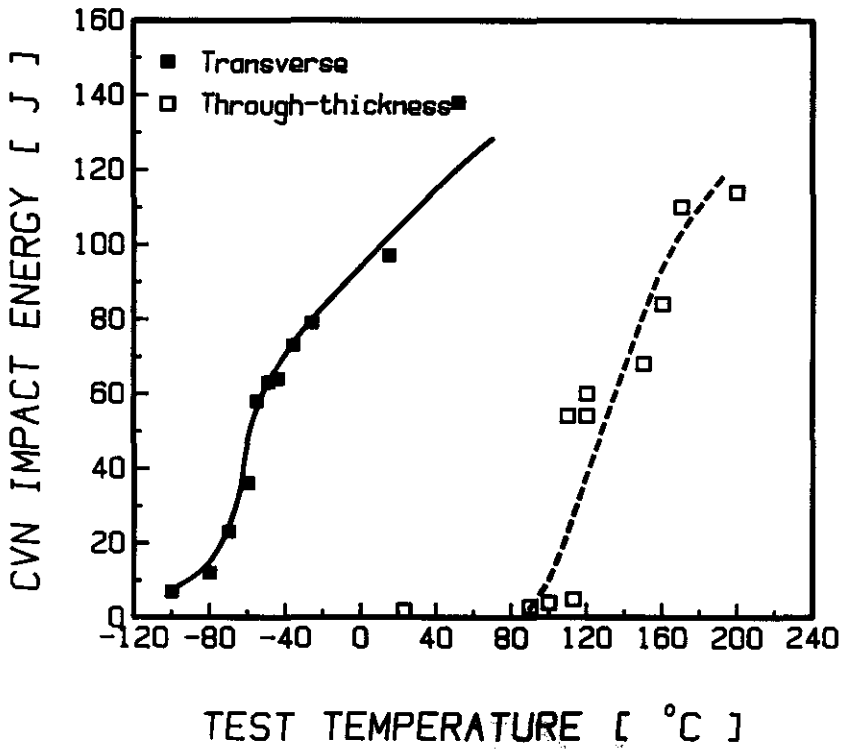

Figure 6.23: Transverse and through-thickness CVN impact curves for steel B

2.2.3c Through-thickness tensile tests

The presence of splits parallel to the rolling plane in transverse Charpy specimens and the high through-thickness ductile-brittle transition temperature (112°C for steel B) raises the issue whether 3CR12 steel is not

highly susceptible to lamellar tearing during welding. Lamellar tearing is usually an inclusion-related phenomenon. Farrar, Ginn and Dolby have shown a good correlation between the short transverse ductility and the susceptibility of a steel to lamellar tearing during welding(29). The susceptibility to lamellar tearing increases with a decrease in the short transverse ductility due to the presence of elongated inclusions. However, the type of splitting which occurs in transverse Charpy specimens of 3CR12, is not an inclusion related phenomenon and the relationship between splitting in transverse Charpy specimens and the short transverse ductility of duplex ferrite-tempered-martensite, 12% chromium steels has as yet not been determined.

A study by De Ardo, on the mechanism of splitting in four high strength low alloy steels, revealed that cementite, either as grain boundary precipitate or as a constituent of pearlite in a particular distribution, appeared to be responsible for splitting(25). No direct correlation between splitting and the short transverse ductility could be found and it was concluded that splitting in transverse Charpy specimens of HSLA steels is not related to the phenomenon of lamellar tearing, which sometimes attends welding.

In the present study the short transverse ductilities of three 3CR12 steels, table 6.1, were determined and the results are summarized in table 6.6. All the specimens exhibited elliptical fracture surfaces (fig. 6.24)

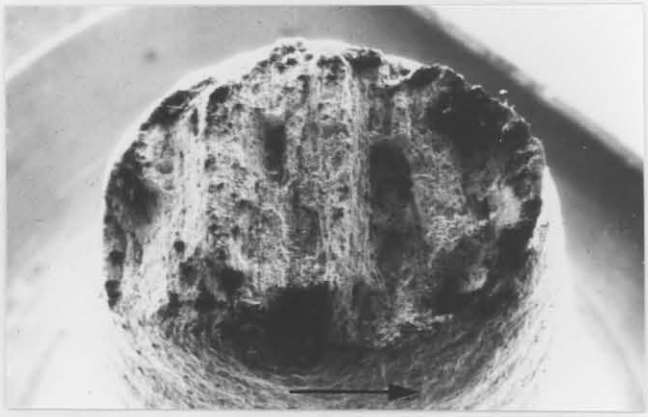

Figure 6.24: Micrograph of the elliptical through-thickness tensile fracture surface of specimen 3 of steel C in table 6.6. The arrow indicates the long transverse direction.

Table 6.6: Through-thickness tensile test results of 3CR12 steel A, B, and C tested in the as-received condition.

Steel	Specimen No.	Tensile strength(MPa)	Reduction in area, pct.	
			L*	Z*
A	1	477	34	55
	2	480	27	27
	3	490	36	52
	4	488	42	56
	Average	484	35	48
B	1	460	56	73
	2	475	57	78
	3	473	50	73
	4	-	17	68
	Average	469	45	73
C	1	465	40	69
	2	473	33	63
	3	-	42	67
	4	456	17	43
	Average	465	33	61

*L : Longitudinal ductility : reduction in area (fig. 6.24)

*Z : Long transverse ductility : reduction in area (fig. 6.24)

as a result of the dimensional anisotropy of the grain structure in the rolling (longitudinal, L) and long transverse (Z) directions. The test results in table 6.6 show that the three 3CR12 steels exhibit a reasonably high short transverse ductility. An SEM analysis of the fracture surfaces revealed complete dimpled ductile fracture surfaces with small patches of inclusions which have been identified as mainly titanium carbonitrides. The few exceptions in table 6.6 were specimens which contained excessive amounts of titanium carbonitride stringers. No relationship between the ferrite factor and the short transverse ductility could be found from the limited number of tests performed.

The high through-thickness ductility of the 3CR12 steels, together with the absence of any brittle transgranular or intergranular fracture in the short transverse tensile specimens, indicate that there is no apparent relationship between planar oriented splitting in transverse Charpy specimens and the through-thickness ductility. This observation indicates that the occurence of splitting in transverse Charpy impact specimens is neither related to, nor a good indicator of, the probability of lamellar tearing that may occur during and after welding. The presence of an abnormally high amount of segregated, planar oriented inclusions can result in lamellar tearing during welding. The absence of splitting during tensile testing of specimens with a through-thickness orientation may probably be attributed to the fact that the fracture stress necessary for splitting is in excess of the true stress when ductile fracture due to micro-void coalescence occurs. Splitting will therefore only be possible when plastic deformation is constrained in such a way that the local stress exceeds the fracture stress required for splitting.

3. GENERAL DISCUSSION

3.1 Mechanism of splitting in transverse Charpy specimens

Various researchers have attempted to relate the splitting or delamination phenomenon in transverse Charpy specimens to specific microstructural features(24-30). It appears, however, that splitting of transverse Charpy specimens is not related to a specific microstructural or crystallographic feature. Careful examination has shown that it is not related to any type of inclusion in the steel.

A model for the phenomenon of splitting in transverse Charpy specimens of 3CR12 can be formulated by comparing the results obtained in this study with those obtained by Emburry(34) on so-called 'crack-divider' laminated Charpy specimens (fig. 6.25). He used standard-size laminated Charpy specimens, containing up to six layers of annealed mild steel, which were prepared by machining transverse Charpy specimens from a composite manufactured by silver soldering thin annealed mild steel plates. The transition temperature and shelf energy were lowered as the number of crack-dividing layers increased. Examination of the fracture surfaces revealed that a pair of shear lips formed on each subunit in contrast to the single set of shear lips associated with a homogeneous specimen. The fracture mechanism of a specimen which allows crack division can be considered to be equivalent to that of a thin plate-like Charpy specimen laterally supported to prevent buckling.

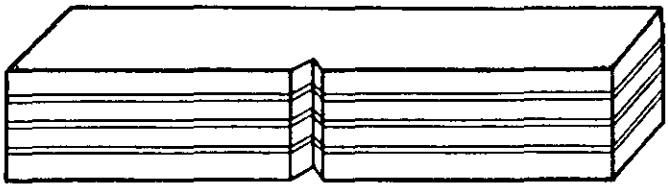

Figure 6.25: A schematic diagram of a 'crack-divider' Charpy specimen. (After Emburry)

Considering the pancake-shaped grain structures (fig. 6.4) normally present in 3CR12 steel, transverse Charpy specimens can also be considered as laminated, 'crack-divider' specimens. During Charpy impact testing, plastic deformation in the plastic zone at the root of the notch is highly restrained. Consequently the stress state just ahead of the root of the notch is characterised by a high degree of triaxiality. As a result of the plastic constraint the tensile bending stress can in extreme conditions be as high as three times the yield stress and the tensile stress induced at right angles to the direction of splitting in transverse Charpy specimens can reach a value of approximately 2.5 times the yield stress(17). If the

tensile stress during transverse Charpy testing is below the fracture stress necessary to induce transverse fracture, and the tensile stress at right angles to the direction of splitting exceeds the fracture strength required for splitting, splitting will preceed transverse fracturing. Depending on the fracture toughness of the material in the direction in which the split propagates, the distance that a split will extend will be governed by the size of the plastic zone which develops at the root of the Charpy specimen. Any local split will cause a relaxation of the local triaxial stress condition in the vicinity of the split. The distance over which the stress is relaxed will depend on the length of the split. Further parallel splits can, therefore, only nucleate some distance from an existing split. The number of splits which develop during testing of a given material will, therefore, depend on the size of the plastic zone at the root of the transverse Charpy specimen. In the brittle transition temperature regime where the size of the plastic zone decreases as the testing temperature is lowered, the distance between splits can also be expected to decrease. Ample experimental proof for this model is to be found in figure 6.11.

When splitting occurs, the triaxial stress condition at the root zone of the notch is relaxed and the stress state altered from mainly plane strain to plane stress(17). The reduction of the stress state in the notch as a result of splitting will therefore reduce the temperature at which cleavage fracture can be expected. Splitting can, therefore, be expected to reduce the brittle transition temperature in accord with Emburry's results. The reduction in the stress state will, however, also cause a reduction in the upper shelf impact energy.

Emburry's laminated 'crack-divider' Charpy specimen can, therefore, be considered as a valid model for laminated fracture of transverse 3CR12 Charpy specimens. Splitting in transverse 3CR12 specimens will probably thus not have a crystallographic origin per se but will occur rather by delamination along planes or interfaces in a laminated structure which has a lower fracture stress than the stress required for transverse fracture. Although a micro analysis showed no significant partition of alloying elements between the ferrite and tempered martensite phases, different possible low fracture-stress planes or interfaces have been identified. Delamination of transverse Charpy specimens occurred by transgranular

cleavage and decohesion of the ferrite-tempered-martensite and ferrite-ferrite grain boundaries (fig. 6.16), whereas through-thickness Charpy specimens fractured by transgranular cleavage (probably through ferrite grains) and decohesion of the ferrite-ferrite grain boundaries.

An elongated grain structure (laminated) and the consequent anisotropic mechanical properties appear to be the most important prerequisite for splitting to occur in transverse Charpy specimens cut from rolled plate. The excellent toughness (low transverse ductile-brittle transition temperature) of hot rolled and tempered 3CR12 plate is, apart from the small grain size, also due to splitting which promotes partial relaxation of the plastic constraint. The very favourable influence of the laminated grain structure on the fracture toughness of 3CR12 is further illustrated by a fractured Charpy specimen in figure 6.26, prepared with the notch in the rolling plane, which absorved 288J energy at -30°C.

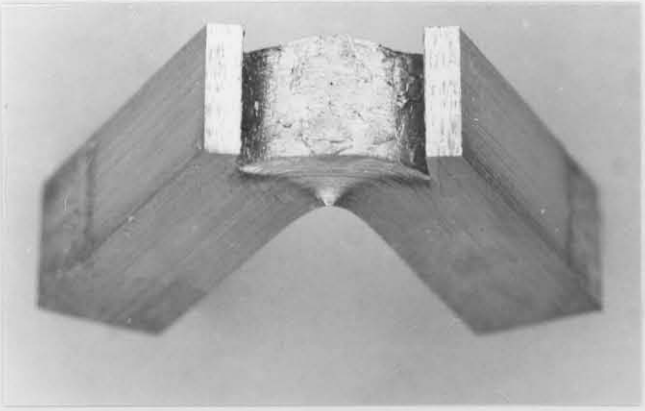

Figure 6.26: Extensive delamination in a longitudinal 3CR12 Charpy specimen prepared from hot rolled and tempered 12 mm plate with the notch in the rolling plane. The specimen absorbed 288J at -30C.

3.2 Influence of heat treatment

Normalising from 1000°C, followed by tempering at 750°C, partially eliminated the dimensional anisotropy of the grain structure (fig. 6.5) without influencing the tensile mechanical properties significantly. It can be expected, however, that the heat treatment reduced the difference in

the transverse fracture stress and the fracture stress required for splitting. In terms of the model of the splitting mechanism, normalising can be expected to increase the distance bertween splits. The ductile-brittle transition temperature can therefore be expected to be increased by normalising (as also predicted by Emburry's results). In fact the ductile-brittle transition temperature was increased considerably from -64°C to +20°C by a normalising and tempering heat treatment. Following the normalising heat treatment, there was still some anisotropy in the fracture stress sufficient to cause some splitting. This is confirmed by the large difference in transition temperature following normalising for specimens with a transverse orientation (20°C) and specimens tested in the through-thickness direction (114°C).

The large increase in the transverse ductile-brittle transition temperature of 3CR12 after a normalising and tempering heat treatment, with the hardness unaffected, indicates that the toughness of this steel is greatly enhanced by the degree of dimensional anisotropy of the grain structure. Hot rolling should therefore be terminated at temperatures low in the two-phase ferrite-austenite phase field in order to obtain the desired toughness levels.

3.3 Relationship between the ferrite factor and splitting in transverse Charpy specimens

It has already been shown that Emburry's laminated 'crack-divider' Charpy specimen is a valid model for the splitting encountered in transverse Charpy specimens of 3CR12. It was also shown that a laminated microstructure, with planes or interfaces parallel to the rolling plane with a low fracture stress, is an important prerequisite for splitting to occur in transverse Charpy specimens. Splits form during the initial stages of the Charpy test, before the initiation and propagation of the main crack, when the lateral stresses which develop as a result of lateral constraint, exceed the brittle fracture stress on the low fracture toughness planes or interfaces. This results in a relaxation of the stress triaxiality in the vicinity of the split.

The number of splits, or the distance between the splits at a given test temperature, will be related to the number of sub-specimens in the

composite specimen, or the distance between the low fracture stress planes in the rolling plane and the amount of stress relaxation in the vicinity of a split. If the transverse size of the stress relaxed zone associated with a split (it is that zone in which the transverse stress is lower than the fracture stress of the low fracture stress plane) is smaller than the distance between the low fracture stress planes, the number of splits will be determined by the number of low fracture stress planes (fig. 6.27).

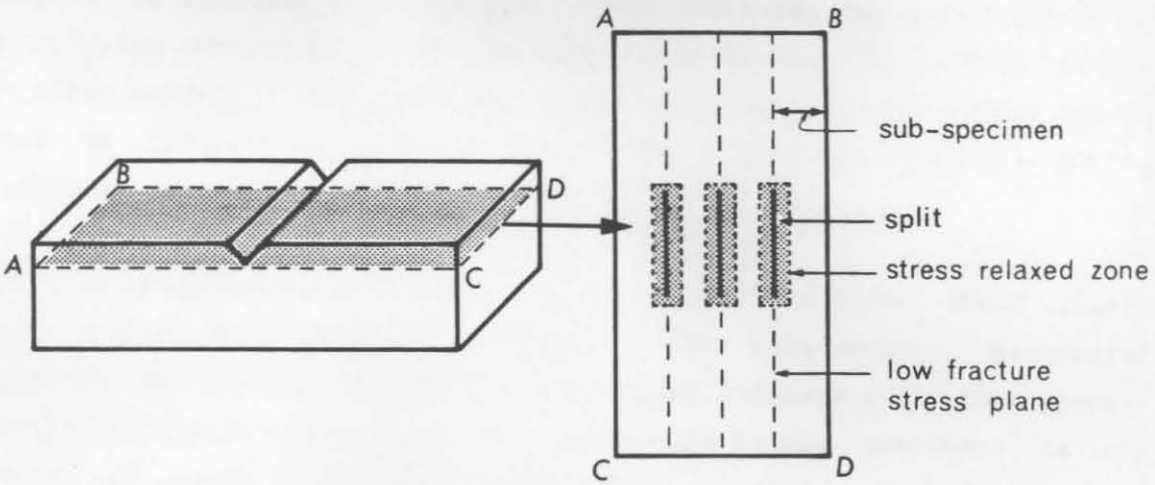

Figure 6.27: Section through the splits which have developed in the rolling plane, ahead of the notch tip of a transverse Charpy specimen prior to initiation of the principal crack at the notch tip during impact loading.

With the distance between the splits much larger than the distance between the low fracture stress planes, the number of splits at a given test temperature will rather be determined by the size of the stress relaxed zone associated with a split. The size of the stress relaxed zone will then approximately be equal to the distance between the splits. Measurements of the distance between the splits at the ductile-brittle transition temperatures of steels A, B and C gave an average value of 0.85 mm. If this is compared with the thickness of the pancake shaped grains (sub-specimens) of steels A (fig. 6.19), B and C (fig. 6.20), which varied between 0.003-0.009 mm, 0.006-0.010 mm and 0.006-0.010 mm respectively, it is evident that the number of splits will not be influenced by the ferrite

factor within the range of 9.7 to 11.26 since the thickness of the pancake shaped grains, which decreases with a decrease in the ferrite factor, is much smaller than the size of the zone in which the lateral stresses are relaxed.

A comparison is made in figure 6.21 of the transverse Charpy curves for steels A, B and C. The differences between the curves for steel B (F.F. = 10.70) and C (F.F. = 11.26) are probably related to the differences in the ferrite factors (table 6.5). The slightly higher transition temperature of steel C is due to the lower percentage tempered martensite in the structure. The ductile-brittle transition temperature of steel A is slightly higher than that expected from the value of the ferrite factor alone, and is probably due to the lower Ti:(C+N) ratio of 6.5 for this steel, compared to a ratio of 11.5 for steels B and C. The results show therefore that there is no direct relationship between the ferrite factor and the incidence of splitting. The small difference between the impact curves can be accounted for by the ferrite factor and by the ratio Ti:(C+N).

3.4 Relationship between splitting and lamellar tearing during welding

The low short transverse ductility of three of the twelve tensile specimens of the three 3CR12 steels shown in table 6.6, was mainly due to segregated stringers of titanium carbonitrides. This indicates the importance of a low inclusion content to prevent inclusion-related lamellar tearing during and after welding. The number of titanium carbonitride inclusions can of course be reduced by limiting the carbon and nitrogen contents during steelmaking.

High through-thickness ductilities were found for the three 3CR12 steels which necked down without splitting. The satisfactory mechanical properties in the through-thickness direction indicate that the planar-oriented splitting associated with transverse Charpy specimens is not expected to result in lamellar tearing during welding. De Ardo reported similar results for high-strength, low-alloy steels(28). The degree of anisotropy in this instance was not as marked as that of the present material. It must, however, be emphasized that the brittle transition temperatures in the through-thickness direction of most other HSLA steels

are much higher than the transverse values. The fracture toughness in the through-thickness direction at room temperature will be quite low. Fortunately 3CR12 also has a fairly low yield strength so that the critical crack length due to planar oriented defects, such as that due to segregated inclusions, will be tolerable. In critical applications where plane strain, rather than plane stress, conditions prevail, such as weld configurations with a high thickness constraint, care should be exercised.

4. SUMMARY

a. A variety of microstructural features are responsible for splitting during shearing of 12 mm thick plate and for the development of laminated fracture surfaces in transverse Charpy specimens.

b. Splitting of 12 mm thick 3CR12 plate during shearing occurs by different mechanisms which are governed by the clearance between the edges of the shear. Fine scaly splitting originated mostly from voids which formed around coarse TiCN inclusions, evenly distributed in the plate. A large clearance of 2.4 mm between the edges of the shear, resulted in long parallel splits, parallel to the rolling plane, by transgranular cleavage.

c. Fine scaly and parallel splits on sheared edges can be controlled, and probably eliminated, by maintaining small clearances between the edges of the shear, and by maintaining sharp edges.

d. Splitting along the rolling plane in transverse Charpy specimens is a phenomenon which arises from the anisotropy of the fracture stress.

e. The mechanism of splitting in transverse and through-thickness Charpy specimens (decohesion of the ferrite-ferrite, ferrite-martensite grain boundaries or transgranular cleavage) is governed by the microstructure (prior heat treatment) and the stress state at the crack tip during fracture.

f. The very low transverse ductile-brittle transition temperature of the hot holled and tempered 3CR12 steels is a feature which is associated with splitting. In order to obtain low ductile-brittle transition

temperatures, hot rolling should be terminated at low temperatures in the two-phase austenite-ferrite phase field in order to obtain a banded grain structure.

g. The tendency for splitting to occur in transverse Charpy V-notch specimens was affected to a limited extent by normalising from 1000°C followed by temperaturing at 750°C. This resulted in a considerable increase in the transverse ductile-brittle transition temperature.

h. The difference between the transverse and through-thickness ductile-brittle transition temperatures decreased from 176°C to 134°C on normalising from 1000°C, followed by subcritical tempering at 750°C.

i. There is no direct relationship between the ferrite factor (in the range 9.7 - 11.26) and splitting in transverse Charpy specimens of 3CR12.

j. The high through-thickness tensile ductility of 12 mm thick plate indicates that splitting is dependent on plane strain rather than plane stress conditions.

k. The through-thickness tensile ductilities of the experimental steels were high in spite of the phenomenon of splitting which is encountered in transverse Charpy specimens. The radius of the plastic zone at the tip of a split is probably fairly large and it is not expected to result in lamellar tearing in the absence of planar oriented inclusions during welding.

CHAPTER 7

GENERAL CONCLUSION

1. WELD HEAT AFFECTED ZONE TOUGHNESS OF 3CR12 AND 3CR14

The important results, concerning the HAZ toughness of 3CR12 and 3CR14, may be summarized as follows:

a. The weld HAZ of 3CR12 and 3CR14 consists of at least three different zones, i.e. the HT HAZ adjacent to the fusion line, the fine grained HAZ adjacent to the HT HAZ and the low temperature HAZ more distant from the fusion line. These different zones in the HAZ exhibit different microstructures, mechanical and toughness properties. For a valid comparison of the HAZ toughness of 3CR12 with that of AISI 409 it will be necessary to compare the respective zones in the HAZ.

b. The fracture toughness of the HT HAZ of 3CR12 is not superior to that of the HT HAZ of the ferritic stainless steel AISI 409 from which 3CR12 was developed.

c. The fracture toughness of the HT HAZ of both 3CR12 and 3CR14 was not significantly improved by the grain refining which resulted from the increase in the low carbon martensite content from 15 percent to 98 percent(35). It is therefore possibly determined by other phenomena which have not yet been identified.

1.1 High temperature heat affected zone

3CR12 was developed by Middelburg Steel and Alloys (Pty), Ltd inter alia in an attempt to improve on the poor weldability of AISI 409. The weld HAZ toughness was evaluated, without differentiating between the different zones in the HAZ, using only the Charpy V-notch test. Although excellent toughness values were reported for the HT HAZ of 3CR12 by Hoffman and others (2,4,8,9,11), no fractographic or metallographic evidence was ever provided to show that the fracture path was limited exclusively to the narrow HT zone in the HAZ during impact testing. The very low toughness values which were obtained (Chapter 4) in this study for the HT HAZ of

3CR12, with the newly developed bead-on-plate bend test, strongly suggests that the high toughness values reported in literature for the HT HAZ of 3CR12 apply rather to the adjacent tough, fine grained zone in the HAZ. It may therefore be concluded that the Charpy V-notch test cannot be used reliably to evaluate the fracture toughness of the narrow HT zone in the HAZ of 3CR12. This is conceivable when the Charpy notch tip radius (0.25 mm) is compared with the size of the HT HAZ which ranges from 0.3 mm to 1 mm. In practice it is very difficult accurately to position the Charpy notch tip in the HT HAZ and guarantee that fracture will occur exclusively in this zone. Another practical limitation as far as the Charpy test is concerned, is the difficulty in producing a welded specimen, especially from 6 mm plate, with a planar HT HAZ oriented normal to the plate surface.

The toughness of both the fine grained and low temperature zones in the HAZ of 3CR12 is higher than that of the corresponding zones in AISI 409. This is due to the grain refining effect which occurs during welding in the fine grained zone in the HAZ of 3CR12, the relatively high HAZ toughness values which were reported in the literature for 3CR12, and the much higher base metal toughness of the dual phase ferritic-tempered-martensite structure of 3CR12, compared to that of the ferritic structure of AISI 409. This does not qualify 3CR12 as a structural steel with a superior weldability over that of AISI 409 since the weldability of AISI 409 is still limited by the low fracture toughness of the HT HAZ. This is especially important when 3CR12 is used in higher strength applications than what is customary for AISI 409, due to its higher yield and tensile strength. Although 3CR12 is specified by Middelburg Steel and Alloys, in some of the most recent technical publications(36) as a weldable structural steel for application in the petro-chemical, metallurgical, pulp and paper, and sugar industries, it is not recommended for critical application in plate thicknesses above 3 mm if adequate as-welded joint toughness is to be maintained.

Although Thomas(10) was actively involved in the developement of 3CR12, he did not realise apparently that the poor HAZ toughness or weldability of 3CR12 could be predicted (as discussed in chapter 1) by using the results of a study of his on the improvement of the weldability of AISI 409 with compositional variations within the specification.

Colt Crucible (USA) has also developed a tough, weldable 11.5 percent chromium ferritic stainless steel from AISI 409, known as Crucible E-4. For plate applications this steel contains 0.06 percent carbon, about 0.2 percent titanium and 0.85 percent nickel(36). Since a predominantly martensitic microstructure develops in the HT HAZ of E-4, this steel may be compared with 3CR12Ni. The major differences between the chemical compositions of E-4 and 3CR12Ni are the higher carbon content (0.06%C) and lower titanium:carbon ratio of 2.5 for E-4. The as-welded HT HAZ toughness of E-4 is expected to be lower than that of 3CR12Ni due to the formation of a higher carbon martensite in the HT HAZ. The HT HAZ ductile-brittle transition temperature of E-4 should therefore be much higher than 100°C. The bead-on-plate bend test described in chapter 4 for 3CR12Ni indicates an HT HAZ ductile-brittle transition temperature higher than 100°C. This is contrary to the weld HAZ Charpy transition temperature of below 0°C which was reported by Eckenrod and Kovach(37) for E-4. This controversy may also be accounted for by the fact that Eckenrod and Kovach failed to differentiate between the different zones in the HAZ. With the edge of the V-notch of their Charpy test specimen located on the fusion line of a welded specimen with a reasonably planar fusion line, the notch tip was positioned at a distance of about 0.8 mm from the fusion line in the tough, fine grained zone in the HAZ. The toughness of the fine grained zone was therefore measured and reported as the toughness of the narrow HT HAZ. The HT HAZ toughness of E-4 is therefore also much lower than the reported values.

1.2 High-temperature embrittlement

The low HT HAZ toughness of 3CR12 and 3CR14, which is nearly independent of the grain size and low carbon martensite content, may be explained by considering the high-temperature embrittlement phenomenon which manifests in high-chromium ferritic stainless steels. After heating commercial high-chromium ferritic stainless steels, containing 16 to 30 percent chromium and moderate-to-high martensite levels, above about 950°C, the steels show an abnormal loss in toughness and ductility at room temperature(38). It is generally agreed that this embrittlement is caused by the precipitation of chromium rich carbides and nitrides on grain boundaries and/or dislocations. The HT HAZ toughness therefore depends on the carbon and nitrogen levels of the steels.

Baerlecken et al. studied the effect of heat treatment on the toughness of vacuum melted 16 to 30 percent chromium ferritic stainless steels(39). They reported a reduction in the transition temperature of an annealed 30 percent chromium steel from 150°C to -30°C by a water quenching treatment from 1050°C and attributed it to a reduction in the amount of chromium-rich carbides and nitrides. Another important conclusion from their work is that grain size has little effect on the toughness of vacuum-melted high-chromium ferritic stainless steels because even with a grain size of ASTM 1-3 a transition temperature of -40°C was obtained. Semchyshen et al. studied the effects of chromium, carbon and nitrogen levels on the toughness of Cr-Fe alloys containing 14 to 28 percent chromium(40). They reported an increase in the ductile-brittle Charpy transition temperature of a 17%Cr-0.01%N steel from -50°C to 130°C with a corresponding increase in the carbon content from 0.002 percent to 0.061 percent. The transition temperature of a 17%Cr-0.004%C steel increased from -50°C to 50°C with a corresponding increase in nitrogen content from 0.010 percent to 0.032 percent.

The general poor weldability of ferritic stainless steels arises from the loss in ductility, corrosion resistance and toughness in the HAZ as a result of chromium-rich carbide and nitride precipitation and excessive grain growth. The as-welded ductility and corrosion resistance is improved tremendously with the addition of stabilizers such as titanium and niobium. Semchyshen et al. and Wright studied the effects of stabilizing additions on the impact properties of ferritic stainless steel plate and found that acceptable room temperature HAZ impact resistance may not be obtained with stabilizing additions(41). For section thicknesses greater than 3.2 mm excellent as-welded HAZ corrosion resistance, ductility as well as toughness can only be obtained with high-purity steel containing extremely low carbon and nitrogen levels. Wright, e.g., reported a decrease in the Charpy transition temperature of 11 mm 26%Cr-1%Mo steel plate from 149°C to -57°C with a corresponding decrease in total carbon and nitrogen content from 0.03 percent to 0.0065 percent.

The high-temperature embrittlement phenomenon which is associated with high-chromium ferritic stainless steels may also be responsible for the low HT HAZ toughness of 3CR12 and 3CR14. Although Rowlands reported that this

phenomenon was suppressed successfully in 3CR12, no conclusive experimental evidence was provided(11). If high-temperature embrittlement is responsible for the poor HT HAZ toughness of 3CR12 and 3CR14 it could not be suppressed using high titanium additions but only by a reduction in the total carbon and nitrogen levels. This high-temperature embrittlement phenomenon should therefore be considered in future research attempts to improve the weldability of 3CR12 and 3CR14. Attention should also be given to the residual elements like P, S and Cu. Wright, for example, found that the HAZ toughness of 26%Cr-1%Mo steels was improved with one or more of these residual elements below the levels normally found in electric furnace processed conventional stainless steels.

1.3 Fine grained heat affected zone

Transverse Charpy 30J ductile-brittle transition temperatures which ranged from -57°C to -68°C were obtained for 12 mm 3CR12 plate in chapter 6. These transition temperatures increased to room temperature after a normalising (after 1h at 1000°C) and tempering (1h at 750°C) heat treatment. It was also found that the excellent toughness of 3CR12 arises, apart from its fine grain size, from the phenomenon of splitting or delamination which releases the triaxial stress field at the Charpy notch tip during testing. This tendency towards splitting is determined by the degree of dimensional anisotropy of the grain structure. The loss in toughness after a normalising and tempering treatment was characterized by a reduction of the degree of dimensional anisotropy of the grain structure. This loss in toughness cannot be restored by a heat treatment since it is not possible to increase the degree of dimensional anisotropy of the grain structure by a heat treatment.

An irreversible loss in toughness will therefore also occur in the fine grained zone in the HAZ of 3CR12 and 3CR14. The transition temperature of 3CR12 was found to increase to about room temperature in this zone as a result of the formation of some untempered martensite and the reduction in the degree of dimensional anisotropy of the grain structure(8). The toughness of the fine grained HAZ can therefore not be improved significantly by a post-weld heat treatment. It may therefore be argued that the as-welded toughness of the fine grained and low temperature HAZ

phenomenon was suppressed successfully in 3CR12, no conclusive experimental

evidence was provided(11). If high-temperature embrittlement is responsible for the poor HT HAZ toughness of 3CR12 and 3CR14 it could not be suppressed using high titanium additions but only by a reduction in the total carbon and nitrogen levels. This high-temperature embrittlement phenomenon should therefore be considered in future research attempts to improve the weldability of 3CR12 and 3CR14. Attention should also be given to the residual elements like P, S and Cu. Wright, for example, found that the HAZ toughness of 26%Cr-1%Mo steels was improved with one or more of these residual elements below the levels normally found in electric furnace processed conventional stainless steels.

1.3 Fine grained heat affected zone

Transverse Charpy 30J ductile-brittle transition temperatures which ranged from -57°C to -68°C were obtained for 12 mm 3CR12 plate in chapter 6. These transition temperatures increased to room temperature after a normalising (after 1h at 1000°C) and tempering (1h at 750°C) heat treatment. It was also found that the excellent toughness of 3CR12 arises, apart from its fine grain size, from the phenomenon of splitting or delamination which releases the triaxial stress field at the Charpy notch tip during testing. This tendency towards splitting is determined by the degree of dimensional anisotropy of the grain structure. The loss in toughness after a normalising and tempering treatment was characterized by a reduction of the degree of dimensional anisotropy of the grain structure. This loss in toughness cannot be restored by a heat treatment since it is not possible to increase the degree of dimensional anisotropy of the grain structure by a heat treatment.

An irreversible loss in toughness will therefore also occur in the fine grained zone in the HAZ of 3CR12 and 3CR14. The transition temperature of 3CR12 was found to increase to about room temperature in this zone as a result of the formation of some untempered martensite and the reduction in the degree of dimensional anisotropy of the grain structure(8). The toughness of the fine grained HAZ can therefore not be improved significantly by a post-weld heat treatment. It may therefore be argued that the as-welded toughness of the fine grained and low temperature HAZ

are dependent on the thermomechanical treatment of the steel plate which determines the degree of dimensional anisotropy of the grain structure.

2. LAMELLAR TEARING

In chapter 6 the through-thickness tensile test, which was also used by De Ardo(27), was used to establish whether splitting in transverse 3CR12 Charpy specimens is related to the phenomenon of lamellar tearing which sometimes attends welding. Satisfactory through-thickness tensile ductilities were obtained and it was therefore concluded that the phenomenon of splitting is not expected to result in lamellar tearing during welding. However, the validity of the through-thickness tensile test, which evaluates the plane stress fracture behaviour, for this purpose is questioned since it was also shown that splitting is dependent on plane strain, rather than plane stress conditions(42,43). The high through-thickness ductile-brittle transition temperatures (112-116°C) and relatively low through-thickness fracture stress of 12 mm 3CR12 plate (chapter 6) strongly suggests that highly restrained welded 3CR12 plate may be susceptible to lamellar tearing initiating from planar defects.

Although the cruciform test is considered as a test with a large degree of restraint in which high through-thickness stresses develop, delamination cracks per se were not found in any of the specimens welded with the different filler metals (chapter 5). Brittle cleavage delamination type fractures did in fact occur in the rolling plane of FLNFT test specimens (chapter 5) welded with AISI 316L, 309L and E3CR12 filler metals, respectively (figure 7.1). In each instance the delamination crack

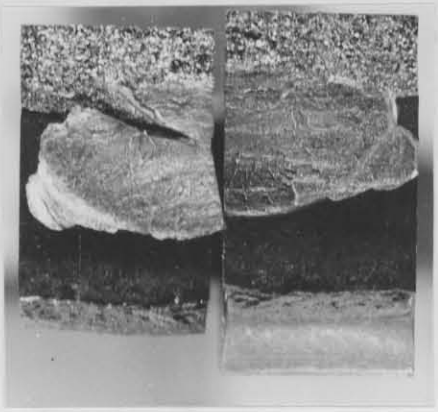

Figure 7.1: Brittle cleavage delamination fracture in a fractured 308L welded FLNFT specimen. The delamination fracture was initiated by the cleavage fracture (bright fracture surface) in the coarse grained HT HAZ.

initiated from a brittle cleavage fracture in the coarse grained HT HAZ. This indicates that the susceptibility of 3CR12 welds to delamination fractures is dictated, apart from TiCN stringers, by the fusion line notch fracture toughness which is usually lower than that associated with delamination. The choice of a filler metal for welding 3CR12 will therefore also influence the susceptibility of welds to subsequent delamination type fractures in the rolling plane.

.....

CHAPTER 8

REFERENCES

1. R. H. Kaltenhauser: 'Improving the engineering properties of ferritic stainless steel', Met. Eng. Quart., May 1971, pp. 41-47.

2. M. L. Melvill, C. S. Mahony, J. P. Hoffman and K. Dewar: 'The development of a chromium-containing corrosion resisting steel' in Proc. Conf. on 'Corrosion', Johannesburg, March, 1980.

3. H. Thielsch: 'Weld embrittlement in chromium stainless steels', Weld. J., Res. Suppl., 1950, vol.29, pp. 126-s-132-s.

4. C. R. Thomas: 'Structure and properties of a duplex ferritic-martensitic stainless steel', in Proc. Conf. on 'Duplex stainless steels', (ed. R. D. Lula), 1983, ASM.

5. R. A. Lula: 'Ferritic stainless steels: corrosion resistance and economy', Met. Progress, July 1976, p. 24.

6. J. F. Lancaster: 'Metallurgy of welding', 3rd ed., George Allen and Unwin, 1980, pp. 173-177.

7. C. R. Thomas and R. L. Apps: 'Weld heat-affected zone properties in AISI 409 ferritic stainless steel' in 'Toughness of ferritic stainless steels', ASTM STP 706, (ed. R. A. Lula), 1980, pp. 161-183.

8. J. P. Hoffman: 'The welding metallurgy of a titanium stabilised 12 percent chromium ferritic-martensitic steel' in Proc. Conf. on 'New developemtns in stainless steel technology', Detroit, Michigan, Sept. 1984, ASM.

9. J. P. Hoffman: '3CR12- An overview of mechanical and corrosion properties', in Proc. Conf. 'Inuagural international 3CR12 conference', Johannesburg, March, 1984.

10. C. R. Thomas and J. P. Hoffman: in 'Speciality steels and hard materials',(ed. N. R. Comins and J. B. Clark), Oxford, Pergamon Press. 1982.

11. D. P. Rowlands: 'Confidence in the reliability of welded stainless steel fabrications in the South-African industry', in Proc. Int. Conf. on 'Reliability in welding', Pretoria, Oct., 1986.

12. A. Ball and J. P. Hoffman: 'Microstructure and properties of a steel containing 12% chromium', Met. Techn., Sept., 1981, pp. 329-338.

13. T. G. Gooch and T. G. Davey: 'Welding of 3CR12 corrosion resisting steel', in Proc. Conf., 'Inuagural International 3CR12 conference', Johannesburg, March, 1984.

14. E. Protopappas: 'The phase equilibria and microstructure of the dual phase steel 3CR12', MSc Thesis, University of Cape Town, 1982, pp. 67-70.

15. S. Pagani: 'The development of the weld metal composition of 3CR12 in relation to mechanical and electrochemical requirements', in Proc. Conf. 'Inuagural International 3CR12 conference', Johannesburg, March, 1984.

16. K. Masubuchi: 'Analysis of welded structures', Pergamon Press, 1982, pp. 363-410.

17. D. Broek: 'Elementary engineering fracture mechanics', Martinus Nijhoff Publishers, 3rd ed., 1983, pp. 219-245.

18. R. W. Hertzberg: 'Deformation and fracture mechanics of engineering materials', John Wiley and Sons, 1976, pp. 359-363.

19. O. H. Wyatt: 'Metals, Ceramics and Polymers', D. Dew-Hudges, 1974, pp. 408-410.

20. N. J. Petch: 'The cleavage strength of polycrystals', JISI, 1953, vol. 173, pp. 25-28.

21. J. R. Low,Jr.: 'Relation of properties to microstructure', ASM, Metals Park, Ohio, 1954, p. 163.

22. A. S. Tetelman and A. J. McEvily, Jr.: 'Fracture of structural materials', John Wiley, New York, 1967.

23. C. Grobler and G. T. van Rooyen: 'The influence of the ferrite factor on the base metal HAZ phase composition of 3CR12Ni and 3CR12', Report to Middelburg Steel and Alloys (Pty) Ltd., 1 Febr. 1985.

24. R. Schofield, G. Rowntree, N. V. Sarma and R. T. Weiner: 'Arrow-head' fractures in controlled-rolled pipeline steels', Met. Techn., July, 1974, pp. 325-331.

25. G. Baldi and G. Buzzichelli: 'Critical stress for delamination fracture in HSLA steels', Met. Science, Oct. 1978, pp. 459-471.

26. D. S. Dabkowski, P. J. Konkol and M. F. Baldy: Met. Eng. Quart, Febr. 1976, pp. 22-32.

27. A. J. DeArdo: 'An investigation of the mechanism of splitting which occurs in tensile specimens of high strength low alloy steels', Met. Trans., March 1977, vol. 8A, pp. 473-485.

28. B. Mintz: 'Influence of grain boundaries on fissure formation during impact testing of ferritic stainless steels', Met. Techn., March 1980, pp. 127-129.

29. Hung-chi Chao: 'Mechanism of anisotropic lamellar fractures', Met. Trans., April 1978, vol. 9A, pp. 509-514.

30. R. K. Ray and Sambhunath Basu: 'Mechanism of splitting of a few Fe-Mn-Ni-base alloys subjected to thermomechanical treatment', Mat. Techn., Steel research 56, 1985, No. 6, pp. 341-345.

31. A. J. McEvily, Jr. and R. H. Bush: 'An investigation of the notch-impact strength of an ausformed steel', Trans. of the ASM, 1962, vol. 55, pp. 654-666.

32. B. L. Bramfitt and A. R. Marder: 'A study of the delamination behavior of a very low-carbon steel', Met. Trans., Aug. 1977, vol. 8A, pp.1263-1273.

33. R. W. K. Honeycomb: 'Steels, microstructure and properties', Edward Arnold, 1980.

34. J. D. Emburry, N. J. Petch, A. E. Wraith and E. S. Wright: 'The fracture of mild steel laminates', Trans. of the Met. Soc. of AIME, Jan. 1967, 239, pp. 114-118.

35. C. Grobler and G. T. van Rooyen: 'The notch-toughness of welded 14% chromium steels', in Proc. Int. Conf. on 'Reliability in welding', Pretoria, Oct. 1986.

36. 'A pocket guide to stainless steel and 3CR12', Middelburg steel and alloys (Pty), Ltd., June, 1986.

37. J. J. Eckenrod and C. W. Kovach: 'Development of a low-chromium stainless steel for structural application', Toughness of ferritic stainless steels, ASTM STP 706, R. A. Lula, Ed., ASTM, 1980, pp. 273-290.

38. J. J. Demo: 'Mechanism of high temperature embrittlement and loss of corrosion resistance in AISI type 446 stainless steel', Corrosion, vol. 27, 1971, pp. 531-544.

39. E. Baerlecken , W. A. Fisher and K. Lorenz: 'Studies of the transformation behavior, the notch impact toughness and the tendency toward intercrystalline corrosion in iron-chromium alloys with chromium contents up to 30% ', Stahl Eisen, vol. 81, no. 12, pp. 1961, 768-778.

40. M. Semchyshen, A. P. Bond and H. J. Dundas: 'Effects of composition on ductility and toughness of ferritic stainless steels', Symp. toward improved ductility and toughness, Kyoto, Japan, 1971, pp. 239-253.

41. R. N. Wright: 'Mechanical behavior and weldability of a high chromium

ferritic stainless steel as a function of purity', Weld. J. Suppl., vol. 50, Oct. 1971, pp. 434-s-440-s.

42. C. Grobler and G.T. van Rooyen: 'A study of the mechanism by which splitting occurs along sheared edges and in transverse Charpy specimens of a 12% chromium steel', in Proc. 25th Annual Conference of Metallurgists, Toronto, Ontario, Aug. 1986. (Accepted for publication in 'Canadian Metallurgical Quarterly').

43. C. Grobler and G. T. van Rooyen: 'An investigation into the influence of the ferrite factor and the occurrence of planar-orientated splitting in transverse Charpy specimens of three 12% chromium steels ', in Proc. 25th Annual Conference of Metallurgists, Toronto, Ontario, Aug. 1986.

****